

STUDIES IN THE RESEARCH PROFILE BUILT ENVIRONMENT
DOCTORAL THESIS NO. 10

Modelling, mapping and visualisation of flood inundation uncertainties

Nancy Joy Lim



Gävle University Press

Dissertation for the Degree of Doctor of Philosophy in Geospatial Information Science to be publicly defended on Monday, 10 December 2018 at 13:00 in Room 12:108, University of Gävle.

Supervisors:

Prof. Stefan Seipel, University of Gävle, Sweden
Dr. S. Anders Brandt, University of Gävle, Sweden
Dr. Eva Sahlin, University of Gävle, Sweden

Opponent:

Prof. Matthew Wilson, University of Canterbury, New Zealand

Evaluation committee:

Prof. Lars Nyberg, Karlstad University, Sweden
Dr. Camilla Forsell, Linköping University, Sweden,
Dr. Jerker Jarsjö, Stockholm University, Sweden

© Nancy Joy Lim 2018

Cover illustration: Nancy Joy Lim

Gävle University Press

ISBN 978-91-88145-33-8

ISBN 978-91-88145-34-5 (pdf)

urn:nbn:se:hig:diva-27995

Distribution:

University of Gävle


Faculty of Engineering and Sustainable Development

Department of Industrial Development, IT and Land Management

SE-801 76 Gävle, Sweden

+46 26 64 85 00

www.hig.se

 Svanenmärkt trycksak, 3041 0736 Kph Trycksaksbolaget 2018

Abstract

Flood maps showing extents of predicted flooding for a given extreme event have wide usage in all types of spatial planning tasks, as well as serving as information material for the public. However, the production processes that these maps undergo (including the different data, methods, models and decisions from the persons generating them), which include both Geographic Information Systems (GIS) and hydraulic modelling, affect the map's content, and will be reflected in the final map. A crisp flood boundary, which is a common way of representing the boundary in flood maps, may therefore not be the best representation to be used. They provide a false implication that these maps are correct and that the flood extents are absolute, despite the effects of the entire modelling in the prediction output. Hence, this research attempts to determine how flood prediction outputs can be affected by uncertainties in the modelling process. In addition, it tries to evaluate how users understand, utilise and perceive flood uncertainty information.

Three main methods were employed in the entire research: uncertainty modelling and analyses; map and geovisualisation development; and user assessment. The studies in this work showed that flood extents produced were influenced by the Digital Elevation Model (DEM) resolution and the Manning's n used. This effect was further increased by the topographic characteristic of the floodplain. However, the performance measure used, which quantifies how well a model produces results in relation to a reference flood boundary, had also biases in quantifying outputs. Determining the optimal model output, therefore, depended on outcomes of the goodness-of-fit measures used.

In this research, several ways were suggested on how uncertainties can be visualised based on the data derived from the uncertainty assessment and by characterising the uncertainty information. These visualisations can be: dual-ended maps; flood probability maps; sequential maps either highlighting the *degrees of certainty* (certainty map) or *degrees of uncertainty* (uncertainty map) in the data; binary maps; overlain flood boundaries from different calibration results; and *performance bars*. Different mapping techniques and visual variables were used for their representation. Evaluations have shown that these mapping techniques, as well as the design of graphical representation, helped users understand the information. Note though that there were visualisations, which the user found easier to comprehend depending on the task given. Each of these visualisations had also its advantages and disadvantages in communicating flood uncertainty, as shown in the assessments. Another important aspect that came out in the study was how the users' background influenced decision-making when using these maps. Users' willingness to take risks depended not only on the map, but their perceptions on the risk itself. However, overall, users found the uncertainty maps to be useful to be incorporated in planning tasks.

The entire research contributes to the understanding of uncertainties in flood maps. Furthermore, investigating ways to effectively communicate flood uncertainty using different visualisation techniques, as well as assessing how

users apprehend and perceive the information provided to them have been important parts of the results derived. These findings and contributions can specifically be summed up as follows: 1) DEM resolution affected the extents of the flooding, and even high resolution data may be limited in producing accurate results; 2) the topographic characteristics of the area under study further enhanced uncertainties produced by models; 3) optimal model results in deterministic maps depended on the quantification method for assessing performance, and thus, are affected by the assumptions of these measures; 4) relying mainly on performance values may not be enough; it also became important to look at the spatial flooding extents generated to determine accuracy of the prediction results; 5) new methods for assessing model performance (mean and median disparities), as well as new a colour map scheme for dual-ended data and visualisation technique to represent uncertainty (i.e. *performance bars*) were presented in the research; 6) the application and implementation of the *Disparity distance* (D_d) algorithm was explored in the research, as an alternative method for accounting uncertainty, and for generating flood uncertainty maps; 7) a cartographic framework was proposed that can help modellers and scientists in visualising flood uncertainty maps; and 8) evaluations showed that users understood flood uncertainty information through maps, but the decisions they made can vary depending on different factors.

Keywords: cartography, flood, GIS, hydraulic modelling, map, uncertainty, visualisation

Sammanfattning

Översvämningskartor som visar utbredningen av förutspådda översvämnningar för vissa extrema händelser har stor användning i all typ av samhällsplanering, samt fungerar som informationsmaterial för allmänheten. Men, de produktionsprocesser som dessa kartor genomgår (inkluderande olika data, metoder, modeller och beslut från de personer som genererar dessa) och som innefattar både geografiska informationssystem (GIS) och hydraulisk modellering, påverkar kartornas innehåll, vilket även återspeglas i de slutliga kartornas utseende. En skarp översvämningsgräns, som är det vanliga sättet att visa gränsen i översvämningskartor, är därför antagligen inte det bästa sättet att representera utbredningen. Sådana gränser ger en falsk trygghet i att dessa kartor är korrekta och att översvämningsutbredningen är absolut, trots att hela processen att producera dem innebär osäkerheter. Denna studie försöker därför undersöka hur översvämningskartering påverkas av osäkerheter i modelleringsprocesser och hur dessa osäkerheter kan representeras, visualiseras och kommuniceras i kartorna. Dessutom försöker studien utvärdera hur olika användare förstår, använder och uppfattar översvämningskartor som innehåller osäkerhetsinformation.

Tre huvudmetoder har använts i denna studie: osäkerhetsmodellering och analys, kart- och geovisualiseringsutveckling samt användarstudier. Resultaten visar att översvämningsgränserna påverkades både av de digitala höjdmoddellernas upplösning (cellstorlek) och markens friktion, representerat av Mannings n , men också av markens topografi. För att kvantifiera skillnaderna mellan modell och referensöversvämningsyta och därefter kunna välja den mest optimala modellen användes olika valideringsmetoder. Dessa lider dock också av olika brister, vilket gör att resultaten varierar beroende på den valideringsmetod som används.

I denna studie föreslås flera sätt att visualisera osäkerheter baserat på resultaten från osäkerhetsmodellering och karaktären av osäkerhetsinformation. Dessa utgörs av kartor med divergerande färgramp (s.k. *dual-ended colour maps*), sekventiella kartor (som framhäver graden av säkerhet, respektive osäkerhet), binära kartor, överlagring av översvämningsgränser från olika modeller samt *värdestaplar*. Olika karteringsmetoder och visuella variabler användes för att representera informationen. Resultat från en användarstudie visade att dessa, samt utformningen av den grafiska representationen, underlättade förståelsen av informationen. Beroende på uppgiften finns det visualisering som är lättare eller svårare att förstå för kartanvändarna. Varje visualisering hade också för- och nackdelar med att kommunicera översvämningsosäkerhetsinformation. En annan viktig aspekt som kom fram i studien var hur användarnas bakgrund påverkar beslutsfattandet när de använde de olika kartorna. Användarnas vilja att ta risker berodde inte bara på kartan, utan också på deras uppfattning av risken i sig. Sammantaget visade det sig emellertid att osäkerhetskartorna är användbara för planeringsuppgifter.

Hela denna forskningsstudie bidrar till förståelsen av osäkerhet i översvämningskartor. I detta ingår även hur information om översvämningsosäkerhet

effektivt kan kommuniceras med hjälp av visualiseringstekniker, samt hur användarna förstår och uppfattar den information som lämnats till dem. Forskningsbidraget kan sammanfattas som följande: 1) höjdmodellens upplösning påverkar översvämningsområdets utbredning, där även högupplösta data uppvisar begränsningar för att få korrekta resultat; 2) de topografiska egenskaperna hos det område som studeras kan ge ytterligare osäkerheter utöver de som producerats av modellerna; 3) optimala modellresultat i deterministiska kartor berodde på valet av kvantifieringsmetod som använts för att validera modeller, och deras antaganden; 4) att huvudsakligen förlita sig på kvantitativt värde från valideringsmetod är inte tillräckligt, det är också viktigt att titta på den översvämningsutbredning som genereras för att avgöra modellens noggrannhet; 5) nya metoder för att bedöma modellers resultat (genom medel- och medianvärdeskillnader) samt nya färgscheman för *dual-ended data* och ny visualiseringsteknik för att representera osäkerhet (dvs. *värdestaplar*) presenterades; 6) tillämpning och implementering av *disparity distance* (Dd)-algoritmen undersöktes som en alternativ metod för att redovisa osäkerheter i översvämningskartor; 7) ett kartografiskt ramverk som kan hjälpa modellerare och forskare att visualisera översvämningskartor som innehåller osäkerhetsinformation föreslogs; och 8) användarstudien visade att användarna förstår osäkerhetsinformation i kartor, men att de beslut som de fattade varierade och beror på olika faktorer.

Nyckelord: GIS, hydraulisk modellering, karta, kartografi, osäkerhet, visualisering, översvämning,

Acknowledgements

I would like to express my gratitude to my supervisors, Prof. Stefan Seipel, Dr. S. Anders Brandt and Dr. Eva Sahlin for all the support, encouragement and guidance. All your comments and feedbacks have been very valuable to me.

To all my colleagues in the divisions of Land Management and IT, as well as the other PhD students in Geospatial Information Science, especially to Markku Pyykönen, Julia Ählén, Ding Ma, and Jonas Boustedt – thank you for the kindness and support.

I would also like to thank Prof. Giuliano di Baldassarre of Uppsala University, for being part of my half-way seminar, and for the important insights he gave to my work. The same goes to Prof. Petter Pilesjö of Lund University. His comments during the final seminar are very much appreciated.

Last but not the least, to my family and friends, for the patience and understanding. I cannot find the right words to show my appreciation to everybody who has been part of my PhD studies and life. All I can say is I am thankful for everything.

Nancy Joy Lim
Gävle, 2018

List of Papers

This thesis is based on the following papers, which are referred to in the text by Roman numerals.

Paper I

Brandt, S. A., & Lim, N. J. (2012). Importance of river bank and floodplain slopes on the accuracy of flood inundation mapping. In R. Murillo Muñoz (Ed.), *River Flow 2012*. (pp. 1015–1020). San José, Costa Rica: CRC Press/Balkema (Taylor & Francis).

Paper II

Lim, N. J., Åhlén, J., & Seipel, S. (2014). Geovisualisation of uncertainty in simulated flood maps. In K. Blashki & Y. Xiao (Eds.), *8th Multi Conference on Computer Science and Information Systems 2014: Proceedings of the IADIS International Conference Computer Graphics, Visualization, Computer Vision and Image Processing* (pp. 206–214). Lisbon, Portugal, 15-19 July: International Association for the Development of the Information Society (IADIS).

Paper III

Lim, N. J., Brandt, S. A., & Seipel, S. (2016). Visualisation and evaluation of flood uncertainties based on ensemble modelling. *International Journal of Geographical Information Science*, 30(2), 240–262. <https://doi.org/10.1080/13658816.2015.1085539>

Paper IV

Brandt, S. A., & Lim, N. J. (2016). Visualising DEM-related flood-map uncertainties using a disparity-distance equation algorithm. In A. H. Schumann (Ed.), *Proceedings of the International Association of Hydrological Sciences (IAHS): The spatial dimensions of water management - Redistribution of benefits and risks* (pp. 153–159). Bochum, Germany: Copernicus. <https://doi.org/10.5194/piahs-373-153-2016>.

Paper V

Seipel, S., & Lim, N. J. (2017). Color map design for visualisation in flood risk assessment. *International Journal of Geographical Information Science*, 31(11), 2286–2309. <https://doi.org/10.1080/13658816.2017.1349318>

Paper VI

Lim, N.J. & Brandt, S.A. (submitted). Flood map boundary sensitivity due to combined effects of DEM resolution and roughness in relation to model performance.

Paper VII

Lim, N.J., Sahlin, E.A.U. & Brandt, S.A. (submitted). A Cartographic framework for visualising flood uncertainties.

Paper VII

Lim, N.J., Seipel, S. & Brandt, S.A. (to be submitted). Assessment of spatial-based decisions and user perspectives in utilisation of flood certainty maps.

Reprints were made with permission from the respective publishers.

Notes on contributions

This thesis is based on the following papers, which are referred to in the text by Roman numerals.

- | | |
|-------------------|--|
| Paper I | Authors are listed in alphabetic order. All authors contributed equally to the paper. |
| Paper II | Lim conceptualised, designed and developed the uncertainty flood geovisualisation model. |
| Paper III | Lim performed the GIS processing, hydraulic modelling and uncertainty analyses, design of questionnaire, conducting the user study, processing of results, analyses and writing. |
| Paper IV | Authors are listed in alphabetic order. All authors contributed equally to the paper. |
| Paper V | Seipel is first author of the paper. Lim contributed in conducting the user evaluation, the processing and analyses of results, and in writing some parts of the paper. |
| Paper VI | Lim planned and executed the study and analyses, and did major part of writing. |
| Paper VII | Lim did the planning of the study and the design of the guidelines. Also, testing of their applicability to hydraulic model results and writing was done by Lim. |
| Paper VIII | Planning, design of maps, user study, analyses and writing were performed by Lim. |

Abbreviations

1D / 2D / 3D	One- / two- / three-dimensional
ASTER	Advanced Spaceborne Thermal Emission and Reflection Radiometer
CS	Cross-section
DEM	Digital Elevation Model
Geovis	Geovisualisation
GIS	Geographic Information Systems
GIScience	Geographic Information Science
GUI	Graphical User Interface
InfoVis	Information Visualisation
LiDAR	LIght Detection And Ranging
SciVis	Scientific Visualisation
SRTM	Shuttle Radar Topography Mission
TIN	Triangular Irregular Network
VTK	Visualisation ToolKit

Nomenclature

Symbols	Description
α	Coefficient
ϑ	Cell width (m)
δ	Resolution (m)
A_i	Overlap size between modelled and reference flood extents
B_i	Size over-estimated by the model
c	Coefficient (D_d algorithm)
C_i	Size under-estimated by the model
C_j	Cost-weighted probability at cell j
D	Distance (m)
D_d	Disparity distance
\bar{D}_i	Mean disparity (m) of simulation i
\tilde{D}_i	Mean disparity (m) of simulation i
$F/F1/F2$	Feature agreement statistics
g	Acceleration due to gravity (m/s ²)
H	Elevation (m)
L_i	Likelihood weight of a model result
n	Manning's roughness parameter
P	Percentile or level of confidence for uncertainty assessment
q	flux
Q	Flow (m ³ /s)
S	Slope perpendicular to the flow
S_j	Entropy-like measure at cell j
t	Time (s)
x, y	Coordinates
w_{ij}	Flooding status at cell j , for simulation i
W	Water depth (m)
W_{flow}	maximum flow depth (m)
WSE	Water surface elevation (m)
z	Exponent (D_d algorithm)

Table of Contents

Chapter 1. Introduction	1
1.1 Background	1
1.2 Problem definition	2
1.3 Aims and research questions	3
1.4 Scope and delimitation	3
1.4.1 Uncertainty definition and type	3
1.4.2 Maps and geovisualisation models as main tool for communication	4
1.4.3 Prediction uncertainty	4
1.4.4 Model performance and uncertainty estimation	5
1.5 Dissertation structure	6
Chapter 2. Theoretical Background	7
2.1 GIS and its application to environmental modelling	7
2.2 Flood inundation modelling	8
2.2.1 Governing equations	8
2.2.2 Flow types	8
2.2.3 Flow dimensionality	9
2.3 Flood mapping and management	11
2.4 Uncertainty	12
2.4.1 Definitions	13
2.4.2 Typologies in GIScience and Geovisualisation	13
2.4.3 Typologies in flood inundation modelling	14
2.5 Flood inundation modelling uncertainty	14
2.5.1 Sources	14
2.5.2 Uncertainty assessment methods	18
2.6 Uncertainty visualisation	21
2.6.1 The role of maps in uncertainty visualisation	21
2.6.2 Uncertainty representation	22
2.6.3 Flood uncertainty representation and visualisation	24
Chapter 3. Methods	29
3.1 Study area	29
3.2 Data and GIS processing	31
3.2.1 Digital Elevation Models (DEM)	33
3.2.2 Validation data	34
3.3 Hydraulic modelling and simulations	35
3.4 Ensemble modelling and GLUE application	36
3.4.1 Accounting for uncertain input and parameters	36
3.4.2 Generation of binary maps	37

3.4.3	Performance assessment and likelihood computation	37
3.4.4	Aggregation and uncertainty map generation	40
3.5	Disparity distance algorithm	41
3.5.1	Data preparation	41
3.5.2	Algorithm implementation and delineation of uncertainty zones	41
3.6	Uncertainty geovisualisation models and maps	46
3.6.1	Interactive 3D flood uncertainty geovisualisation model	46
3.6.2	2D and 3D flood uncertainty geovisualisation	52
3.6.3	Flood certainty maps	56
3.7	User evaluation	62
3.7.1	User evaluations 1 and 2	62
3.7.2	User evaluation 3	64
Chapter 4.	Summary of papers, discussion and contributions	69
4.1	Paper I: Importance of river bank and floodplain slopes on the accuracy of flood inundation mapping	70
4.2	Paper II: Geovisualisation of uncertainty in simulated flood maps	71
4.3	Paper III: Visualisation and evaluation of flood uncertainties based on ensemble modelling	74
4.4	Paper IV: Visualising DEM-related flood map uncertainties using a disparity-distance equation algorithm	75
4.5	Paper V: Color map design for visualisation in flood risk assessment	76
4.6	Paper VI: Flood map boundary sensitivity due to combined effects of DEM resolution and roughness	78
4.7	Paper VII: A cartographic framework for visualising flood uncertainties	82
4.8	Paper VIII: Assessment of spatial-based decisions and user perspectives in the utilisation of flood uncertainty maps	84
Chapter 5.	Conclusion, research contributions and future work	87
5.1	Conclusion	87
5.2	Research contributions	88
5.3	Future work	91
References		95
Appendix		105

List of Figures

Figure 1. Location of study area just north of the city Gävle. Flow direction is going south-southeast. ©Lantmäteriet.....	30
Figure 2. (a) The LIDAR and (b) bathymetric data used for generating the (c) TIN model.....	33
Figure 3. The different resolution DEMs used in the research.....	34
Figure 4. The reference data used for validating the model prediction results. This corresponds to the extent of the actual flooding in the Testebo river in 1977 at 160 m ³ /s.....	34
Figure 5. Ensemble modelling and GLUE methodology implementation....	36
Figure 6. Conversion of one of the original simulation results (i.e. water depth map, left) to a binary map showing the flooding status of a given cell (w_{ij} , right).	37
Figure 7. Example simulation result showing how the overlap, areas under- and over-estimated were accounted for.....	38
Figure 8. The sampling performed in one of the simulation results (left), and from the reference data (right).	39
Figure 9. The relationship between the C_j and S_j values.....	40
Figure 10. Data processing flow for the D_d algorithm.....	42
Figure 11. Direction of the node-to node calculation at the left part of the cross-section.....	43
Figure 12. Algorithm's implementation in deriving the uncertain elevation values.	44
Figure 13. Delineation of uncertain boundaries in GIS for the 50 m data.	45
Figure 14. Steps for generating the different maps layers used in the geovisualisation model and the visualisation pipeline followed.	46
Figure 15. (a) S_j result in raster grid format (5 m resolution), after eliminating all certain to be flooded and dry areas. (b) the original LiDAR point cloud data in the same location where the S_j values were present. (c) Filtered point cloud data that was used for extracting the uncertainty values.	47
Figure 16. (a) Channel, (b) flooded areas and (b) uncertainty band.	48
Figure 17. The (a) DEM and (b) slope maps converted to USGS DEM format, readable by VTK.	49
Figure 18. Display hierarchy of the different maps.....	49
Figure 19. The different map layers in VTK.	50
Figure 20. Cartographic elements included in the main window of the geovisualisation.	51
Figure 21. The graphical user interface, with the different functionalities.	52
Figure 22. 2D contextual information and flood uncertainty map.....	53
Figure 23. 3D contextual information and flood uncertainty map.....	53
Figure 24. The performance bars used for the geovisualisation. Flood and dry statuses were represented by red/green in <i>Paper III</i> (left), and blue/brown in <i>Paper V</i> (right).	54

Figure 25. The dual-ended colour scheme applied to the cost probability (C_j) map in <i>Paper V</i>	55
Figure 26. The original aggregated maps based on applying the C_j (left) and S_j (right) equations.....	56
Figure 27. The three dual-ended certainty maps showing (a) continuous predicted flooding status through a surface map, and the discretised maps using (b) choropleth, and (c) graduated symbol mapping techniques.....	57
Figure 28. (a) Continuous and (b) discrete flood probability maps.....	59
Figure 29. Sequential maps showing degrees of certainty to be dry/flooded using the different mapping techniques: (a) surface map; (b) choropleth map; and (c) graduated symbol map.....	60
Figure 30. The binary map representing certain (blue) and uncertain (red) conditions.	61
Figure 31. (a) One of the stimuli to be assessed by the participants. The <i>preferred</i> homeowner's location is marked in green, while the location that will be allowed for construction (<i>decided position</i> , <i>purple</i>), can be chosen anywhere along the yellow line. (b) The equivalent stimulus in 3D used in one of the conditions in <i>Paper III</i>	62
Figure 32. The preferred locations in the 14 different stimuli used in user evaluations 1 and 2.	63
Figure 33. (a) The positions of the requested sites, and (b) a sample task to be solved, where they have to decide whether the requested location will be allowed or nor allowed for construction.	66
Figure 34. (a) Areas where participants had to select locations for project development, and (b) the sample task to be solved for Task 2.	67
Figure 35. Example map pairs used for the pairwise comparison in Task 3.....	68
Figure 36. Main research topics in the dissertation.	69
Figure 37. The 3D geovisualisation model with flood uncertainty information.	72
Figure 38. The effect of using randomly distributed points to represent uncertainty.	73
Figure 39. Uncertainty zones generated when using the LiDAR data and 50 m DEM.	76
Figure 40. The proportion of the statuses chosen by participants when using the different geovisualisation models. Total n per visualisation was 1162.....	77
Figure 41. Flood extents grouped according to roughness value used.	79
Figure 42. Optimal model performance from the different goodness-of-fit measures.	80

List of Tables

Table 1. Examples of different flow dimensional models, their advantages and disadvantages, as well as common applications.....	9
Table 2. Users of flood maps.....	12
Table 3. Spatial data quality elements, their descriptions and common indicators (from MacEachren et al. (2005) and Thomson et al. (2005)).	14
Table 4. Uncertainty representations using the different visual variables in geovisualisation.	23
Table 5. Colours used for representing certainty and uncertainty conditions.	24
Table 6. Graphical methods for representing flood model uncertainty.....	25
Table 7. Uncertainty representations using colour and value with continuous and discrete data, as presented in different uncertainty flood modelling studies.	26
Table 8. Presentation approaches for visualising flood uncertainties.	27
Table 9. Methods employed in the different papers.....	29
Table 10. Summary of primary data used in the entire research.....	32
Table 11. Pivotal points and the corresponding based colours assigned for the dual-ended colour map presented in <i>Paper V</i>	55
Table 12. Different map types used, and the classification and colour assignment for the different categories in the dual-ended map.....	58
Table 13. Reclassification of original C_j values and the colour assignment used for the sequential probability surface and choropleth maps.....	59
Table 14. The reclassified values and representation used for the sequential certainty status.	61
Table 15. The statuses of the sites in the different certainty maps.....	66

Chapter 1.

Introduction

1.1 Background

Flood modelling is important for predicting flood events, particularly those with high magnitudes. The results derived from these forecasts constitute an important part of information for authorities, planners and the general public, for awareness, and to manage flooding and the risks associated with it. The main outputs from flood modelling are flood inundation and hazard maps that are used for visualising the extents, depth and velocity of flood water, which are all vital for determining and analysing areas that are at potential risk during a flood event. These maps form the basis for flood risk maps, which are utilised in assessing costs and impacts of floods. Therefore, they are significant parts of Flood Risk Management (FRM) tasks (Schanze, 2006) and planning. Development plans, policies, emergency response, etc., rely on these maps as part of decision-support (Moel, van Alphen, & Aerts, 2009).

Nevertheless, these maps are not perfect. The entire modelling process used in generating them involves the combination of Geographic Information Systems (GIS) and hydraulic modelling, which are both subject to different uncertainty issues. Flood maps reflect the specific modelling assumptions, processes, data and decisions made and performed by the modeller who produced the information. Yet, map users may or may not be aware of these sources and causes of uncertainties in the modelling process. The representation of these maps, which often shows deterministic information (Di Baldassarre, Schumann, Bates, Freer, & Beven, 2010) (either through crisp flood boundaries, or depth-related information based on one simulation result), may give an impression that the information presented is true. Even if a model is calibrated to get an optimal result, there is no guarantee that it is accurate. Determining the correctness of the information is relative to the methods employed for quantifying accuracy. Additionally, there can also be imperfections in the reference data that is used for comparing the model. Hence, information presented in a deterministic map, can be misleading (Di Baldassarre et al. 2010; Di Baldassarre, 2012) as there will always be inexactness in the position of flood boundaries, as well as the water depths, for different reasons. To avoid these, uncertainties should be incorporated and represented in the flood maps. Uncertainty assessment and flood uncertainty visualisation should therefore be relevant parts of the flood modelling and prediction processes, and flood communication.

1.2 Problem definition

Deterministic representation of floods that are used for hazard and risk mapping may not be the most appropriate representation of flood information. It may seem to convey absolute information (Di Baldassarre et al., 2010), despite the uncertainties in the map generation process. Different data, models, modelling parameters and processing methods employed will all have effects on the flood maps. This is part of the equifinality problem (Beven & Freer, 2001; Beven, 2006) in modelling. The *equifinality* problem recognises that there can be numerous combinations of factors that can produce acceptable results, as part of the modelling processes' output. An optimal result derived, therefore, is only valid for the conditions, parameter ranges, study area, model etc. that are used and applied in the current setting. It cannot be guaranteed that the same optimal output will be derived if tested under different conditions (Beven, 2006, 2009). Hence, a deterministic map, which represents the single best result from the modelling conducted, will not be the most appropriate representation to be used. The maps can be misinterpreted to be true, despite the uncertainties associated with their generation.

This is the reason why earlier studies suggest the incorporation of uncertainties in flood model results (Pappenberger & Beven, 2006; Faulkner, Parker, Green, & Beven, 2007; Beven, 2009; Di Baldassarre et al., 2010). Users of the information have to be made aware of the important conditions used in the modelling, their limitations and how they affect the results. The incorporation of uncertainty in planning and in the decision-making process, as well as its communication, have been seen to become more and more important (Hall & Solomatine, 2008) and necessary. Nevertheless, although methods for estimating flood uncertainties exist and are well documented, and various flood uncertainty representations are suggested in different literature, they are hardly used to produce flood information that will cater the needs of practitioners and decision-makers. Even in some cases, practitioners can be reluctant when presented with uncertainty from any modelling process (Slocum, Cliburn, Feddema, & Miller, 2003). Scientists are adept in using quantitative analyses for estimating and visualising uncertainty. Statistics is often used to indicate how uncertain the information is. However, statistical representations may not be intuitively viewed by lay persons to suffice the decisions they make (MacEachren et al., 2005). They often rely on experience, best knowledge and reasoning to deal with decisions, rather than numbers. Moreover, there is other information that they have to consider and weigh upon in the decisions they make. Flood information is only one of them.

If flood uncertainty information is to be practically used, the maps should be simple and easy to understand by their potential users. Hence, determining how uncertainty can be quantified, in a way that it can easily be visualised, may possibly help scientists and modellers (i.e. the producers of information) to communicate the information to lay persons and decision-makers (i.e. the users). This may help address reducing the cognitive gap between these two important groups. Possibly, this can also lead to uncertainties in modelling being considered in decision-making and planning.

1.3 Aims and research questions

The aims of the research are to: 1) determine how uncertainties in the modelling process, as brought about by the effects of the Digital Elevation Model (DEM) resolution, the Manning's n , and methods for estimating model performance can affect the model prediction results, in terms of the flood inundation maps generated from them; 2) find out in what ways flood uncertainties can be represented, cartographically designed and visualised in maps; and 3) evaluate how different users utilise and perceive flood uncertainty maps. Specific questions that will help meet the aims are as follows:

1. How are prediction results affected by the modelling processes and the performance estimation used? What are the assumptions of these techniques that affect the output flood inundation map?
2. How can uncertainties be represented in maps and other geovisualisation models?
3. Which cartographic design elements can be adopted in flood uncertainty visualisation? How important are they in communicating uncertainty to different users?
4. Which design guidelines can be suggested to modellers for visualising uncertainty to users?
5. How effective and useful are uncertainty flood maps and geovisualisation models when making spatial decisions?
6. How do laypersons and practitioners perceive uncertain information presented to them?

1.4 Scope and delimitation

1.4.1 Uncertainty definition and type

The uncertainty definition adopted in the entire research is derived from Hunter and Goodchild (1997) and MacEachren et al. (2005). Here, uncertainty will generally refer to as the *lack of knowledge of the true value*, or any inconsistency [in the data, results or processes] (Sec. 2.4.1), and the main research focus is on *epistemic uncertainty*. This type of uncertainty results from subjectivity and the limited knowledge of the system being studied (Merz & Thielen, 2005; Hutter & Schanze, 2008;). In modelling, this can arise from the imperfections of the data used, the parameter estimates, and the assumptions of the utilised model, as well as the uncertainty analysis method employed.

1.4.2 Maps and geovisualisation models as main tool for communication

The entire uncertainty communication approach is not adopted in this research, but rather, the focus is on visualisation, as an important tool for communication (Faulkner et al., 2007). If models produced by scientists are to be used in planning, then flood uncertainty information must be thoroughly communicated to its potential users. The two groups have different understanding of the uncertainty information. Inadequateness of the visualisation technique can pose cognitive difficulty to the information, which is already deemed difficult to comprehend by laypersons.

Flood inundation maps and geovisualisation models are the main visualisation focus. The former, in particular, are generally utilised in all planning and management tasks, as well as in information awareness campaigns. This is due to the simplicity of the information being conveyed. The flooding extents visualised in these maps usually serve as the initial information used for flood risk assessment, i.e. for identifying possible locations that are at risk of flooding.

1.4.3 Prediction uncertainty

Flood modelling prediction uncertainties that affect flood maps are accounted for in the entire research. There are two sources of uncertainties that are looked at primarily in the studies: the topographic data, in terms of the DEM resolution (input data), and the roughness parameters, through the Manning's n (model parameter) (Sec. 2.5.1). In different literature, these two sources of uncertainties are widely recognised to significantly affect the flood inundation extents generated (Dottori, Di Baldassarre, & Todini, 2013).

The topographic data is an important input that gives the geometry of the area (Casas, Benito, Thorndycraft, & Rico, 2006), and is created through GIS techniques. Two important properties derived from the DEM are the resolution (or the grid size) and the height values. Both are used by hydraulic numerical models to discretise space and to extract elevation in order to derive water depths. In this research, the focus however is the effect of the resolution to the flood model results. DEMs come from different sources and can have different resolution and accuracy. Details in the topography are dependent on the resolution of the DEM. High resolution DEMs, particularly LiDAR-based data, are known to give better representation of the topography (Casas et al., 2006; Schumann et al., 2008), allowing smaller features to be represented, and accounted in the modelling. It has also better accuracy. On the other hand, details are eliminated in lower resolution DEMs. The elimination of details in the topography has an impact in changing the flow patterns of water (Savage, Pianosi, Bates, Freer, & Wagener, 2016). Thus, flood extents produced from coarser DEMs differ from high resolution data. The resulting uncertainties in results as effect of resolution are widely investigated with one-dimensional models. However, with two-dimensional models, medium to lower resolution

DEMs are often investigated due to the higher computational cost of simulations using fine resolution DEMs (Savage et al., 2016). This poses limitation of understanding whether there is a real benefit in using high resolution DEMs in modelling, or if it will suffice with medium to lower resolution DEMs, particularly with 2D models.

On the other hand, the roughness coefficient, which determines the channel and floodplain's resistance to the flow, is also an important model parameter. It is often derived from land cover classes and assigned with recommended values from literature. Yet, all models manifest different sensitivity to the Manning's n (as shown e.g. Aronica, Hankin, & Beven, 1998; Pappenberger, Beven, Horritt, & Blazkova, 2005). It can produce different model results. Accordingly, this makes it difficult to determine the exact value to be used when modelling. Thus, the roughness parameter is often calibrated to match a reference data for the specific study site, model and even resolution to determine the Manning's coefficient to be used.

1.4.4 Model performance and uncertainty estimation

There are different quantification methods used for accounting prediction uncertainty in modelled flood extents. These performance or goodness-of-fit measures tell how the output is produced in relation to a reference flood extent (i.e. historical data). They are the bases for determining "optimal" model results that are used for deterministic flood maps. Moreover, they are important in uncertainty assessment methods such as the Generalised Likelihood Uncertainty Estimation (GLUE) methodology. In GLUE, they are utilised for deriving the likelihood weights, which are used for producing the flood probability and uncertainty maps. Nevertheless, each of these quantification methods can also have assumptions on how model performance is quantified (Beven, 2009). This may also affect the uncertainty map outputs that are produced.

In evaluating the effects of performance in deterministic mapping, there are four goodness-of-fit measures assessed (Sec. 3.4.3). The two feature statistics (F) methods are the most commonly used for extent validation studies. They compare the total size of the predicted inundation with a known (observed or reference) extent. Aside from the feature statistics, two new proposed methods are presented, i.e. the mean and median disparities, which take into account the difference (i.e. error) between the modelled and the reference flood boundaries.

In accounting for flood model's prediction uncertainty, there are two main methods employed in the uncertainty assessment. These are the Generalised Likelihood Uncertainty Estimation methodology (Beven & Binley, 1992) and the Disparity Distance (D_d) algorithm (Brandt, 2016) (Sec. 2.5.2). Both methods consider uncertainties in flood extents, and can be used to produce different types of flood uncertainty maps that are used for the geovisualisation and user evaluation parts of the research.

1.5 Dissertation structure

In chapter 2, relevant literature to the study is reviewed. This includes putting into context three important aspects of the research: Geographic Information Systems (GIS), flood modelling and uncertainty visualisation. The third chapter presents the approach employed in the entire research to help answer the research questions. These are divided mainly into six main parts: data pre-processing within GIS; hydraulic modelling; uncertainty estimation; uncertainty mapping, visualisation and design; and user assessments. The results of the different studies conducted through the different publications are summarised in the fourth chapter. This chapter also shows how the different papers address the different research questions presented in Sec. 1.3, together with their contributions and discussions. The last chapter presents the conclusion, the overall research contribution and recommended future work.

Chapter 2.

Theoretical Background

2.1 GIS and its application to environmental modelling

The utilisation of GIS and different spatial analysis methods is important for solving geographical problems and for investigating spatial phenomena (Mark, 2000). This is a reason why GIS has been employed in different fields to help answer geographic problems related to them. One of the most common applications of GIS is in environmental modelling and research (Fedra, 1993). Environmental models are used to simulate processes, in order to gain better understanding of the environmental system's behaviour (Skidmore, 2002), as well as for prediction of future events (Beven, 2009). The latter is particularly important from management, planning and decision-making perspectives. Predicting the magnitude of phenomena can help visualise different scenarios and their possible consequences. From this information, authorities can take precautionary measures or actions that can help minimise (if not prevent) drastic impacts of a disaster (Mulligan & Wainwright, 2004).

Like any other models, environmental models are simplifications of reality (Mulligan & Wainwright, 2004; Beven, 2009). This is because real-life processes are complex that involve many interacting factors. In a model, the processes and their components are transformed to mathematical equations to help quantify and explain system behaviours (Mulligan & Wainwright, 2004). Each equation implemented has certain assumptions that may neglect several aspects that it deems irrelevant in the modelling process, to reduce complexities and computational costs.

The spatial aspect of environmental modelling is supported by both remote sensing and Geographic Information Systems. Remote sensing acts as an important data source for modelling. Satellite imagery, radar and LIDAR data, as well as aerial photographs are used for deriving the topography, land cover/land use, vegetation, geologic data, etc. which provide the geographic characteristics of the area. GIS, on the other hand, is applied mainly as a tool for capturing, storing, manipulating and displaying spatial data (Fedra, 1993; Skidmore, 2002). Most spatial data need further processing to be used in an environmental system. For instance, these datasets have to be added geometry and attributes that will help classify and identify landscapes. Some of the data also needs to be transformed to specific formats required by the model to be used. It is within GIS that these datasets are prepared before they can serve as inputs in a model, which is often external to a GI system (Fedra, 1993).

But aside from this pre-processing functionality, GIS helps further analyse and visualise results from environmental modelling processes. Its analytical capacity lies in the different spatial modelling methods that can be employed to give insights of the geographic trends in results. Its visualisation capability enables the spatial and non-spatial display of information (Skidmore, 2002).

Therefore, GIS is also important for visual and exploratory analyses, and in scenario building, which are all valuable tools for planning and decision-making.

2.2 Flood inundation modelling

Flood inundation modelling is used mainly for predicting the impacts of a given flood event, by simulating the flow behaviour. Hydraulic models are often used in the modelling to determine the movement and timing of flow along the channel. They give approximation of the flood or wave propagation that help determine water depth, velocity or flood extents, which are important outputs of the model. Their complexity depends on the equations they apply in simulating flows, and the assumptions that they consider in the modelling.

2.2.1 Governing equations

Hydraulic models are built on two main governing equations based on the laws of physics. These are the continuity (conservation of mass) and momentum equations. The continuity equation simply states *that net change of mass in the control volume as caused by the inflow and outflow, is equal to the net rate of change of mass in the control volume*. The momentum equation is based on Newton's second law of motion. It states that *the rate of change in the momentum is equal to the net forces acting on it* (French, 1986; Cruise, Sherif, & Singh, 2012). With flowing water, external forces such as gravity, friction, pressure and inertia are considered in the momentum equation. Hydraulic models implement these governing equations in different ways, to reduce the complexity in the approximation of flow movement and to make the model more stable. Therefore, they apply these equations to meet certain assumptions, e.g. how the flow being modelled is to be characterised (flow types), or how the flow will be represented (dimensionality of the flow).

2.2.2 Flow types

Flow characteristics tell whether depth, flow and velocity change with time (steady or unsteady) or location (uniform or non-uniform) (French, 1986). In steady flow, these variables do not change over time, as opposed to unsteady flow, where they vary with time. In uniform flow, there is no change in flow depth along the river, as against non-uniform (varied flow). Non-uniform flow can further be classified as gradually-varied and rapidly-varied. With gradually-varied flow, there is no excessive change in the flow depth along the stream. If there is a large, sudden change in depth, specifically at shorter intervals, the flow is characterised to be rapidly-varied (French, 1986; Wurbs, 1997).

2.2.3 Flow dimensionality

The governing equations and solutions applied to models may be described using different spatial dimensions on how flow is represented by the model. Although, real-life flow characteristics are three-dimensional (3D) (i.e. in x , y and z) in nature, this may pose limitations in solving the flow problem due to more complex equations and data needed (Cruise et al., 2012). Therefore, the most common flow representations used are provided by one-dimensional (1D) and two-dimensional (2D) models. 1D models implement the simplest approximations, followed by 2D models. Table 1 shows the different flow representations and their advantages and disadvantages, as well as their common applications.

Table 1. Examples of different flow dimensional models, their advantages and disadvantages, as well as common applications.

FLOW DIMENSION	EXAMPLE	ADVANTAGES	DISADVANTAGES	COMMON APPLICATIONS
1D	HEC-RAS (steady and unsteady) MIKE 11 (unsteady) TufLOW 1D	<ul style="list-style-type: none"> - Fast simulation time - Manageable data requirement - Easy to conduct model calibration - Can consider effects of bridges and other structures along the river 	<ul style="list-style-type: none"> - Sensitive to cross-section spacing and positioning - May not be able to capture flow dynamics in complex channels 	<ul style="list-style-type: none"> - Straight channel - Steady or unsteady river systems
2D	Telemac-2D RMA-2 FEWWMS-2DH MIKE 21 (unsteady) TufLOW LISFLOOD-FP	<ul style="list-style-type: none"> - Discretisation of space through mesh or grid - Better for modelling floodplains with complex geometry - Balances the simplicity and complexity of 1D and 2D models 	<ul style="list-style-type: none"> - Long simulation time for high resolution data - More data and parameter requirements 	<ul style="list-style-type: none"> - Shallow - Braided channel
3D	Flow 3D (unsteady)	<ul style="list-style-type: none"> - Fulfills the limitations of 2D models 	<ul style="list-style-type: none"> - Long simulation time - More data and parameter requirements 	<ul style="list-style-type: none"> - Complex river systems - Depth varying velocities

One-dimensional flow models

In a one-dimensional flow model, the flow is considered to be one-directional, parallel to the channel (Néelz & Pender, 2009; Teng et al., 2017). Channel and floodplain geometries are represented by cross-sections (Pender & Néelz, 2007), which are used for solving flow equations. 1D hydraulic models are based on the St. Venant equations. There are several assumptions in these equations, which characterise 1D models. These include: 1) there is uniform velocity over the cross-section, and the water level at each cross-section is horizontal; 2) the small streamline curvature and vertical accelerations are insignificant; 3) flow resistance can account for both boundary friction and turbulence; and 4) the average channel slope is small (Litrice & Fromion, 2009).

One-dimensional models are in practice used because of their efficiency in modelling, due to the simple assumptions of the equation, as well as the utilisation of cross-sections to define geometry. This leads to lesser computational time even when using high resolution data (Bates & de Roo, 2000; Néelz & Pender, 2009) with larger study area. The input data requirements and hydrologic data needed are also more manageable, making them easier to use (Bates & de Roo, 2000; Samuels, 2006). Shorter reach lengths with less complex geometries can appropriately be modelled with 1D models (Bates & de Roo, 2000). Even so, 1D models are also known for their limitations in modelling. One of the sensitivities of the model is caused by the cross-sections' spacing, (Cook & Merwade, 2009), position (Hunter, Bates, Horritt, & Wilson, 2007), and the representation of areas in between the cross-sections (Bates & de Roo, 2000). Also, in modelling more complex and larger streams, 1D models may not capture the flow dynamics well (Merwade, Cook, & Coonrod, 2008), especially when flow is spread out horizontally.

Two-dimensional flow models

With two-dimensional models, both water depth (W) and depth averaged velocities (u, v) are accounted for in two spatial dimensions (x, y) (Teng et al., 2017). These x and y directions are derived from the topographic data used, which is discretised in either a triangular mesh or through grid cells, that represents a continuous surface. The usage of a continuous surface gives better representation of the topography (Bates & de Roo, 2000) than by using cross-sections, allowing better computation of depth and velocity. It also allows capturing the flow dynamics in more complex channels.

In 2D models, both the continuity and momentum equations are in most cases solved by applying the St. Venant's shallow water equation, which is integrated with the 2D Navier Stokes equations (Teng et al., 2017). These models also vary in the solutions they apply when using the momentum equations, allowing them to neglect some of the components of the full equation (Néelz & Pender, 2009), to simplify flow calculation. The kinematic and diffusive wave are the most common approximations used. In the former both the gravitational and frictional forces are retained, while in the diffusion wave model, gravity and friction are accounted, together with pressure (Bedient, Huber, & Vieux, 2013).

According to Horritt and Bates (2001a), 2D models balance the modelling disadvantages of 1D and 3D models, in terms of simplicity and complexity, respectively. However, like the 1D model, 2D models also have certain issues. First, the accuracy of the flow representation will depend on the resolution of the discretised mesh or grid used. Second, the number of elements (triangles and cells) used in the modelling, is affected by the resolution (Fewtrell, Bates, Horritt, & Hunter, 2008) and size of the modelled area. This has a direct impact on the simulation time. Although better computer processors and model optimisation techniques speed up the modelling (Leedal, Neal, Beven, Young, & Bates, 2010), typical simulation time for 2D models can still take several hours or days (Néelz & Pender, 2009), depending on the resolution and size of the study site. Thus, the usage of high resolution data remains a restriction to 2D models (Savage et al., 2016). This time constraint also poses the limit to performing several calibrations and sensitivity analyses, specifically when using fine resolution DEMs. Additionally, they also need more input data, model parameters and variables than 1D models.

Three-dimensional flow models

In the computation of 3D velocities, 3D models are used (Pender & Néelz, 2007). They are also employed to predict water depths and extents at more local scale. According to Horritt and Bates (2001a), three-dimensional models try to compensate the limitations of 2D models. However, the numerical solutions applied in them are more complex. Due to this complexity, there are technical problems that are associated with their full implementation (Néelz & Pender, 2009). The technical complexities also increase with the scale of the site being studied. This leads to practical limitations for its application to flood hazard mapping and inundation studies (Néelz & Pender, 2009).

2.3 Flood mapping and management

Flood model results are used for generating different flood hazard maps (i.e. flood inundation extent, depth and velocity maps). These maps provide relevant information for different practitioners in both public and private sectors, in managing and mitigating the impacts of flooding (Table 2). They are mainly used for arriving at measures and instruments that are needed to reduce risks. These measures are either permanent or temporary physical actions undertaken to control floods and protect those that can be affected. Instruments are mechanisms that can help alleviate risk. Examples are policies, communication and financial supports (Schanze, 2006). Communities, homeowners and other citizens also benefit from flood maps as source of information to make them aware if they are safe or unsafe from flooding.

Table 2. Users of flood maps.

PUBLIC	PRIVATE	OTHERS
Municipal/regional/national government Policy makers Engineers/Surveyors Disaster/emergency workers Flood managers Planners and designers	Insurance companies Stakeholders and developers Contractors Utility companies Non-government organisations (NGOs)	Communities Homeowners General public

Flood extent maps are the most general among inundation and hazard maps. They display the flood boundaries derived from simulating a given event. Because of their contents, they are easier to read and understand, and are often used in initial risk assessment tasks (EXCIMAP, 2007). These maps are also the most widely adopted in land use and urban planning, especially as basis for issuance of building permits.

Flood depth maps show the water level at the given flood frequency, while the velocity of the water is displayed in a flood velocity map. Both are used for producing flood vulnerability and risk maps, which further help estimate possible consequences (social, cultural, economic, and environmental) of flooding. The depth and velocity maps have also their usage in planning, but velocity maps are particularly important for emergency and engineering tasks (EXCIMAP, 2007). Emergency workers use the latter to determine how fast the water flows in areas where rescue operations take place. In constructing flood defence structures, velocity of water is also needed to be known.

At the European Union (EU) level, the EU Flood directive 2007/60/EC requires member states to develop flood hazard and risk maps, as well as flood management risk plans. The flood directive aims to comprehensively evaluate the associated flood risk in all water bodies in EU countries. This helps in arriving at mitigation measures to better manage possible consequences of flooding to avoid drastic human, economic and environmental impacts.

2.4 Uncertainty

Uncertainty is an issue in both GIS and flood inundation modelling. This is mainly due to the various sources of uncertainty that affect results produced from these processes. Therefore, accounting for uncertainty in the results is recognised to be important in both fields.

2.4.1 Definitions

Uncertainty can have different definitions that can be subjective to people who are using the term. It is synonymously referred to inaccuracy, error, limited knowledge, unreliability, doubt, ambiguity, vagueness, etc. (Beven, 2009). In some contexts, there are clear differences among these terms, which can be distinguished according to the uncertainty source and types, and the methods employed for measuring it.

Hunter and Goodchild (1997) use uncertainty to refer to the *lack of knowledge of the true value* of a data. According to them, this true value is the actual field/observation value derived for the data using an accurate instrument. This definition given by Hunter and Goodchild (1997) provides a general depiction of uncertainty that encompasses any inconsistency in a data (MacEachren et al., 2005), which is brought about by different sources, such as the instrument's imperfection in collecting and recording the data, data manipulation processes, generalisation effects in visualisation, etc.

2.4.2 Typologies in GIScience and Geovisualisation

In both GIScience and geovisualisation, a formalised approach for typifying uncertainty is based primarily on the different components that affect the quality of spatial data (MacEachren et al., 2005; Thomson, Hetzler, MacEachren, MarkGahegan, & Pavel, 2005). Spatial data is an important product of GIS processes, and are also the usual inputs for modelling. Since these data come from different sources and are generated through different processing techniques, their quality can change. Therefore, different information that can help determine their quality must be made known to its users by describing and indicating them in the metadata. The five quality components of spatial data are lineage, positional accuracy, attribute accuracy, logical consistency, and completeness (Table 3), which help indicate some parts of uncertainty affecting the data (Thomson et al., 2005).

Lineage tells about the history of the data (MacEachren, 1992). This includes its source, the processes it underwent to attain its final form, and its currency. Positional accuracy determines the closeness of the coordinate values in the maps to known true positions in the ground (absolute), and the closeness of measurement on how objects are placed relative to each other (relative). The most common indication of this is through error or accuracy measurements (e.g. root means square error, RMSE). Accuracy of the attributes is related to correctness of the non-spatial information associated with spatial data. Attribute accuracy can be measured by deriving random samples and comparing them to the "true" value (ground truth data) through classification error matrices. This provides a measure of agreement between the sample and the ground truth data through the overall accuracy, or the omission or commission errors. Logical consistency refers to the topological accurateness of the data. Completeness indicates whether all objects are included or not included in the database (MacEachren et al., 2005; Thomson et al., 2005).

Table 3. Spatial data quality elements, their descriptions and common indicators (from MacEachren et al. (2005) and Thomson et al. (2005)).

SPATIAL DATA QUALITY ELEMENT	DESCRIPTION	COMMON INDICATORS
Lineage	Spatial data history (source, currency, data generation process, reason for production)	Descriptive statements
Positional accuracy	Closeness to true position in the ground or in relation to other objects	Error measurements (e.g. RMSE)
Attribute accuracy	Correctness of the attributes associated to the spatial data, to the real-world features that they represented.	Classification error matrices to determine Kappa values
Logical consistency	Topological accurateness of the data	Descriptive documentation
Completeness	Indication whether objects are represented and included in the database; definitions used; selection criteria, etc.	Descriptive statements

2.4.3 Typologies in flood inundation modelling

In flood inundation modelling, two widely recognised types of uncertainties are *aleatory* and *epistemic* uncertainties (Apel, Thielen, Merz, & Blöschl, 2004; Merz & Thielen, 2005; Hutter & Schanze, 2008). Aleatory uncertainty is related to the randomness of the phenomena. These uncertainties are inherent because of the complex processes involved in real events, and there is interplay of different factors associated with them. Yet, this type of uncertainty is rather hard to quantify due to the variability of the phenomena itself, which is difficult to measure. The second type of uncertainty is related to the modelling process and may be affected by the data and the model used, as well as the measurements applied. This is known as epistemic uncertainty. Unlike aleatory uncertainties, these uncertainties are quantifiable through different statistical methods.

2.5 Flood inundation modelling uncertainty

2.5.1 Sources

There are several studies that recognise different sources of uncertainties in flood inundation modelling. According to the *Handbook on good practices on flood mapping in Europe* (EXCIMAP, 2007), the uncertainty sources can be classified mainly into three types: input data, measurements and model.

Input data

Flood models require various data. The most commonly used are topographic, land cover and hydrologic data. Topographic and land cover data are derived from remote sensing, surveying, maps and application of GIS techniques. The hydrologic data are derived from gage measurements and through hydrologic modelling.

Topographic data

The topographic data, which is primarily used for providing the geometry of the river and floodplain, are derived from remote sensing and surveying techniques. Popular sources are Light Detection and Ranging (LiDAR), Advanced Spaceborne Thermal Emission and Reflection Radiometer (ASTER, 30 m), Shuttle Radar Topography Mission (SRTM with 90 m resolution), as well as bathymetric surveys and topographic maps. Bathymetric data are used for deriving channel elevation, which is not captured in remote sensing products (Casas et al., 2006; Cook & Merwade, 2009). Providers of these datasets can be government or federal agencies (e.g. National Aeronautics and Space Administration, NASA), or private consulting companies who perform surveying.

Topographic data used in flood modelling are processed to meet the hydraulic model's requirements for input data. Combining different data from different sources (LiDAR and bathymetric data) is also needed to compensate for the missing information from one source (Casas et al., 2006). Therefore, before they are finally used in the hydraulic model, they undergo different manipulation and transformation within GIS. All these steps influence how the geometry of the channel and the floodplain are represented, as well as the eventual results derived from the hydraulic simulation.

Uncertainty in flood maps as effect of topographic data has been extensively studied (e.g. Tate, Maidment, Olivera, & Anderson, 2002; Casas et al., 2006; Cook & Merwade, 2009). The uncertainties caused by these datasets are brought about by the different remote sensing data (SAR, LiDAR), which can also be associated by their resolution. High resolution data, particularly LiDAR in combination with bathymetric data (Casas et al., 2006; Cook & Merwade, 2009), has been recognised to produce better model results. This is due to the more accurate representation of the river and floodplain, and the more precise height values LiDAR data provides.

Land cover data

Land cover data (which is often referred to as land use data in hydraulic modelling literature and software) is used for assigning the roughness parameter (Manning's n , see *Parameter Uncertainty*), which determines the floodplain and the channel's resistance to flow. It provides the information as to the type of (surface) materials lining the channel and the floodplain. Examples can be light to heavy grasses, trees, shrubs, paved surfaces, etc. Land cover data is generated from classification of satellite images (Schumann et al., 2007), provided by local authorities, or can also be derived from existing land use data or maps. The detail of the land cover information can vary from one source to

another. Small-scale land cover maps are mostly homogenised to dominating classes. They give an overall view of the land cover at the larger area, but may fail to give the variation at the local level. On the other hand, land cover maps derived from classification using satellite images, can be affected by the classification technique performed, the processes involved in their preparation, as well as the resolution of the satellite image used.

Hydrologic data

Hydrologic data consist of flow data, water stages and their corresponding time. They are used as boundary conditions for the model. Raw hydrologic data are initially collected from measuring instruments (e.g. stream gauges), observations or from surveying methods at different parts along the river. They are used for deriving rating curves (to estimate discharges), hydrographs that show either the change in discharge or water elevation over time, discharge, velocity or water depths (Di Baldassarre & Montanari, 2009). Some of the raw data and already processed hydrologic data can also be available from meteorological/hydrological agencies.

Measurement errors

The different input data are collected using different instruments. These instruments can be affected by external factors when recording raw data, aside from human errors involved during the acquisition and processing of the measurements. Sensors are used for obtaining satellite images and elevation information, which are used for creating the land cover and topographic maps. The recorded raw digital images can be affected by weather conditions (e.g. clouds and rain), atmospheric factors and noise during the data gathering process (Lillesand, Kiefer, & Chipman, 2004). Hydrologic data, which are recorded from river gauges and field measurements, are also affected by environmental factors, as well as human errors. Thus, they are associated with uncertainties, as what was exemplified in Di Baldassarre and Montanari (2009).

Inclusion of measurement errors in uncertainty modelling can be difficult particularly for topographic data and land cover maps. The former is usually derived from different providers, which publish already corrected information. Exact ways of how the different corrections in raw digital images (which are also based on different methods and equations) and the accuracy information may sometimes be left out in the accompanying metadata. Therefore, its quality is difficult to determine. Some data, like LiDAR, may have accompanying accuracy information provided by its producer.

With hydrologic data, measurement errors can be based on the specifications indicated in the instruments. Nonetheless, uncertainties in methods employed for processing or deriving products based on these raw data readings may also be difficult to track, unless one processes the data to be used, and account for errors in the measurements. The latter can be considered in the modelling by varying the boundary conditions based on the associated error in the input data, or by varying discharges (see section on *Information uncertainty: initial and boundary conditions*).

Model

Model uncertainties are caused by the model structure, parameters, and information used for modelling (i.e. the initial and boundary conditions). Model structure is affected by the model used, as well as its assumptions in applying mathematical solutions to the problem. Parameter uncertainty is the effect of limited knowledge of the parameter values, which can vary from one model or study case to another. Information uncertainty can be associated to the errors in the model input that affect the results (Loucks & Beek, 2005).

Model structure

As mentioned earlier, the governing equations (continuity and momentum equations) are applied in variety of ways in the different models, either to simplify model solutions or to introduce stability when modelling. Therefore, alternative equations are implemented in different models, with specific assumptions. The momentum equation for instance, can be used fully (i.e. dynamic wave models) to account for all external forces influencing the flow rate of water (Bedient et al., 2013). However, its application will require more data and numerical computations, making it more complex to handle. Therefore, approximations are applied, wherein some of the external forces are assumed to be unimportant and eliminated in the equation. For example, in the kinematic wave model, which is the simplest approximation for the momentum equation, only the gravitational and frictional forces are retained. In the diffusive model, pressure, gravity and friction are accounted.

Parameter uncertainty

One of the important parameters to which hydraulic models manifest sensitivity is the roughness parameter represented by the Manning's n . These Manning's n values are typically derived from literature, e.g. Chow (1959), and assigned according to the land cover (vegetation or the surface material of the bed and floodplain). However, models behave differently when using the same roughness value. Horritt and Bates (2002) for instance showed how the optimum channel and floodplain roughness differ with the models used (HEC-RAS, Telemac and LISFLOOD-FP). Some models may also require heterogeneous Manning's n values as specified in the land cover map, while there are some which only need a specific value assigned to the channel and floodplain.

Furthermore, the roughness parameter used can also change with the resolution of the input topographic data (Romanowicz & Beven, 2003; Yu & Lane, 2006; Savage et al., 2016), boundary conditions (Hall, Tarantola, Bates, & Horritt, 2005; Pappenberger et al., 2006; Yu & Lane, 2006; Savage et al., 2016), the discharge used (Aronica, Hankin, & Beven, 1998; Romanowicz & Beven, 2003; Di Baldassarre & Montanari, 2009), as well as the study site to which it is tested. Therefore, the roughness coefficient cannot just be based on standard values suggested in literature, which are empirically derived in specific test sites.

Information uncertainty: initial and boundary conditions

Models require different information prior to starting the simulations. The basic information needed are the initial and boundary conditions, which are derived from the hydrological data. Initial condition determines the initial modelling status, at the starting time of $t = 0$. This condition is provided through a specified water level or discharge. Boundary conditions are the statuses that are often specified at specific locations along the reach. The most common locations are the upstream and downstream parts of the channel. The requirements for the initial and boundary conditions may vary among models. Some may only require an initial boundary condition. There are models that only need a boundary condition at the upstream of the river, while in some cases it has to be assigned at both ends of the channel. Information used for boundary conditions are the rating curves (stage-discharge relationship), hydrographs (showing changes in discharge or water elevation over time), water stage/level and discharge. Since they are all outputs from the hydrologic data, initial and boundary conditions are subject to the uncertainty of the hydrologic data. The sensitivity of the model to the boundary condition, particularly to the rating curve and inflow are shown in Hall et al. (2005) and Pappenberger et al. (2006). This effect is manifested mainly in the changes in water depth (Pappenberger et al., 2006).

2.5.2 Uncertainty assessment methods

There are several ways of how uncertainties are regarded in different inundation studies. In assessing flood model prediction uncertainties through the inundation extents produced, two methods that are usually employed are sensitivity analysis and the Generalised Likelihood Uncertainty Estimation (GLUE). The former is used for understanding the effects of the model input or parameter to the output, while the latter is for understanding uncertainty in the model prediction. A third method for accounting uncertainty, i.e. the *disparity distance*, algorithm, is also introduced in this section. It considers the uncertainty in the model output as an effect of the topography in the area.

In these methods, not all sources of uncertainties in the modelling are accounted for. Only specific input data or parameters, or combinations are considered to be uncertain, while other information remains constant in the modelling. This helps avoid the problem of over-parameterisation, which can hinder understanding the impact of specific input/parameter that is/are being analysed.

Sensitivity analysis

Sensitivity analysis allows to determine model output's response to incremental changes in the input or parameters being tested (Mulligan & Wainwright, 2004). Multiple simulations are carried out, where input data or parameters, or combinations of both, are altered in each run. Every simulation produces a unique result that is dependent on the input data/parameter used. This process

is often termed as ensemble modelling because the factors to which it is tested for is derived from given sets or an ensemble.

Generalised Likelihood Uncertainty Estimation (GLUE)

The Generalised Likelihood Uncertainty Estimation (Beven & Binley, 1992) accounts mainly for prediction uncertainty or how the model results are affected by the uncertainties in the modelling process. There are four requirements that have to be decided in following the GLUE methodology, namely: 1) a likelihood measure; 2) model parameter or input to be considered uncertain; 3) sampling distribution from where the samples are to be derived; and 4) implementation.

An important part of the methodology is deciding a likelihood measure, which is used to weight the model output, based on how well the result is generated. The likelihood measure can be based on any performance (goodness-of-fit) measure that quantifies model results in relation to a reference data, where the model is validated. Therefore, in this methodology, a historical flood data is needed. These performance measures are then converted to likelihood weights assigned to each model. Beven (2009) also mentioned that a threshold should be set, that will distinguish acceptable (i.e. models that received performance values above the threshold given) from rejected models (which will be assigned with likelihood values of 0), before the modelling is performed.

After the likelihood measure and threshold have been decided, the uncertain parameters have to be considered, together with the prior distribution where they will be sampled. This is performed by following the Monte Carlo procedure where samples are derived randomly from a given distribution. Also important to determine at this stage is the number of random samples to be derived, which will be the basis of the number of simulations to be performed. This has also an implication to the last GLUE requirement, which is the implementation or realisation of the methodology. The number of realisations can be affected by the hydraulic model, the resolution used and the size of the study area. 1D models such as HEC-RAS, can be used to perform simulations at a faster time. However, with 2D models, it is still time consuming to conduct hundreds of simulations, especially when using high resolution data, which can take hours or days to perform a single simulation (Néelz & Pender, 2009). The output type to be generated from the analyses is also important to be considered together with the earlier factors mentioned. For analyses that only require model outputs in the form of data plots and graphs, hundreds or thousands can easily be extracted from the data. Nevertheless, when accounting for spatial uncertainties and visualising them through maps, these require additional GIS processing of individual results. Thus, the number of simulations is multiplied with the number of processing steps to be undertaken for each model output.

Disparity distance (D_d) algorithm

With the *Disparity distance* (D_d) method, uncertainty bounds around a specific model output are generated, to further deal with the uncertainties as effect of the topography in the modelling process and in the output. In producing these uncertain zones, the D_d algorithm is implemented. This is based on an empirical equation formulated by Brandt (2016), which was grounded in two previous studies (Brandt, 2009, and the results from *Paper I*). The D_d algorithm assumes that the disparity between the model and the reference data decreases with increasing slope value (and vice versa), and that lower resolution DEMs further contribute to an increased disparity. This relationship can be modelled through Equation 1, where D_d or the disparity becomes a function of the river valley side slope (i.e. the slope perpendicular to the flow, (S)), the DEM resolution (δ) in m, and the percentile (P) or level of confidence used for the assessment of uncertainty.

$$D_d = f(S, \delta, P) \quad (1)$$

This can be expressed as:

$$D_d = cS^z \quad (2)$$

where S (Equation 3) is computed by dividing the difference between the elevation (H) at a given node and the water surface elevation (WSE , i.e. the flood boundary), and by taking the distance between the two points (D) (Equation 4).

$$S = \frac{H - WSE}{D} \quad (3)$$

$$D = \sqrt{\Delta x^2 + \Delta y^2} \quad (4)$$

The coefficient c and the exponent z were derived from the regression analyses of disparity results of the Eskilstuna study area. Using the DEM resolution that was used for modelling and the percentile, these two can be computed as Equations 5 and 6. According to Brandt (2016), both values increase with coarser resolution DEMs.

$$c = 0.000792P^{1.303}\delta^{0.970} \quad (5)$$

$$z = (0.1124 \ln \delta) + (0.0709 \ln P) - 1.0064 \quad (6)$$

2.6 Uncertainty visualisation

Uncertainty visualisation aims at informing users of inaccuracies associated with the information they are using (Pang, Witterbrink, & Lodha, 1997). It can help improve data analysis and decision-making, by being able to communicate the limitations of the presented results (Pang et al., 1997; Mahoney, 1999; Drecki, 2002; Johnson & Sanderson, 2003). The topic on uncertainty visualisation has been important in the fields of Geovisualisation (GeoVis), Scientific Visualisation (SciVis) and Information Visualisation (InfoVis) since the early 1990s. However, their focus in handling uncertainties and their representations vary from each other. InfoVis and SciVis are geared towards the creation of visual representations of uncertainties using different dimensions in their representations (Pang, 2001). In Geovisualisation, maps are the main tools for conveying the uncertain information. Additionally, GeoVis seeks to understand the types, nature, character and sources of uncertainty (Pang, 2008). Both GIScience and Geovisualisation were first to consider a formal approach to handling and visualising uncertainties (MacEachren et al., 2005; Brodlie, Osorio, & Lopes, 2012). The primary reason for this is that both the spatial data and the GIS processes can considerably affect the quality of the resulting information produced based on them (Goodchild, 1992; MacEachren, 1992).

2.6.1 *The role of maps in uncertainty visualisation*

Although computer generated geovisualisation models have been common with the advancements in technology, maps in all forms remain relevant tools in planning. The effectiveness of maps for communicating geographic information relies on the cartographic rules adhered in their design and development (MacEachren, 1995; Kraak & Ormeling, 2003). The cartographic rules and principles followed are based on psychology, communication (graphic) and geography (Dent, 1999). They have significant roles in communicating and explaining spatial phenomena through maps and other means of spatial display of information (Drecki, 2002).















Important parts of graphic communication in maps are their visual elements, which serve as stimuli for the map reader to react when viewing the information (Robinson, Morrison, Muehrcke, Kimerling, & Guptill, 1995). A visual element can be perceived according to its location and how it looks like in relation to the rest of the objects presented. However, individuals may have different ways of processing and reconstructing information provided in a map to derive meanings from them. Thus, designing the map is an important task for the cartographer. The effectiveness of the map as a communication medium will therefore depend on how well the message conveyed by the cartographer agrees with the interpretation of the map reader (Robinson et al., 1995).

2.6.2 Uncertainty representation

Uncertainty can be represented in maps and geovisualisation models by using the different visual variables, namely: colour, texture, value, size. In addition, saturation, fuzziness, arrangement, and transparency are also used (Bertin, 1983; MacEachren, 1992; MacEachren et al., 2012). Certainty is often associated with darker value, finer texture, saturated colour, larger size, regular patterns/arrangements, crisp and opaque objects. Uncertainty on the other hand is often symbolised by lighter values, coarseness, unsaturated colour, smaller size, irregular patterns, fuzziness and transparency. Yet, the logic in the representation can also depend on what is being conveyed in the visualisation. Uncertainty can be expressed using two semantics: *degrees of certainty* and *degrees of uncertainty*. The former indicates the progression in certainty status from low/minimum (i.e. uncertain) to high/maximum certainty. According to Beven et al. (2014), this implies a positive state by giving emphasis on the certainty of the condition. Therefore, the association between low–high certainty with light–dark, coarse–fine, unsaturated–saturated, transparent–opaque, etc. follows the progression of the magnitude/quantity being represented. *Degrees of uncertainty* stresses the gradation of uncertain condition, where the maximum uncertainty is highlighted. Hence, if the magnitude or quantity will be the basis of representation, the order of the representation will be the same as the first semantics used, but the connotative meanings associated with them will be opposite. An example is how size is used to indicate *degrees of uncertainty* by Sanyal, Zhang, Bhattacharya, Amburn, and Moorhead (2009) and Kunz, Grêt-Regamey, and Hurni (2011). There, size increases with uncertainty. Thus, the lowest uncertainty (i.e. the most certain condition) using this semantics is represented by smallest size, which gets an opposite representation in the other semantics used. However, how value is used in Scholz and Lu (2014) when using *degrees of uncertainty* is consistent with the first semantics. Darkest value is assigned to the most certain condition while the most uncertain has the lightest representation.

Table 4 shows a list of the different visual variables used in earlier literature that were considered to be intuitive in representing uncertainty. The semantics used in these studies are also indicated.









Table 4. Uncertainty representations using the different visual variables in geovisualisation.

VISUAL VARIABLE	SEMANTICS USED			
	DEGREES OF CERTAINTY Low (uncertain) → High (certain)		DEGREES OF UNCERTAINTY Low (certain) → High (uncertain)	
Value		*Leitner & Bутtenfield (1997, 2000); *Edwards & Nelson (2001); *Aerts, Clarke, & Keuper (2003); *Bisantz et al. (2009); *Kubiček & Šašinka (2011); *MacEachren et al. (2012)		*Scholz & Lu (2014)
		Cheong et al. (2016)		
Size		*Drecki (2002); *MacEachren et al. (2012); *Lim, Brandt, & Seipel (2016); *Seipel & Lim (2017)		*Sanyal, Zhang, Bhattacharya, Amburn, & Moorhead (2009); Kunz et al. (2011)
Texture		*Leitner & Bутtenfield (1997, 2000)		
Arrangement		Goodchild, Bутtenfield, & Wood (1994); Interrante (2000); *MacEachren et al. (2012)		
Opacity		*Drecki (2002)		
Transparency		*MacEachren et al. (2012)		*Scholz & Lu (2014)
Saturation		Howard & MacEachren (1996); *Bisantz et al. (2009)		*Sanyal et al. (2009)
Fuzziness /Crispness		*Edwards & Nelson (2001); *MacEachren et al. (2012)		*Scholz & Lu (2014)

* intuitiveness based on outcomes of experiments/user studies

The usage of colour for representing uncertainty may depend on its association with the object or condition being represented. For instance, red is often associated with more risks or hazard, in contrast to green or blue, as depicted in the study of Smith-Jackson and Wogalter (2000). Colour is mainly used for selective purposes to easily identify a given class visually (Bertin, 1983). Unlike the other visual variables presented in Table 4, colour indicates no order. Some colours used to represent certain and uncertain statuses are shown in Table 5.

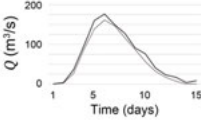
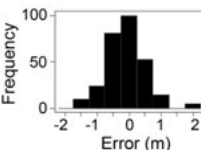
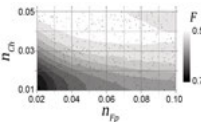
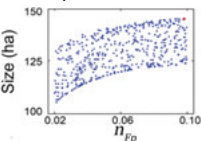
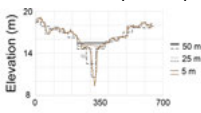
Table 5. Colours used for representing certainty and uncertainty conditions.

COLOUR REPRESENTATION			SOURCE
Single	Uncertain		Aerts et al. (2003); Tak & Toet (2014)
			Tak & Toet (2014)
	Certain		Tak & Toet (2014)
Bicolour	Uncertain-certain		Aerts et al. (2003)
			Tak & Toet (2014)
Tricolour	Uncertain→Certain		Tak & Toet (2014)
			Tak & Toet (2014)
			Howard & MacEachren (1996)

2.6.3 Flood uncertainty representation and visualisation

Uncertainties in flood modelling studies are represented in variety of ways in different studies. Graphs and diagrams are often used to show variation in flood stages, model performances, depths, inundation sizes, etc. (Table 6). They are useful in displaying multiple results from the models simultaneously (even up to millions of them). A drawback, however, is that they lack giving the geographic context of the uncertainty (Hunter, Goodchild, & Robey, 1994; Merz, Thieken, & Gochi, 2007).






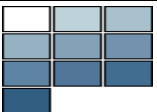






Table 6. Graphical methods for representing flood model uncertainty.

DIAGRAM TYPE	EXAMPLE APPLICATIONS
<p>Line graph</p> 	<ul style="list-style-type: none"> Changes in water stage, discharge, flow duration (Hunter, Horritt, Bates, Wilson, & Werner, 2005; Pappenberger et al., 2006; Hunter et al., 2008; Di Baldassarre, Laio, & Montanari, 2009; Di Baldassarre & Montanari, 2009; Neal et al., 2009, 2012; Bates, Horritt, & Fewtrell, 2010; Domeneghetti, Vorogushyn, Castellarin, Merz, & Brath, 2013), and areal size (Yu & Lane, 2006) Comparison of errors (Di Baldassarre & Montanari, 2009), entropy (Horritt, 2006); model reliability (Horritt, 2006), CDF plots (Romanowicz & Beven, 2003); and accuracy (Yu & Lane, 2006) Variation in predicted forecasts (Pappenberger et al., 2005)
<p>Bar graph</p> 	<ul style="list-style-type: none"> Histogram of errors (Neal et al., 2009) Model effect of DEM to WSE, velocity or timing (Neal et al., 2012)
<p>Contour plot</p> 	<ul style="list-style-type: none"> Model response to using parameter combinations (Horritt & Bates, 2001b; Aronica, Bates, & Horritt, 2002; Horritt, 2006; Fewtrell et al., 2008; Neal et al., 2009)
<p>Scatterplot</p> 	<ul style="list-style-type: none"> Likelihood or performance of model (Hunter, Bates, Horritt, De Roo, & Werner, 2005; Pappenberger, Frodsham, Beven, Romanowicz, & Matgen, 2007; Blazkova & Beven, 2009;) Inundation size in relation to parameter used, model reliability, correlation plots
<p>Cross-section profile plot</p> 	<ul style="list-style-type: none"> Comparison of depth and bed elevation (Cook & Merwade, 2009)

In representing uncertainties in flood maps, colour and value are the commonly used visual variables for indicating uncertainty statuses (Table 7). There are also different semantics used in presenting the information, which also affects the colour or values used. *Degrees of uncertainty* are often represented by grey-scale, which is the safest choice for this type of information to avoid misinterpreting the condition being represented. *Flooding probability*, which is being conveyed using values from 0 (lowest probability to be flooded) to 1 or 100% (highest probability), is either represented by sequential colour scheme (black-


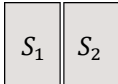
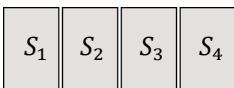
to-white or lightest-to-darkest blue colour), or dual-ended schemes, where the extreme values are assigned with different colours. In Romanowicz and Beven (2003), the authors used *probability of being safe* from flooding, which gives emphasis on areas with safe condition in the maximum value. The safest condition was assigned to the lightest value. When discretising the conditions to different classes, the number of categories (from three to ten classes), types of classification (equal interval or manual classification) and colour used varied in different studies.

Table 7. Uncertainty representations using colour and value with continuous and discrete data, as presented in different uncertainty flood modelling studies.

SEMANTICS USED & DATA SCHEME		CONTINUOUS	DISCRETE
Degrees of uncertainty/ entropy	Sequential	 Horritt (2006) Low (0) High (1)	 Faulkner et al. (2007) Low Med. High
		 Lim et al. (2016) Min. Max.	
Flood probability/ hazard	Sequential	 Horritt (2006); Pappenberger et al. (2007); Di Baldassarre et al. (2010) Low (0) High(1)	 Smemoe, James, Zundel, & Miller (2007)
			 Domeneghetti et al. (2013)
	Dual-ended / Diverging	 Leedal et al. (2010) 0 1	 National Oceanic and Atmospheric Admin. (NOAA) Coastal Services Center (2010)
		 Beven et al. (2014); Beven, Lamb, Leedal, & Hunter (2015) Low (0) High (1)	
		 Seipel and Lim (2017) Dry Unc. Flooded	
Probability: safety from flooding	Sequential	 Romanowicz & Beven (2003) 0 1	
Dual conditions: certain and uncertain	Binary		 Brandt (2016); Brandt & Lim (2016)

When presenting uncertainty information, there are three approaches that are used: overlay, map pair or multiple map display (Table 8). In most cases, uncertainty is depicted by overlaying several flood boundaries from different calibrations results to show changes in the model output. Usually, these boundaries are represented by lines differentiated by different colour or thickness. In other cases, probability of flooding is represented through a surface map. The reference flood boundary or the flooding extents with the highest probability are delineated as lines and overlain on these maps (e.g. Papaioannou, Vasiliades, Loukas, & Aronica, 2017). Map pairs or multiple maps are also used to show different model results, and to compare the variations from the model as effect of the tested variable. Yu and Lane (2006), for instance, used multiple maps to visualise evolution of flooding with time as influenced by the input data used in the modelling.

Table 8. Presentation approaches for visualising flood uncertainties.

PRESENTATION APPROACH	USAGE
Overlay 	<ul style="list-style-type: none"> – Difference in extents produced by the different inputs/parameters (e.g. Mason, Cobby, Horritt, & Bates, 2003); – Model results vs. reference or validation data – Deterministic (i.e. the most optimum) vs. probabilistic result (Papaioannou et al., 2017)
Map pair 	<ul style="list-style-type: none"> – Water level/depth variation in different quantiles (Pappenberger et al., 2005), or in use with different models (Bates et al., 2010)
Multiple map display 	Comparisons of: <ul style="list-style-type: none"> – Predicted water levels at different percentiles (Pappenberger, Beven, Hunter, et al., 2005); or as effect of model used (Hunter et al., 2008) – Model result variations (Horritt, 2006) – Time series evolution of inundation based on different DEM resolution (Yu & Lane, 2006) – DEM/topographic data effect in inundation (Yu & Lane, 2006; Cook & Merwade, 2009;) – Structures or geometric configuration effects (Fewtrell, Neal, Bates, & Harrison, 2011)

Chapter 3.

Methods

Methods applied in the different studies presented in the papers included: pre-processing the spatial data inputs within GIS, hydraulic modelling, uncertainty assessment, designing and creating the visualisation models, and user evaluations. These are summarised in Table 9.

Table 9. Methods employed in the different papers.

METHODS	PAPER							
	I	II	III	IV	V	VI	VII	VIII
GIS modelling (data pre-processing and post-processing)	•	•	•	•	•	•	•	•
Hydraulic modelling			•			•		
Disparity-distance algorithm implementation				•				
Sensitivity analyses/GLUE			•			•		
Design and/or creation of flood uncertainty geovisualisation models/maps		•	•		•		•	•
User studies (quantitative and qualitative)			•		•			•
Statistical analyses	•		•	•	•	•		•

3.1 Study area

The whole Testebo River (*Testeboån*) stretches from Åmot, upstream from Ockelbo to its drainage in Gävle, Sweden. The river flows in a flat and blocky moraine landscape. Due to its rich flora and fauna, Testeboån is classed under the Natura 2000 sites (Länstyrelsen Gävleborg, 2016).

Testeboån in the municipality of Gävle extends from the E4 highway in the north, downstream to its outlet at the delta. The studied area focused within the parts of the river in Varva, Forsby and Strömsbro (Figure 1) in Gävle. The entire site measures about 4 km². This size of the study area is computationally manageable for the 2D hydraulic simulation and ensemble modelling to be performed using high to low resolution DEMs.

From E4 going downstream, the river consists of single stream. The upstream part is relatively steep, surrounded by mixed forests, and some cleared areas. As it goes south towards the study site, the surrounding area around the river becomes flat. In the northern and eastern parts (Varva), arable lands constitute the floodplain with some mixed forests. These topographic characteristics of the floodplain (constituting steep and flat areas) are suitable conditions

for testing the hydraulic model's capability to model the flow. This also allows to examine how variable the model results will be in these topographies, at the specific model conditions to be implemented. As mentioned in earlier studies, flat areas can produce more uncertainties in the model results (Fewtrell et al., 2008). However, how big these uncertainties produced can also vary among different study areas and models due to the differing characteristics and complexities in the flow pattern in the river. Furthermore, since one of the aims of the study is to visualise uncertainties, these locations where they can be high, will be good examples to be used in the uncertainty visualisation parts of the research, where maps and visualisation models are to be created from the modelling results.

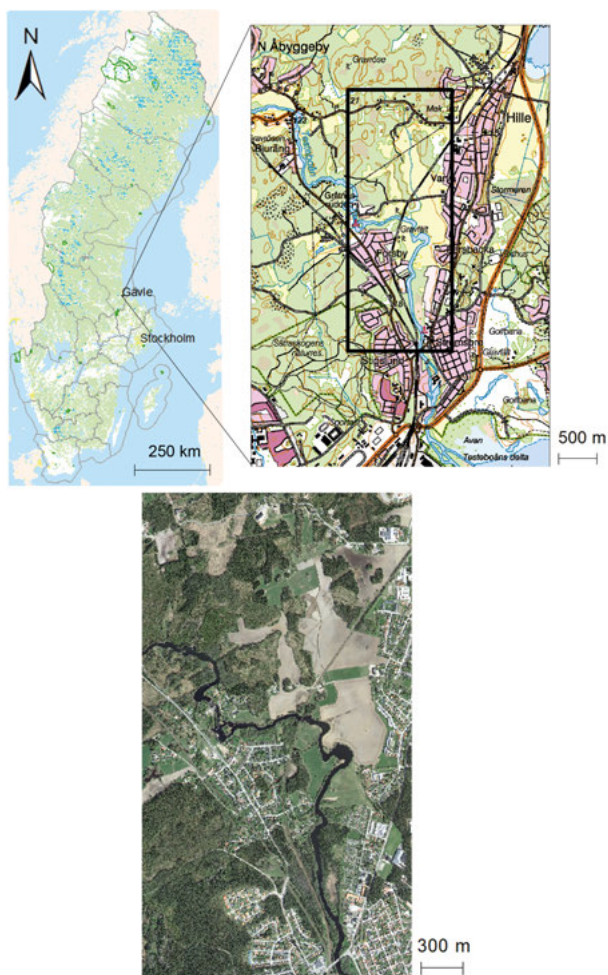


Figure 1. Location of study area just north of the city Gavle. Flow direction is going south-southeast. ©Lantmäteriet

There are also arable lands in the western part of the study area, and at the south of Varva (i.e. Forsby) But most of the residential areas are concentrated here. Some of these residences in Forsby and Strömsbro were just outside the border of the 100-year flood that was initially modelled for Testeboån using the 1D hydraulic model HEC-RAS (Lim, 2009). But whether these will be predicted to be flooded or non-flooded using 2D model and different conditions is also uncertain. Thus, from planning perspective, these areas, particularly residential areas at the border can be at risk of flooding.

Testeboån has a mean discharge of 12.1 m³/s. There were four recorded major spring floods in the river: 1916 (177 m³/s); 1937 (127 m³/s, 1966 (180 m³/s) and 1977 (160 m³/s) (Olofsson & Berggren, 1966).

One of the earlier published studies of the river was made by Olofsson and Berggren (1966). They analysed its observed maximum discharges and water depths during extreme events. In 2002, the report *Översiktlig översvämningskartering längs Testeboån (sträckan från Åmot till utloppet i Bottenhavet)* (SMHI, 2002) was published. It contains the mapping information conducted and the corresponding maps derived for the 100-year and highest probable flood for the Testebo River using the 1D hydraulic software MIKE11. This was based on the 50 m resolution data from the Swedish Mapping, cadastral and land registration authority (*Lantmäteriet*). The Swedish Meteorological and Hydrological Institute (*Sveriges meteorologiska och hydrologiska institut*, SMHI) performed the mapping, as commissioned by the Swedish Civil Contingency Agency (*Rädningsverket* by that time). In 2015, an updated version of the maps were produced by WSP for the Swedish Civil Contingency Agency (now known as *Myndigheten för samhällskydd och beredskap*, MSB), for the 100-yr., 200-yr. and highest probable floods using MIKE11 software (WSP, 2015). They used the 2 m resolution DEM that is said to improve the results of the modelling. According to MSB, these maps can be used for rescue operations and for risk management and spatial planning.

3.2 Data and GIS processing

The primary data used in the entire research are presented in Table 10. Most of them were used for generating secondary data that were needed for specific studies. Methods of how these secondary data were produced are further described in the succeeding parts of the paper.

Table 10. Summary of primary data used in the entire research.

	PAPER							
PRIMARY DATA	I	II	III	IV	V	VI	VII	VIII
LiDAR point cloud and bathymetric data		•	•			•		
LiDAR TIN (from 1D simulation)	•	•		•				
Lantmäteriet 50 m TIN	•			•				
Validation data	•		•	•		•		
Stream centrelines	•			•		•		
Channel		•						
Cross-sections based on:								
Brandt's LiDAR DEM	•			•				
Lantmäteriet 50 m DEM	•			•				
LiDAR DEM	•		•	•		•		
Flood extents from 1D modelling:								
Brandt's	•			•				
Lantmäteriet	•			•				
LiDAR	•			•				
Monte Carlo simulation results (1D flood modelling):								
S_j map		•						
Flood depth map		•						
Most optimal map result from the ensemble		•						
Other maps:								
Orthophoto		•	•		•		•	•
Topographic map							•	
Results from modelling, analyses and mapping performed in:								
<i>Paper III</i>					•			
<i>Paper IV</i>							•	
<i>Paper VI</i>							•	•
<i>Paper VII</i>								•

3.2.1 Digital Elevation Models (DEM)

The Digital Elevation Models used for the 2D hydraulic modelling were created from a combination of the LIDAR point cloud and bathymetric data. The point cloud data consisted of 4 million filtered ground points, with point spacing ranging from 0.2 to 1.8 m. The said data has an accuracy of 0.10 m horizontally. From these data, all points at the location of bridges were removed. The original bathymetric data composed of ca 30 000 points. To account for missing data in some parts of the river, which were impossible to echo-sound, bottom elevation data were interpolated (Lim, 2009) and added to the original bathymetric data (Figure 2). A Triangular Irregular Network (TIN) model was created by combining the two datasets. The advantage of using TIN is that it can well represent the banks and the floodplain, or the changes in the topography (Casas et al., 2006), which are needed for the model to calculate the flow. It is also practical for interpolating millions of points, which will be more difficult to achieve with interpolation methods such as kriging.

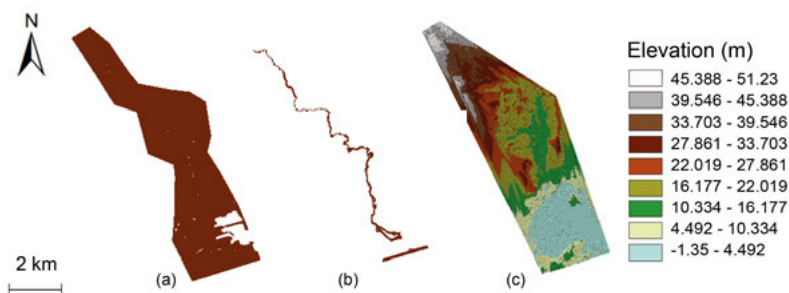


Figure 2. (a) The LIDAR and (b) bathymetric data used for generating the (c) TIN model.

The hydraulic model used in the study requires raster data as input. Thus, after creating the TIN model, it was rasterised to different DEMs with resolutions of 1 to 5 m, 10, 15, 20, 25 and 50 m (Figure 3). Motivation for using different resolution DEMs and including high resolution DEMs of 1 to 5 m is to be able to see their effects in the extents of the flood generated and the quantified performance, particularly in two-dimensional flood models. Earlier studies that analysed sensitivity of 2D hydraulic models to the effects of DEM resolutions in combination with different model/parameters or boundary conditions (e.g. Horritt & Bates, 2001; Horritt & Bates, 2002; Neal. *et al.*, 2009; Savage *et al.*, 2016) utilise medium to lower resolution (10 to 90 m) DEMs. Fine resolution data (1 to 5 m) were seldom tested in ensemble modelling, due to increased simulation time (Savage et al., 2016). Therefore, high resolution DEMs were included in this research. Also, in the studies conducted in the different papers, DEMs poorer than 50 m were excluded due to higher inaccuracies they can produce, particularly at the scale used in the study area (which is more local).

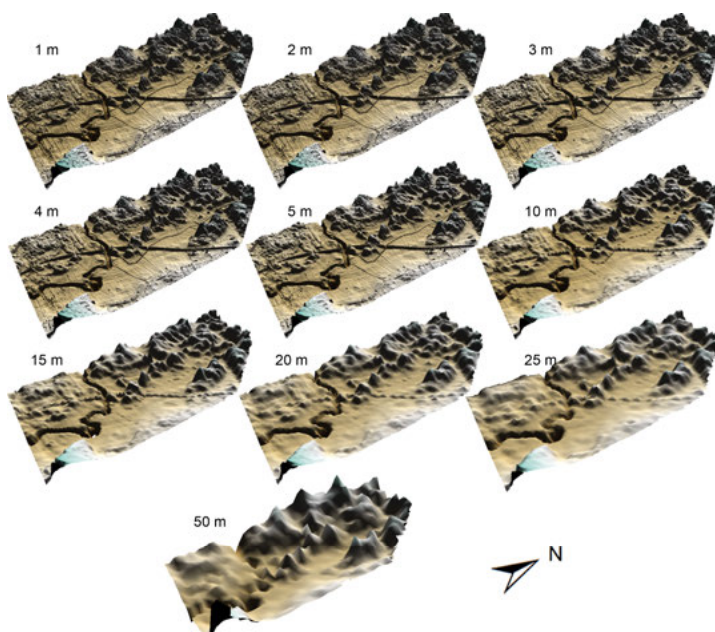


Figure 3. The different resolution DEMs used in the research.

3.2.2 Validation data

The validation data used was provided by the municipality of Gävle. This covers the extent of the flood that happened on 12 May 1977. According to the provider of the information, this was digitised from the aerial photo. The original data was in digital format, but it only shows the boundaries of flooding, without the channel. Since this information is needed in the validation, they were added to the original data (Figure 4).



Figure 4. The reference data used for validating the model prediction results. This corresponds to the extent of the actual flooding in the Testebo river in 1977 at $160 \text{ m}^3/\text{s}$.

3.3 Hydraulic modelling and simulations

The hydraulic numerical model used was CAESAR-LISFLOOD (Coulthard et al., 2013), which is a 2D raster model that is based on the modified LISFLOOD-FP model (Bates et al., 2010). There are three primary equations implemented in the model. The first equation (Equation 7) calculates the flow (Q), by considering the flux (q) and maximum flow depth (W_{flow}) between cells, acceleration due to gravity (g), roughness parameter (i.e. Manning's n), elevation (H), cell width (ϑ), water depth (W), and time (t).

$$Q = \frac{q - gW_{flow}\Delta t \frac{\Delta(W+H)}{\Delta\eta}}{1 + gW_{flow}\Delta t n^2 |q|/W_{flow}^{10/3}} \Delta\vartheta \quad (7)$$

The second equation accounts for the computation of the water depth of given cell (at coordinates x, y), using the computed discharges of the previous cells (Equation 8):

$$\frac{\Delta W^{x,y}}{\Delta t} = \frac{Q_{\vartheta}^{x-1,y} - Q_{\vartheta}^{x,y} + Q_{\eta}^{x,y-1} - Q_{\eta}^{x,y}}{\Delta\vartheta^2} \quad (8)$$

The last equation accounts for the computation of time step, using coefficient α , the grid size, the acceleration to gravity and water depth. This equation is needed for the stability of the model. The coefficient α can have values between 0.2 and 0.7 (Bates et al., 2010), depending on the DEM resolution used. The lowest value should be assigned to higher resolution DEMs, while the largest values for the coarsest resolution.

$$t_{max} = \alpha \frac{\Delta\vartheta}{\sqrt{gW}} \quad (9)$$

In the simulations performed, a steady-state flow was implemented. This is due mainly to the length of the river and the output that was to be derived for the simulation, i.e. the flood extents (cf. Di Baldassarre et al., 2010). The discharge of 160 m³/s was used for simulating the flow. This is equivalent to the 100-year flood of the river, and the flow that corresponds to the reference data. The Courant values used with the different DEMs were: 0.02 (1 to 5 m); 0.4 (10 m); 0.5 (15, 20 and 25 m); and 0.7 (50 m). These were based on the suggestions made in Bates et al. (2010).

3.4 Ensemble modelling and GLUE application

Ensemble modelling, following the GLUE methodology, was adopted to assess model input/parameter sensitivity and prediction uncertainty. The flowchart in Figure 5 shows the implementation of the modelling and uncertainty assessment.

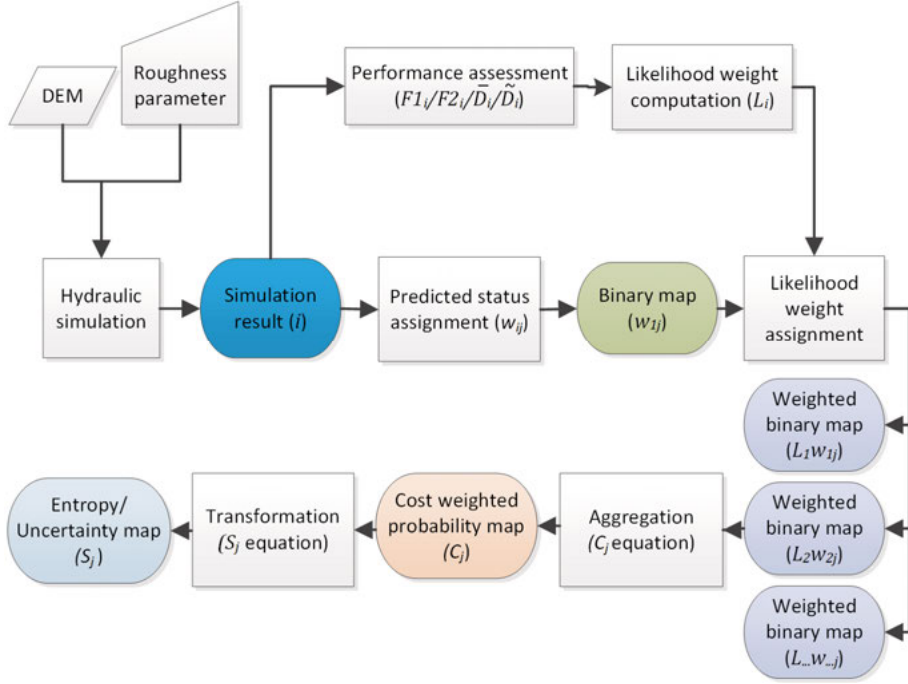


Figure 5. Ensemble modelling and GLUE methodology implementation.

3.4.1 Accounting for uncertain input and parameters

To assess the sensitivity of the model to the topographic data input and the hydraulic model parameter (Manning's roughness, or n), there were 50 (*Paper III*) and 100 simulations (*Paper VI*) conducted to produce different model prediction outputs. DEM resolutions used in *Paper III* were 5, 10, 15, 20, and 25 m, while for *Paper VI*, higher and low resolution DEMs (1 to 5 m and 50 m) were included.

A uniform Manning's roughness was used for both the channel and floodplain, considering that the flow is more overland. Manning's n that were assessed ranged from 0.01 to 0.1, with increments of 0.01. These values were based on Horritt and Bates (2002). According to the authors, this range of roughness values allows to see where the concentration of high or low performance occur in the parameter space.

The main motivation for conducting the ensemble modelling in this way was the main outputs produced and analysed were the extents of flooding. Increasing the number of simulations can be a limitation for comparing the extents of the outputs produced. Moreover, small increments in the tested DEM or Manning's n , may not capture big changes in the flood extents. The DEM and Manning's n used may be sufficient to see and compare geographic trends in the results.

3.4.2 Generation of binary maps

The output from the simulation result (i) using a given DEM and Manning's n combination is a flood (water) depth map (Figure 6, left). Each water depth map was converted to binary maps, where each cell j was assigned a value indicating whether its predicted status (w) is either flooded or dry. This was done through reclassification, where all depths > 0 were assigned to $w_{ij}=1$ or inundated, while depths $=0$ or areas having no data were $w_{ij}=0$ (non-flooded) (Figure 6, right).

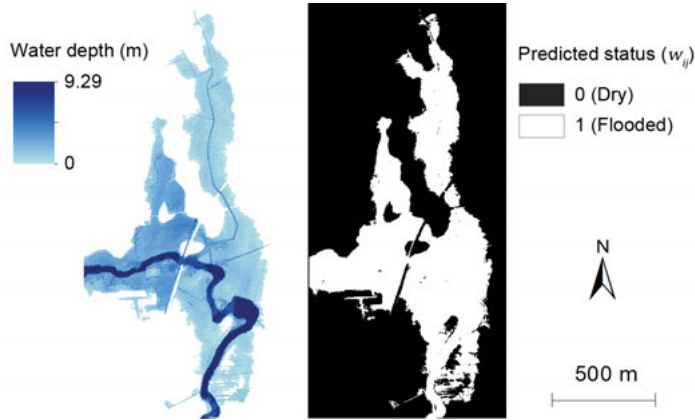


Figure 6. Conversion of one of the original simulation results (i.e. water depth map, left) to a binary map showing the flooding status of a given cell (w_{ij} , right).

3.4.3 Performance assessment and likelihood computation

To find out how well the model predicted the flood at the given discharge and using the different input and parameter pairs, four different performance measures were used to quantify the results.

Feature agreement statistics ($F1$ and $F2$)

Feature agreement statistics are commonly used for validating extents produced by the flood model. F uses the set theory to account for the intersection and union between the observed (Obs) or the actual data, and the predicted flooding (Mod) (Bates & de Roo, 2000) (Equation 10).

$$F = \frac{Obs \cap Mod}{Obs \cup Mod} \quad (10)$$

There are two versions of F statistics applied in extent validation studies. $F1$ is based on assessing how big the size of overlap (A) between the model and the observed flood extent, in relation to the total size of overlap (A), overestimation (B) and underestimation (C) produced in simulation i , using a particular input/parameter (Mason, Bates, & Dall' Amico, 2009) (Equation 11).

$$F1_i = \frac{A_i}{A_i + B_i + C_i} \quad (11)$$

The other is $F2$, which is presented in Hunter et al., (2005) (Equation 12). In the equation, the size of over-estimation is subtracted to the size of overlap in the numerator. This penalises the over-estimation produced by the model to reduce the bias in $F1$.

$$F2_i = \frac{A_i - B_i}{A_i + B_i + C_i} \quad (12)$$

When implementing this with GIS, each flood extent produced by the model, was overlaid on the reference flood extent, to get A, B and C (Figure 7), prior to applying Equations 11 and 12. F values range from 0 to 1, where 1 is the maximum performance.

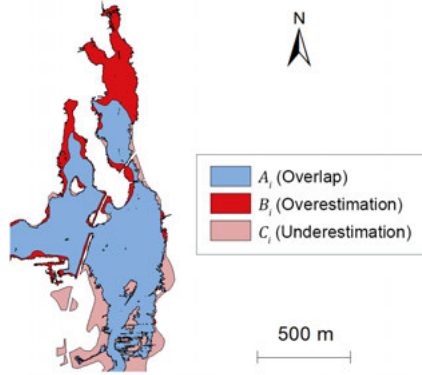


Figure 7. Example simulation result showing how the overlap, areas under- and over-estimated were accounted for.

After computing the feature agreement statistics of all simulation results, the minimum (F_{min}) and maximum (F_{max}) values were derived and used for calculating the likelihood weight (L_i) of each model result (Equation 12). This equation is applicable for both $F1$ and $F2$.

$$L_{i,F} = \frac{F_i - F_{Min}}{F_{Max} - F_{Min}} \quad (13)$$

Mean and median disparities

Two additional performance methods were presented in *Papers III* and *VI* for assessing flood extents. Mean (\bar{D}_i) and median (\tilde{D}_i) disparities employ sampling methods as a means of quantifying the disparity. In both methods, the difference (error) between the modelled and reference flood extents is considered. The usage of \tilde{D} was presented as an alternative to \bar{D} , as there can be cases when the data sampled can be highly skewed, and the median will be a better performance determinant.

In both methods, sampling was performed using the cross-section data and the flood extent from a given simulation. Each cross-section was numbered and divided to left and right sides using the stream centreline (looking downstream the channel), which were used for coding them with their unique identifiers. The flood map and the reference flood map were then used with the cross-section data to extract points where they intersected (Figure 8), that were used as samples for the computation. Each point was assigned with the unique identifier of the cross-section, in addition to getting their x, y coordinates and elevation (H) values. Afterwards, the distance (D) between the two points (simulation and reference maps), at a given cross-section location, was computed (Equation 4). To get the overall performance of the given simulation, either the mean (Equation 14, where N is the total number of point samples) or the median (Equation 15 if the number of point samples is odd, and Equation 16 if N is even) of the disparities was taken.

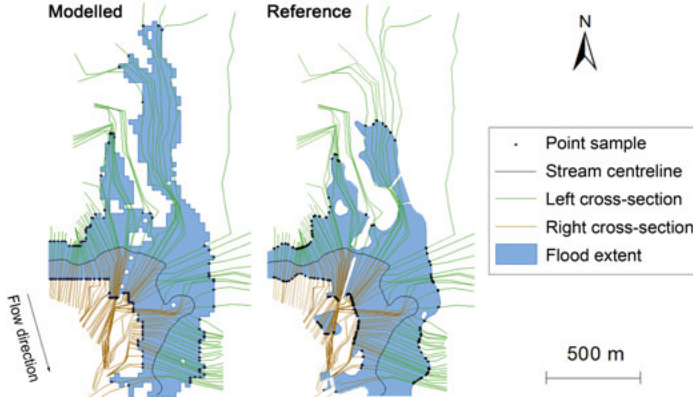


Figure 8. The sampling performed in one of the simulation results (left), and from the reference data (right).

$$\bar{D}_i = \frac{\sum D}{N} \quad (14)$$

$$\tilde{D}_i = D_{\frac{N-1}{2}} \quad (15)$$

$$\tilde{D}_i = \frac{1}{2} (D_{\frac{N-1}{2}} + D_{\frac{N-1}{2}+1}) \quad (16)$$

The lower the disparity means the better the model performance. This has an inverse performance relationship compared with F . Thus, when getting the L_i for the mean disparity, Equation 17 has to be applied. This equation is also valid for getting the likelihood weight for \tilde{D} .

$$L_{i,\tilde{D}_i} = \frac{\bar{D}_{Max} - \bar{D}_i}{\bar{D}_{Max} - \bar{D}_{Min}} \quad (17)$$

3.4.4 Aggregation and uncertainty map generation

The computed L_i from the performance measure was assigned as weights to its corresponding binary map ($L_i w_{ij}$). The weighted maps were then aggregated using Equation 18:

$$C_j = \frac{\sum L_i w_{ij}}{\sum L_i} \quad (18)$$

This results to a map indicating a cost-weighted probability status, considering the ensemble of results and the likelihood weights. The value, which is encoded to each cell is from 0 to 1. The most certain conditions are represented by the minimum ($C_j=0$, dry) and maximum ($C_j=1$, flooded) values, while the most uncertain condition is the middle value ($C_j=0.5$).

However, according to Horritt (2006), the representation by the C_j values may not clearly distinguish certain and uncertain conditions, because of the duality of the statuses being represented, while uncertainty is in the middle of the two. Thus, Horritt (2006) proposed an entropy-like measure that will separate certain from uncertain statuses by transforming the C_j result using Equation 19. The resulting flood map still ranges from 0 to 1, but this time, those that are certain to be dry or flooded will have a value of 0, while those with maximum uncertainty will be 1. The relationship between the C_j and S_j values is further illustrated in Figure 9.

$$S_j = -\{(C_j \log_2 C_j) + [(1 - C_j) \log_2 (1 - C_j)]\} \quad (19)$$

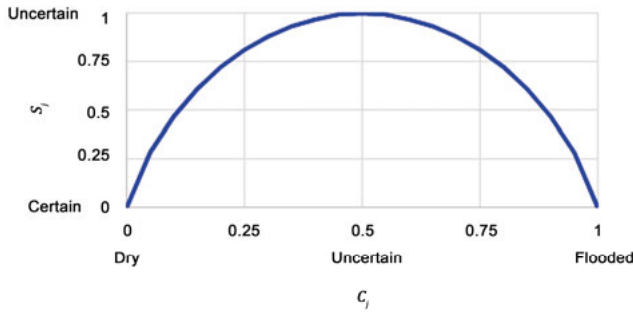


Figure 9. The relationship between the C_j and S_j values.

3.5 Disparity distance algorithm

In *Paper IV*, the disparity distance algorithm was used for estimating uncertainty. In implementing the algorithm, three 1D (HEC-RAS) model results were used: Brandt's simulation of the Testebo River using the LIDAR data, and Lim's simulation results using LiDAR and the *Lantmäteriet* 50 m DEM.

3.5.1 Data preparation

For each simulation result, there were four datasets needed to apply the algorithm: 1) the cross-section (CS) data corresponding to the DEM used; 2) stream centreline; 3) flood extent of the predicted flooding; and 4) the TIN model of the elevation (Figure 10). The cross-sections were initially numbered and assigned with unique identifiers, in a similar way performed in the computation of mean and median disparities (cf. 3.4.3). This unique identifier contained the CS number and an indication of whether it is positioned to the left (*l*) or right (*r*) part of the stream centreline.

Two sets of sample points were then derived that were used later for the computation: 1) points intersecting the CS and the flood boundary polygon; and, 2) CS nodes that were sampled along the cross-sections, using the TIN model. Both datasets were assigned the unique identifier from the CS, in addition to getting their *x*, *y* coordinates, and elevation values (*H*). The CS nodes were also identified whether they were positioned on the inner (*I* or flooded) or outer (*O* or dry) side of the modelled flood extent.

3.5.2 Algorithm implementation and delineation of uncertainty zones

The delineated uncertain boundaries are derived by implementing the algorithm. For each cross-section (*m*), four uncertain elevation values have to be derived: left inner (*lIH*) and outer (*lOH*), as well as right inner (*rIH*) and outer (*rIH*).

The algorithm was initiated at the first left cross-section's outer side (i.e. the non-flooded side). Sampled nodes (*k*) were numbered starting from the outermost node ($k_{lO}=1$) going towards the modelled flood boundary (*K*). This was also the same direction that the algorithm followed in the node-to-node iteration (Figure 11). Starting from $k_{lO}=1$, distance (*D*, Equation 4) and slope (*S*, Equation 3) between this node and the point sampled (*K*) at the flood boundary were computed. Afterwards, coefficient *c* (Equation 5) and exponent *z* (Equation 6) were computed, using $P=95$, $\delta=2.1$ (for Brandt and Lim using the LiDAR-based DEM data), and $\delta=50$ for the 50 m DEM resolution. D_d was then derived using Equation 2.

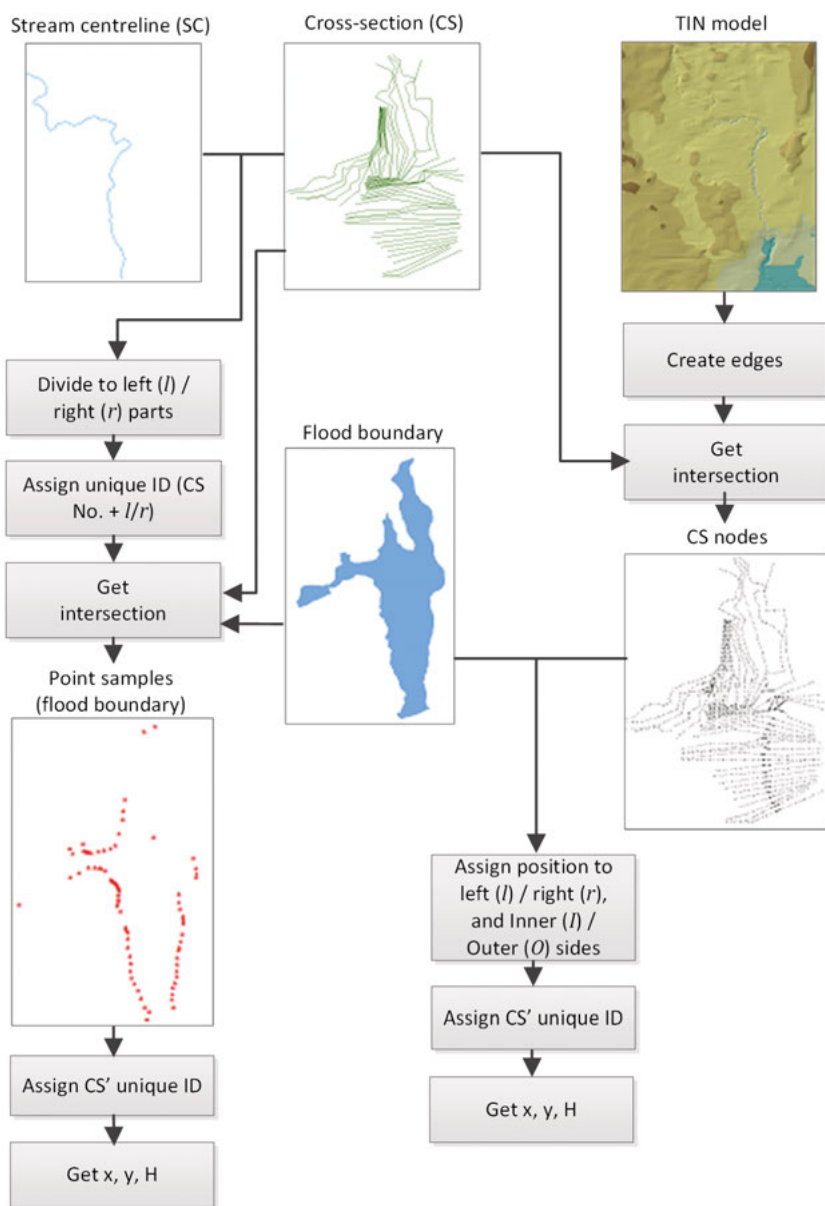


Figure 10. Data processing flow for the D_a algorithm.

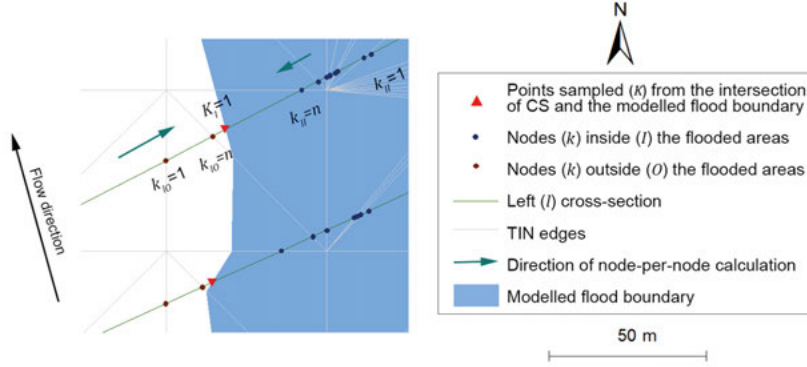


Figure 11. Direction of the node-to node calculation at the left part of the cross-section.

After the calculation of D , S and D_d , the node was assessed with the following conditions:

- If $S > 0$ AND $D_d < D$, node is *Not flooded*;
- If $S < 0$ and $D_d < D$, node is *Flooded*;
- If $S > 0$ AND $D_d > D$, node is *Uncertain*.

If the node gets a certain condition (of either flooded or not flooded), the iteration proceeds to the next node ($k_{II} = k + 1$). Otherwise, if D_d exceeds D , then this node is uncertain. The algorithm stops at this node, and an outer left elevation value is computed for this boundary. Preliminarily, this is assigned to the previous node's elevation value (H_{k-1}). However, according to Brandt (2016), this height has to be initially assessed for any wall effect, to avoid getting very high elevation values. To account for this, the elevation of the sampled point at the flood boundary (H_K) and the current node's D were used with Equation 20.

$$H_K + \exp\left(\frac{\ln D - \ln c}{z}\right) \times D \quad (20)$$

If the result is less than H_{k-1} , then the result from Equation 20 is used as the left outer uncertain elevation for the given cross-section. But, if the result is greater than H_{k-1} , then the outer uncertain elevation used is the preliminarily assigned elevation value from the previous node (H_{k-1}). This is recorded as the left outer uncertain elevation (*LOH*) boundary for the specific cross-section.

After the calculation of the CS' outer part, the algorithm was iterated for the inner left part of the cross-section, but the calculation of the wall effect is altered to Equation 21. Also, the result of the equation is checked if it is greater than H_{k-1} , for it to be used as the left inner uncertain elevation value (*LIH*), otherwise H_{k-1} is used.

$$H_K - \exp\left(\frac{\ln D - \ln c}{z}\right) \times D \quad (21)$$

The algorithm was repeated for the right inner nodes, and lastly to the right outer nodes, following the same procedure when calculating the wall effects and in assigning the uncertain elevation values for the left CS' outer and inner sides. Then the algorithm continued to the next cross-section (Figure 12).

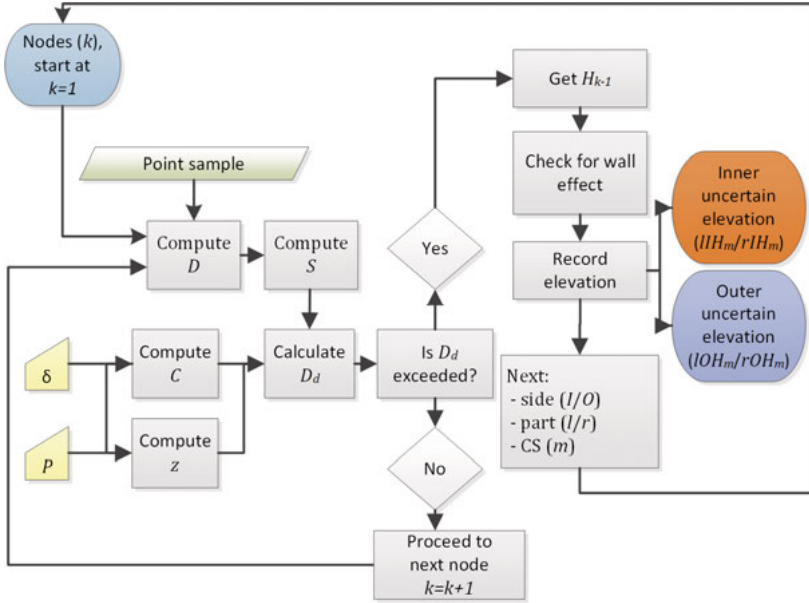


Figure 12. Algorithm's implementation in deriving the uncertain elevation values.

When all uncertain elevation values were derived, two new point datasets were generated: one that was assigned with the inner uncertain (LIH , RIH) elevation values, while the other with all outer elevation values (LOH , ROH) (Figure 13). These were used for creating a TIN model that was later rasterised, and compared with the DEM to identify flooded and uncertain zones. When comparing the inner and outer raster elevation, they were subtracted from the DEM. The results were then reclassified. In the reclassification, all cells that had difference < 0 (i.e. the DEM is lower than the inner/outer elevation value) were flooded and assigned a value of 1. If difference > 0 (i.e. the DEM is higher than the inner/outer elevation value), the cell's condition was assigned to dry and are not represented in the map (i.e. NODATA). The reclassified raster datasets were then converted to polygons. To finally map the uncertain boundaries, the two datasets were overlaid (using union). The parts where the two polygons intersect are areas that are certain to be flooded, at 95% percentile confidence. The remaining areas are uncertain.

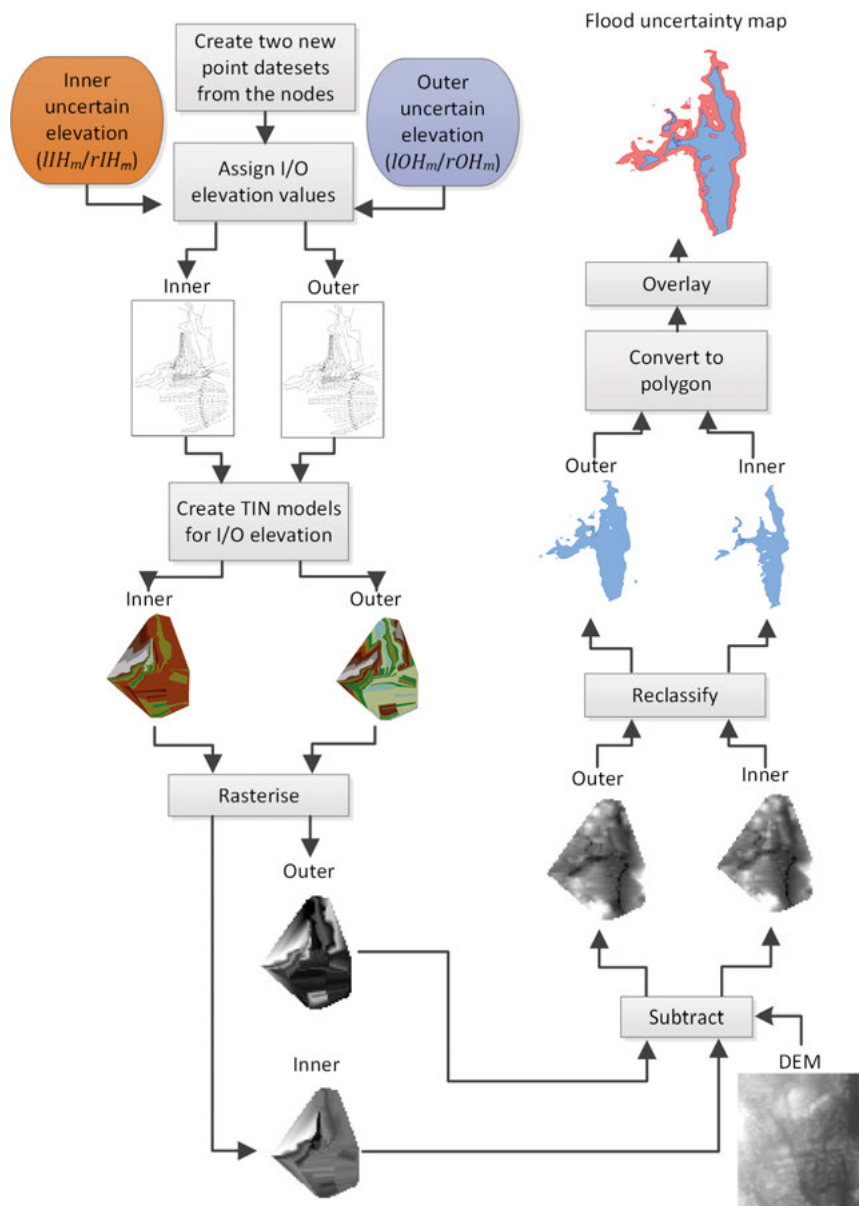


Figure 13. Delineation of uncertain boundaries in GIS for the 50 m data.

3.6 Uncertainty geovisualisation models and maps

In the previous methods, there were different flood uncertainty information and maps produced. In this section, the main focus is the design considerations for representing uncertainty, as well as the creation of different geovisualisation models and maps that can be used for communicating flood uncertainty.

3.6.1 Interactive 3D flood uncertainty geovisualisation model

A 3D geovisualisation model presented in *Paper II* was developed to show how flood uncertainty information can be used for visualising a flood scenario together with other maps. There were two main steps employed in the creation of the model. The first step was the data preparation/pre-processing stage. Here, all the spatial data to be used for the model were extracted for the study area, filtered/transformed and converted to a format readable by the visualisation software. In the second step, the model was developed in Python, by first creating the graphic visualisation using the Visualisation Toolkit (VTK), which is an open source package for computer graphics and visualisation (Schroeder, Martin, & Lorensen, 2006). The visualisation pipeline followed was reading the source/map layer data, filtering/transformation of the data, mapping and display. Afterwards, the Graphical User Interface (GUI) was created using TkInter (Figure 14).

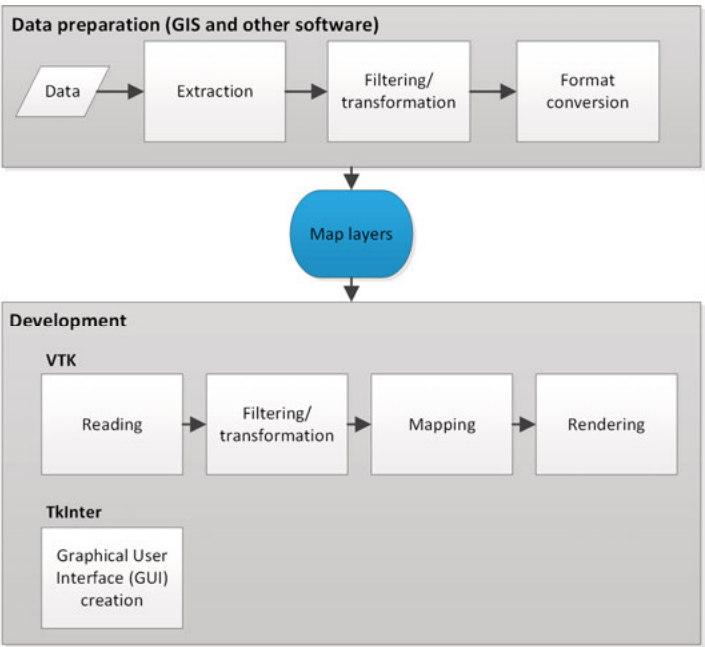


Figure 14. Steps for generating the different maps layers used in the geovisualisation model and the visualisation pipeline followed.

Data pre-processing in GIS and other software

There were different maps used in the geovisualisation model. These are the uncertainty information and the different map layers that give context to the information. The maps used were both in vector and raster formats. The processing for the different vector maps was divided according to the feature types represented (i.e. point or polygon), as similar processing steps were applied to data with the same features.

Point features

There were three point feature maps that were used: uncertainty, slope and flood depth. The uncertainty information was derived from the available Monte Carlo simulation results using the one-dimensional model HEC-RAS. This takes into account the effects of varying roughness parameters for the channel and the floodplain. The uncertainty was represented by the entropy-like measure, S_j , indicating the degree of uncertainty of a cell. Cells with highest uncertainty have $S_j=1$, while those that have low uncertainty (i.e. certain), have $S_j=0$. To further simplify the representation, all conditions that were certain to be flooded or dry (i.e. $S_j=0$) were eliminated in the data, as shown in Figure 15a.

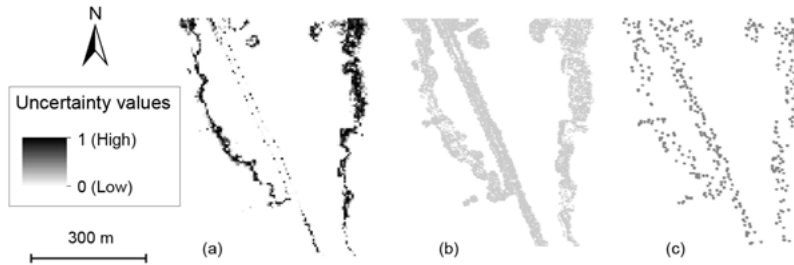


Figure 15. (a) S_j result in raster grid format (5 m resolution), after eliminating all certain to be flooded and dry areas. (b) the original LiDAR point cloud data in the same location where the S_j values were present. (c) Filtered point cloud data that was used for extracting the uncertainty values.

As the original uncertainty data was in raster format, this would result in a gridded appearance when transformed into points. To make them appear more random, the points from the LiDAR data (Figure 15b) were used, to geographically represent the uncertain conditions. To further reduce cluttering in the data, which can make it difficult to read and interpret, the points were further filtered, by using every 50th point in the data (Figure 15c). This reduces the number of points to 400, making them less cluttered. These filtered points were then used to extract the values from the S_j map in Figure 15a.

In addition to the uncertainty map, a slope map and a flood depth map were also created. For the slope, the same point data as in Figure 15c was used to extract the values of the slope map, which was created from the DEM. The data used for the water depth came from the water surface elevation map from

the Monte Carlo simulation with the highest computed model performance (using F). Unlike the uncertainty and slope data, the original gridded data was used for creating equally spaced points to where the depths were assigned. The point features were then converted to text files, with their corresponding x , y coordinates, and z -values, which served as input to VTK.

Polygon features

Polygon feature maps comprised the channel, flood map, and the area predicted to be uncertain (Figure 16). The channel map came from digitising the banks of the river. The flood map of the predicted 100-yr flood event came from the highest performing model from the ensemble. The uncertainty data was derived from the S_j raster map in Figure 15a. This gives an area delineation of uncertainty, to supplement the information provided by the point uncertainty map. The border can show up to which extent the prediction is uncertain. Since the original map data were all shapefiles, they had to be converted to VTK readable format using VisIt (Lawrence Livermore National Laboratory, <https://wci.llnl.gov/simulation/computer-codes/visit>).



Figure 16. (a) Channel, (b) flooded areas and (b) uncertainty band.

Background maps

The background maps consisted of the DEM, slope map and the orthophoto. The orthophoto gives a realistic overview of the area, while the DEMs and slope maps can be used with the uncertainty and flooding information to visualise possible flow patterns in relation to the topography. The DEM used came from the TIN model that was used for the 1D hydraulic simulation. This data was converted to raster format with 1 m resolution. It was also used for deriving the slope map. Both the DEM and slope datasets were converted to USGS DEM format using Global Mapper (Blue Marble Geographic, <http://www.blumarblegeo.com/products/global-mapper.php>), which is readable by VTK (Figure 17). The transformation into this format also allowed these two maps to be extruded at a given value once in the Visualisation ToolKit. However, a disadvantage was the loss of details during the conversion. Thus, another DEM with more detailed features was produced from the original raster data, by using ParaView (<https://www.paraview.org/>). Nevertheless, this data cannot be extruded nor assigned with graded colours.

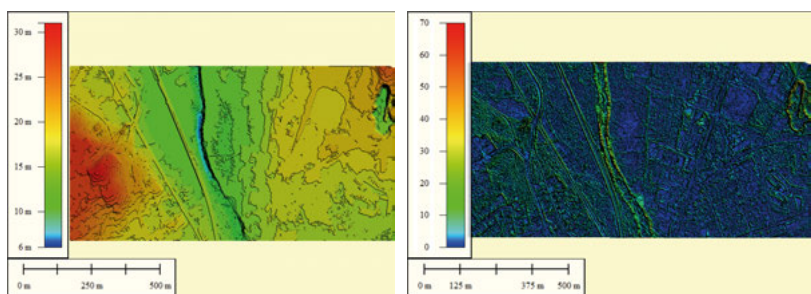


Figure 17. The (a) DEM and (b) slope maps converted to USGS DEM format, readable by VTK.

Geovisualisation development

When importing the different maps in VTK, an important preliminary step undertaken was to consider how the layers were to be displayed. This is relevant if maps are to be overlaid during visual analyses, thus, their hierarchy must be considered. Point symbols were positioned on top of the hierarchy (Figure 18), allowing them to be visible, even without changing the opacity of the background map. This was followed by the polygon, and the background maps, which were lowest, allowing them to be displayed underneath the point and polygons features. It must be noted that even within each feature type group, a particular map can be positioned at a higher level.

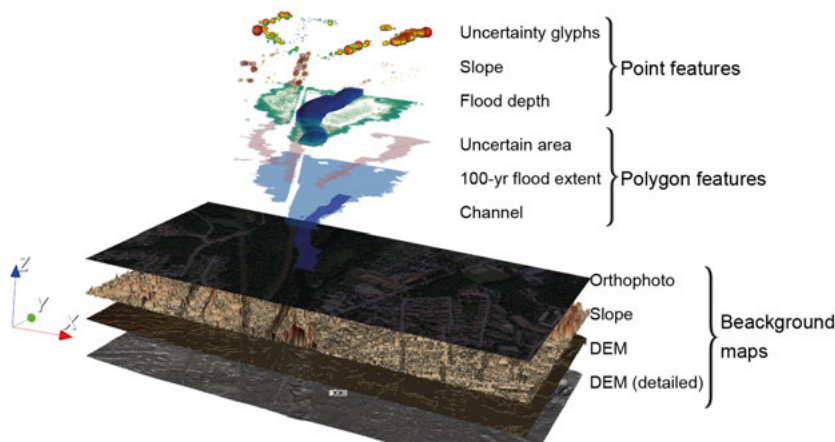


Figure 18. Display hierarchy of the different maps.

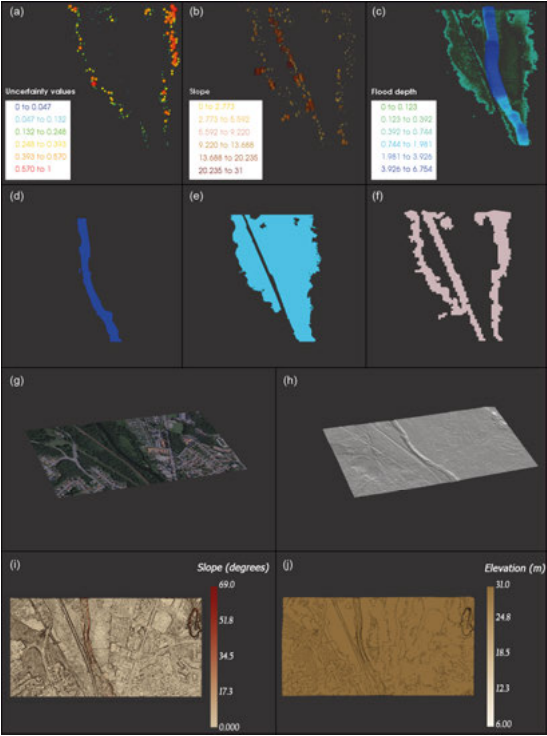
Graphics and visualisation modelling in VTK

The point features were all transformed into glyphs (spheres for the uncertainty, cylinders for the slope and cubes for the flood depth) in VTK (Figure 19a–c). The uncertainty information was assigned with graduated sizes according to the uncertainty value (i.e. the bigger the glyph, the more uncertain it is). They were also classified into six classes using natural breaks, which was

used for assigning the colours. Red was used to represent the highest uncertainty, and blue for the lowest. The cylindrical glyphs for the slopes were also set with varying sizes and colour based on the slope values. The flattest areas were represented by the smallest glyph size in yellow. The steeper the slope gets, the bigger the size and the darker the brown colour it becomes. The layer was also assigned with a default opacity of 0.25, to allow the uncertainty glyphs to be visible when turned on. The cubes representing the flood depths were scaled according to water heights and were coloured from green (lowest depth) to darkest blue (highest depth).

All polygon features (Figure 19d–f) were assigned a default opacity value of 0.5 so that they would be visible when overlaid with other map layers. The colour assignments for the maps were: darker blue (i.e. representing deeper water) for the channel; light blue for the 100-yr flood extent; and light red for the uncertainty boundary, to indicate caution in these areas.

The DEM and slope background maps were shown by default as non-extruded layers. The DEM was assigned with colours from dark to lighter brown colours (i.e. low to high elevation), which is commonly used for representing geographic features according to elevation. For the slope, dark reddish brown was used for steep slopes, and light colours for the flattest areas.



Addition of cartographic elements

Map elements necessary to facilitate reading and interpreting the information were included in the main geovisualisation window (Figure 20). The compass (upper right corner) and the coordinate axes (lower left) were added for orientation purposes. The compass was basically used for controlling the orientation of the scene, while the coordinate axes gives the orientation of the map being displayed. The legend and scalar bars provide information on the meaning of the colours used in the map. The legends were used for representing point feature data, with discrete attributes. They were placed in the left part of the window, without overlapping each other. The *scalar bars* were used mainly for surface maps (i.e. the DEM and slope maps) that have continuous data. They were placed in the right-hand portion of the window. The visibility of the legends and *scalar bars* depended on the visibility of the map layer they represent. Additionally, a camera widget was added to record scenes.

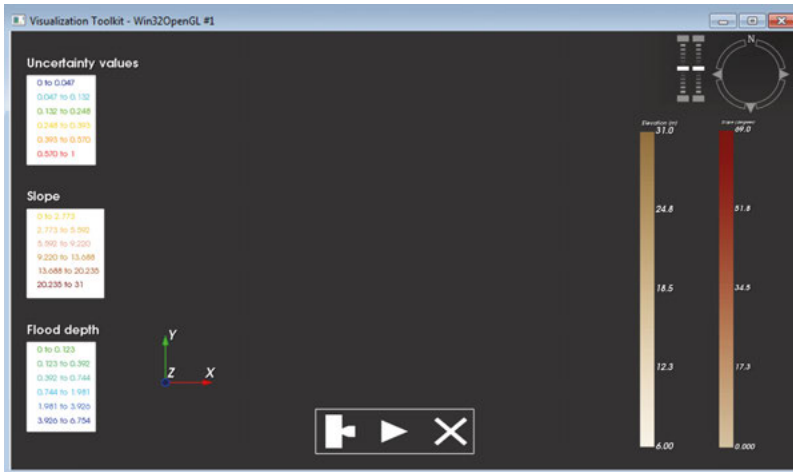


Figure 20. Cartographic elements included in the main window of the geovisualisation.

Graphical User Interface (GUI) development

Using the TkInter package, a graphical user interface was embedded in the visualisation model, to enable users to take more control of the visibility of the map layers (Figure 21). This added control from the user side can facilitate visual analyses of the flooding scenario. There were three main functions controllable in the GUI: visibility, opacity and object size. Visibility lets a user choose the map, which will be visible (ON) or hidden (OFF) when using the geovisualisation model. Thus, all map layers were added with this functionality. The control for opacity in the GUI was added primarily for the slope and flood depth glyph maps and the three polygonal maps. Since these layers can be overlaid on the background maps or to each other, users may opt to change their transparency when visualised with the other layers. Adjustment of glyphs' sizes, and extrusion of elevation heights and slope values at the z-direction can

also be changed by the user to add distinctiveness to the features being represented.



Figure 21. The graphical user interface, with the different functionalities.

3.6.2 2D and 3D flood uncertainty geovisualisation

For *Papers III* and *V*, there were four different flood uncertainty representations created that were later on evaluated in the two different user studies. Each visualisation is described briefly in the following subsections. All visualisations employed map pair presentation approach (MacEachren, 1992).

2D contextual information and flood uncertainty map

In the *2D contextual model and flood uncertainty map* geovisualisation model, both the orthophoto and the flood uncertainty map were displayed in 2D (Figure 22). The flood uncertainty information was derived from the entropy-like measure produced by applying the S_j equation (Equation 19). This gives a sequential continuous predicted uncertain flooding status ranging from 0 (certain) to 1 (uncertain). The certain condition ($S_j=0$) was assigned to black, while the highest uncertainty ($S_j=1$) was white. This is similar to the representation used by Scholz and Lu (2014), in using value to express *degrees of uncertainty* (from i.e. minimum to maximum uncertainty). This type of data representation also gives more contrast, by highlighting medium to highly uncertain regions, which makes them immediately visible.



Figure 22. 2D contextual information and flood uncertainty map.

3D contextual information and 2D flood uncertainty map

The *3D contextual information and 2D flood uncertainty map model* used the same uncertainty map as the first model, but the contextual information was displayed in 3D. The orthophoto, was draped over an extruded digital elevation model (Figure 23). The contextual information was also added with functionalities to allow rotating and zooming in and out of the model. With the 3D model, a clearer topographic and environmental perspective that is necessary for understanding the physical processes that contribute or affect, e.g. the flow of flood water is made possible (Price & Vojinovic, 2008; Mitsova, Harmon, Weaver, Lyons, & Overton, 2012). Moreover, users can have more control of the 3D visualisation, which can help them to further explore, or investigate the area.

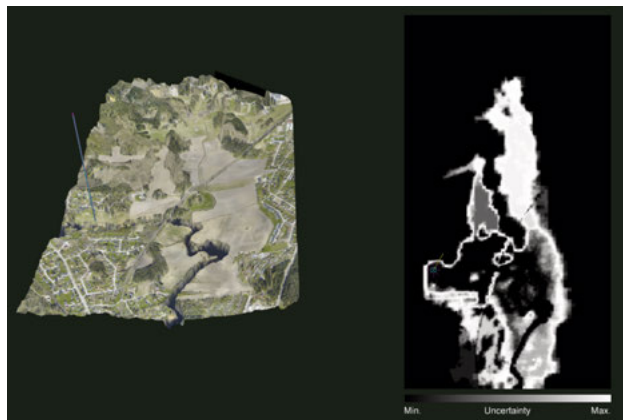


Figure 23. 3D contextual information and flood uncertainty map.

Performance bars

Instead of using a map to represent uncertainty, *performance bars* were used to depict the predicted uncertain status at the location where the cursor was pointed (Figure 24). There were 50 bars used to represent the individual simulation result from the binary map (w_{ij} , Figure 6). Each bar has its corresponding size, which was based on its computed likelihood weight (L_i), i.e. how likely it is to reference data, based on the performance measure. The longer the size of the bar, the higher its likelihood value is. This is a similar uncertainty representation used, e.g. in MacEachren et al. (2012), when using size. The bars were arranged from longest to shortest in the visualisation.

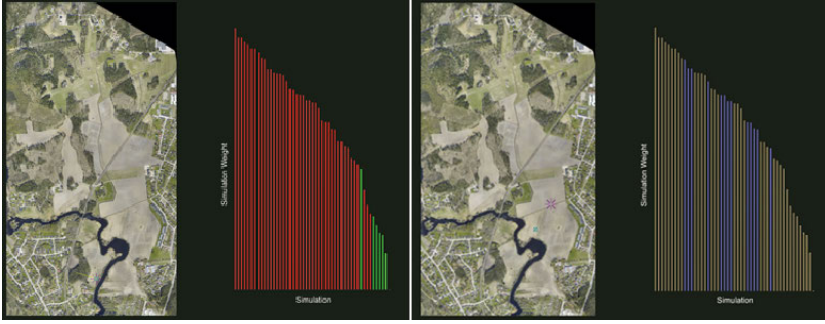


Figure 24. The performance bars used for the geovisualisation. Flood and dry statuses were represented by red/green in *Paper III* (left), and blue/brown in *Paper V* (right).

The predicted status at the given location was indicated by the bar's colour. A binary colour scheme was employed to indicate flooding and dry conditions of the cell at the cursor position. In *Paper III*, red/green were used to indicate flooding/dry statuses due to the association that can be made to unsafe/safe regions (Van der Wel, Hootsmans, & Ormeling, 1994). However, in *Paper V*, the colours adopted were blue/brown, which were based on the association of these colours to water/land, according to an informal survey.

Dual-ended colour map

A new colour map for dual-ended information was proposed in *Paper V*. The main uncertainty information to which this colour scheme was applied was the results based on the C_j equation (Equation 18). This equation produces a cost-weighted probability map, wherein there are two separate conditions being represented by the extreme values (i.e. $C_j=1$ is flooded, while $C_j=0$ is dry). Uncertainty is denoted by the middle critical value ($C_j=0.5$). This type of information can be represented using a dual-ended/diverging colour scheme (Brewer, 1994, 1996). For the minimum and maximum values, binary colours, which can be associated to the represented statuses, are suggested by Brewer (1994) to be applied. Thus, blue/brown were used for representing the oppos-

ing statuses. Highly uncertain status was depicted by grey. The usage of unsaturated colour, such as grey to signify uncertainty is a logical choice according to MacEachren (1992).

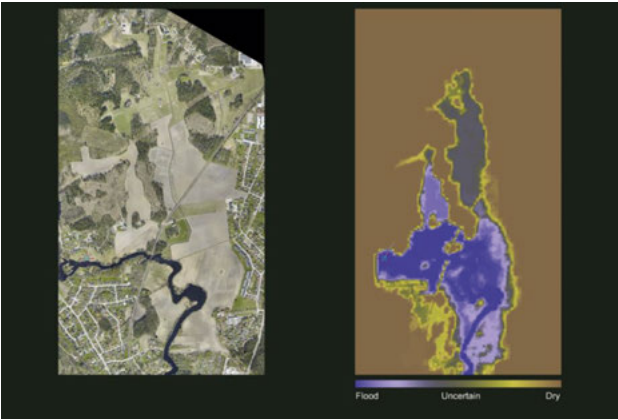







Figure 25. The dual-ended colour scheme applied to the cost probability (C_j) map in *Paper V*.

In designing the colour scheme, several pivotal points were assigned to different base colours that served as control points in the colour interpolation performed (Table 11). The interpolation allows the generation of colour sequences to be applied. Additionally, linearization was performed to attain perceptually equal differences between the colours used. The suggested colour map can also be used to indicate the S_j condition, based on its relationship to C_j values (cf. Figure 9).

Table 11. Pivotal points and the corresponding based colours assigned for the dual-ended colour map presented in *Paper V*.

C_j	S_j	CONDITIONS	BASE COLOUR	RGB		CONTINUOUS PALETTE
1	0	Certain to be flooded	Blue	R: 70 G: 62 B: 174		
0.75	0.81		Blue-grey	R: 166 G: 153 B: 204		
0.5	1	Uncertain	Grey	R: 89 G: 89 B: 89		
0.25	0.81		Brown-grey	R: 189 G: 186 B: 62		
0	0	Certain to be dry	Brown	R: 130 G: 106 B: 74		

3.6.3 Flood certainty maps

The quantified uncertainty or sensitivity of the model can be visualised in different ways, as what is presented in the previous sections. There can be different visual variables, map types and even abstraction that can be employed to facilitate reading the map. However, users may also have different ways of interpreting them, based on their understanding of the information. Thus, different types of uncertainty information were produced and created using different mapping techniques, to find out how users employ them in planning-related decision-making tasks.

In creating these maps, the two main uncertainty data used were the aggregated maps from applying the C_j and S_j equations (Figure 26). The data used here were not the same as the ones used in the previous geovisualisation models under 3.6.2, since model sensitivity accounted for here included higher and lower resolution DEMs (1–5, 10, 15, 20, 25 and 50 m), comprising an ensemble of 100 simulations. Both maps originally contain continuous data, which is usually presented as surface maps. The C_j data can be used to produce a dual-ended, sequential (probability) or even a binary (if reclassified in only two classes) maps. The S_j data, on the other hand, can only produce a sequential map. However, unlike the sequential probability map, the semantics used for expressing certainty is not the same, since the uncertainty of the condition is being emphasised in this map. The colours used were derived from Color-Brewer (Brewer, Hatchard, & Harrower, 2003), and were selected to be suitable for colour-blind persons.

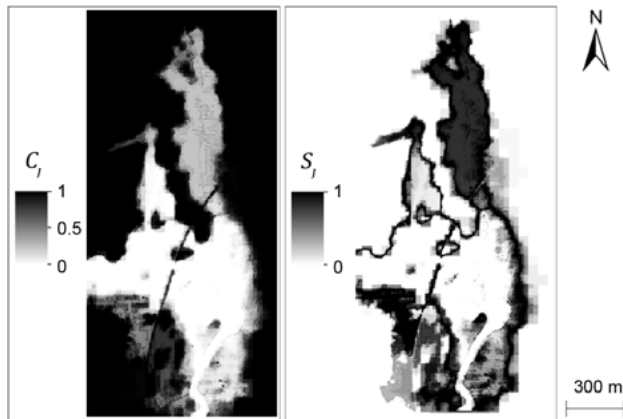


Figure 26. The original aggregated maps based on applying the C_j (left) and S_j (right) equations.

Dual-ended certainty maps

There were three static certainty flood maps created from the original C_j data. The coloured surface map (Figure 27a) gives a continuous representation of the certainty status. The choropleth (Figure 27b) and the graduated symbol maps (Figure 27c) were used for discretised information.

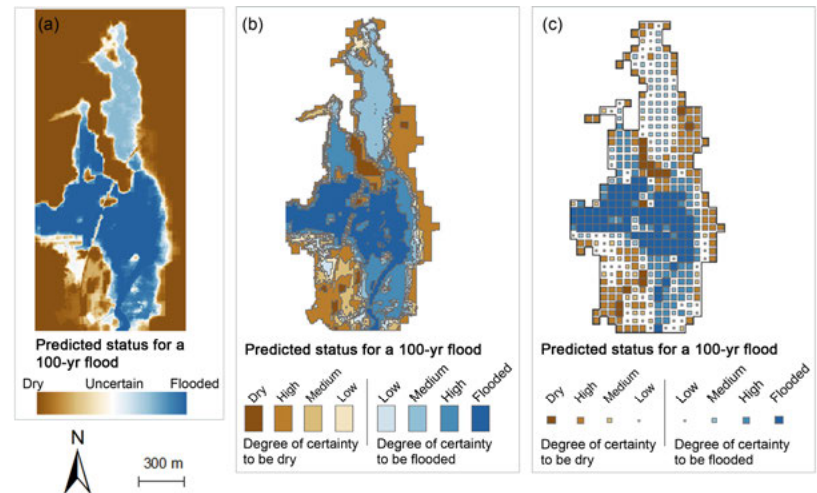







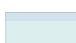


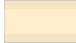









Figure 27. The three dual-ended certainty maps showing (a) continuous predicted flooding status through a surface map, and the discretised maps using (b) choropleth, and (c) graduated symbol mapping techniques.

The surface map was created directly from the original C_j data, without altering the original data values. A dual-ended colour scheme was adopted for representing the two conditions: flooded=blue and dry=brown. The degree of certainty was represented by colour lightness: the darkest colour was the most certain condition, while the lightest was the least. This was based on the same representation for certainty used in Edwards and Nelson (2001), Aerts, Clarke, and Keuper (2003), and MacEachren et al. (2012). In the legend used in the map, the conditions representing the values were used, instead of the original numeric information

In the choropleth dual-ended map, the original conditions were reclassified into eight categories. The first half represented *certainty to be dry* ($C_j=0$ to 0.5), while the other half is *certainty to be flooded* ($C_j=0.5$ to 1). Both certain to be dry ($C_j=0$) and flooded ($C_j=1$) belonged to separate class. The rest of the values were classified using equal intervals (Table 12). Furthermore, the big dry area outside of flood zones, was also eliminated in the map to further simplify the visualisation.

Table 12. Different map types used, and the classification and colour assignment for the different categories in the dual-ended map.

ORIGINAL C_j	CATEGORICAL CONDITIONS		BASE COLOUR	RGB	MAP AND DATA TYPES		
					Surface map (cont.)	Choro- pleth map (disc.)	Grad. sym- bol (disc.)
1	Certainty to be flooded	Flooded	Blue	R: 33 G: 102 B: 172			
0.833–0.999		High		R: 67 G: 147 B: 195			
0.667–0.833		Med.		R: 146 G: 197 B: 222			
0.5–0.667		Low		R: 209 G: 229 B: 240			
0.333–0.5	Certainty to be dry	Low	Brown	R: 246 G: 232 B: 195			
0.167–0.333		Med		R: 223 G: 194 B: 125			
0.001–0.167		High		R: 191 G: 129 B: 45			
0		Dry		R: 140 G: 81 B: 10			

In the graduated symbol map, size was used additionally to provide an immediate cue of the estimated quantities being represented, and to improve the readability of the difference in the data being presented (Bertin, 1983). Largest size was used to indicate certainty, while smallest size signifies the lowest certainty status (MacEachren et al., 2012). In producing this map, the original C_j , which has 1 m resolution, was transformed to 50 m grid. This was then converted to point symbols (squares). The squares were then assigned with sizes, according to the C_j value extracted at the particular location. A certain location was represented by a square having a size of 50 m \times 50 m, covering the entire grid. High to low certainty statuses were assigned with 37.5 m \times 37.5 m, 25 m \times 25 m, 12.5 m \times 12.5 m sizes, respectively. The symbol sizes compensated the scale used for mapping, allowing them to be visible and discernible.

Sequential certainty maps

Two sequential maps were produced from the original data. The first sequential maps show the weighted flooding probability status (Figures 28a and b). They were derived from the C_j data by multiplying the value with 100. Highest probability is indicated by 100, while the lowest is 0. Since the information being represented is the flooding status, a base colour of blue was used. The degree of certainty was again signified by value, i.e. the most certain being the darkest. As the flooding probability gets lower, the colour gets lighter. White areas represent the non-flooded areas in the map. In the discretised flood probability map, the original values were classified into five equal intervals, and were assigned using the colour scheme presented in Table 13. The white (dry areas) were eliminated from the legend, to indicate that they are dry areas.

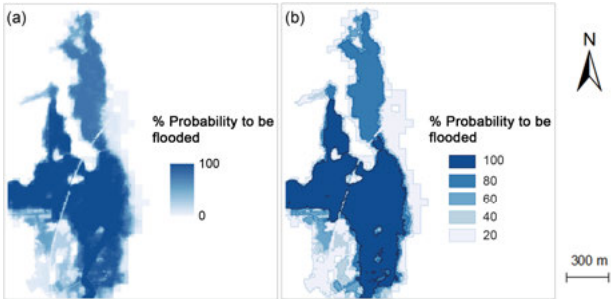


Figure 28. (a) Continuous and (b) discrete flood probability maps.

Table 13. Reclassification of original C_j values and the colour assignment used for the sequential probability surface and choropleth maps.

ORIGINAL C_j	PROBABILITY TO BE FLOODED	RGB	MAP AND DATA TYPE	
			SURFACE MAP (CONTINUOUS)	CHOROPLETH MAP (DISCRETE)
80-100	100	R: 8 G: 81 B: 156		
60 –80	80	R: 49 G: 130 B: 189		
40–60	60	R: 107 G: 174 B: 214		
20–40	40	R: 189 G: 215 B: 231		
1–20	20	R: 239 G: 243 B: 255		

The remaining sequential maps were derived from the S_j data, where highly uncertain status is numerically equivalent to $S_j=1$, while certain to be dry/flooded is $S_j=0$. To make the values' representation consistent with the recommendations of Brewer (1994a) and MacEachren et al. (2012), according to which higher certainty status should be represented by the highest values and vice versa, the original S_j data was inverted by applying Equation 22. This highlights the certainty condition, rather than the uncertainty, which is what the original information represents.

$$S_{j,inv} = (S_{jMax} - S_j) + S_{jMin} \quad (22)$$

The different maps produced from this data are shown in Figure 29. When discretising the information, four classes were used. The certain condition was again separated from the rest of the classes, and the remaining statuses were classified to high, medium, and low certainties to be flooded. For the graduated symbol map, the same technique was applied in producing the graduated symbol maps for the dual-ended certainty information.

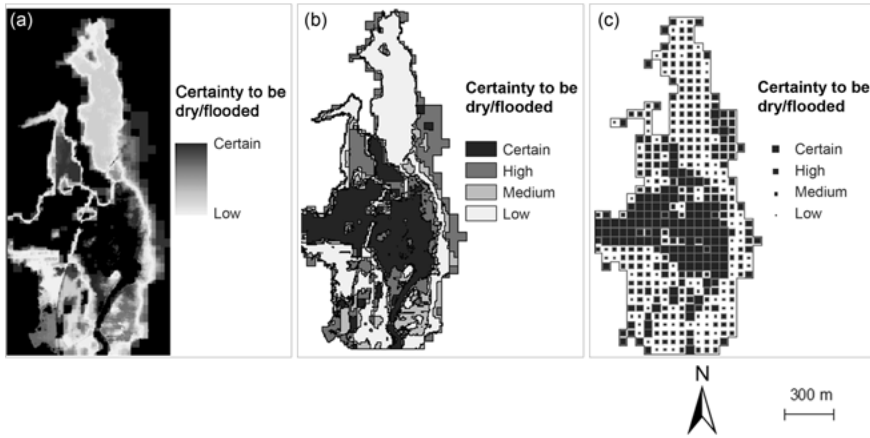


Figure 29. Sequential maps showing degrees of certainty to be dry/flooded using the different mapping techniques: (a) surface map; (b) choropleth map; and (c) graduated symbol map.

Colour and value were the main visual variables used for the surface (Figure 29a) and choropleth (Figure 29b) maps. A grey colour scheme following a sequential lightness step (certain=dark, and low certainty=light, Table 14) was mainly used, to avoid misinterpretation of the status being depicted, which is either dry or flooded. The graduated symbol map only used size as the graphical variable for representing the condition. All symbols were assigned with the same colour (R:37, G:37, B:37).

Table 14. The reclassified values and representation used for the sequential certainty status.

INVERTED S_j	CERTAINTY TO BE DRY/FLOODED	MAP AND DATA TYPE			
		SURFACE MAP (CONT.)	CHOROPLETH MAP (DISC.)		GRAD. SYM- BOL (DISC.)
1	Certain		R: 37 G: 37 B: 37		
0.666–0.999	High		R: 115 G: 115 B: 115		
0.333–0.666	Medium		R: 189 G: 189 B: 189		
0–0.333	Low		R: 240 G: 240 B: 240		

Binary map

The binary map was also derived from the original C_j data by discretising the values into two classes: flooded and uncertain. All cells having C_j values from 0.05 to 1 were classified as certain to be flooded, while those having values from 0.01 to 0.5 were classified as uncertain. This reclassification categorises the predicted condition on the upper half of the C_j values (i.e. $C_j > 0.5$) to be flooded, to avoid selecting these areas. While those on the dry side were all uncertain. The certain to be dry areas ($C_j = 0$) were eliminated in this map, which is automatically the white area in the background having no information.

When representing the statuses, colour was the main visual variable used, primarily for being able to easily identify the conditions displayed. Blue was assigned to flood zones, while red was used to imply uncertainty in a similar way used in Aerts et al. (2003), and Tak and Toet (2014) (Figure 30).

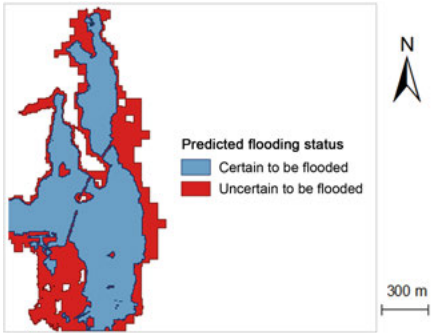


Figure 30. The binary map representing certain (blue) and uncertain (red) conditions.

3.7 User evaluation

Flood geovisualisation models (Sec. 3.6.2) and the static certainty maps (Sec. 3.6.3) were evaluated in different user studies to be able to assess how users make decisions using them, and to find out how effective or intuitive they are in conveying their messages. Both quantitative and qualitative methods were employed in the user assessment. The quantitative method was mainly used for measuring decision-making task performances using the different geovisualisation models and maps, while questionnaires were used for understanding the users, their perspectives of the tasks and using the uncertainty information.

3.7.1 User evaluations 1 and 2

In the first (*Paper III*) and second (*Paper V*) user studies, it was assumed that the different geovisualisation can lead users to choose different locations, depending on how they interpret the displayed uncertainty information. Furthermore, different visualisation models can affect users' times to solve the tasks.

Task design and procedure

The task was designed where participants have to act as planners and decide whether they will permit construction at the site (Figure 31) proposed (*preferred location*) by the homeowner, on the basis of the flood condition in the area. If deemed risky, participants are allowed to move the site to another location (i.e. *decided position*), which they think is safer. To limit the participants from randomly choosing locations anywhere in the study area, they were only allowed to select the location from a *pre-defined line*, extending from the *preferred* site to some extent along the floodplain.

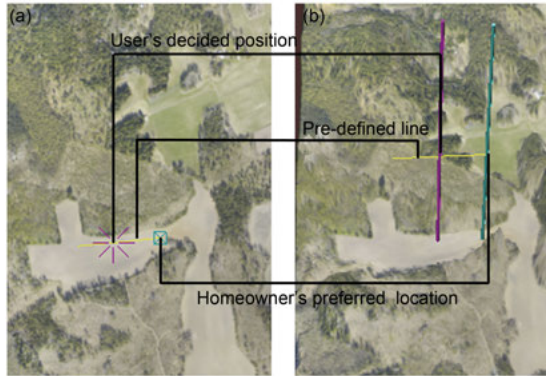


Figure 31. (a) One of the stimuli to be assessed by the participants. The *preferred* homeowner's location is marked in green, while the location that will be allowed for construction (*decided position*, purple), can be chosen anywhere along the yellow line. (b) The equivalent stimulus in 3D used in one of the conditions in *Paper III*.

To make the participants take into account possible consequences of their decisions, different dilemmas were presented to them: (1) homeowners will be more likely to pursue with the project, if the site is located closer to the preferred site; this can be advantageous to the municipality in terms of generating new revenues through property tax; (2) deciding on a location farther from the homeowner’s site preference may lead to backing out from the project, which can be a loss to the municipality; and (3) if building permit is released in a site that can possibly be flooded, the municipality is legally responsible to damages incurred due to inundation, for the next 10 years.

In both user studies, the stimuli used were based on 14 preferred positions (Figure 32). The different conditions used for the assessment were the different uncertainty geovisualisation models presented in Section 3.6.2. For *Paper III*, these were the S_j (uncertainty) maps with 2D (Figure 22) and 3D (Figure 23) contextual information, and the performance bars (Figure 24a). In *Paper V*, the dual-ended C_j map (Figure 25) was additionally used, aside from the 2D S_j map and performance bars (Figure 24b), which was altered in colour. All conditions used were presented in map pairs, where the contextual information (orthophoto) was displayed next to the uncertainty map. The user tests were programmed using VizardTM (WorldViz, <http://www.worldviz.com/>). Each test comprised 42 trials (3 conditions \times 14 stimuli), which were randomly displayed to the participants. They were self-paced, with no imposed time limit to solve the trials. It was emphasised to participants that solving the task is more important than speed.

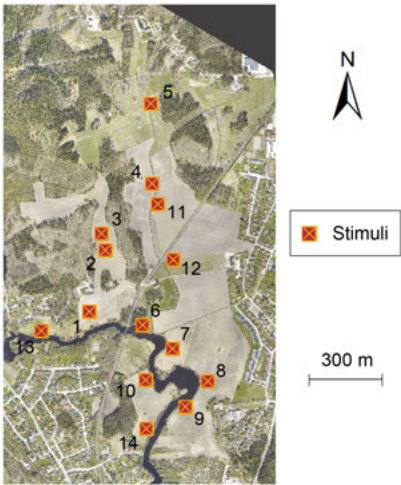


Figure 32. The preferred locations in the 14 different stimuli used in user evaluations 1 and 2.

Questionnaire design

The questionnaires in both user studies comprised of open and close-ended questions. The former allowed free text answer possibilities, while the latter consisted of Likert Scales, Yes/No, and multiple-choice type questions. There were 16 (*Paper III*) and 20 (*Paper V*) questions used in the two user studies. They were categorised to five themes, namely: (1) familiarity on flood maps and flood-related questions; (2) applicability of the different visualisations in decision-making; (3) helpfulness of the uncertainty information in decisions made; (4) strategies used when making decisions using the different visualisation. The fifth theme varied with the user evaluation. In user evaluation 1 (*Paper III*), the question focused on the 3D visualisation used, while in the second evaluation (*Paper V*), the effects of the contextual information in the decisions were explored.

Procedure and implementation

Prior to the actual user evaluation, written instructions, together with the questionnaire, which was sealed in an envelope, were distributed to the participants. The instructions provided background on flood uncertainties, descriptions of the different visualisation used, an explanation of the tasks to be performed, and the control keys to be used.

Participants

The first user study (*Paper III*) was conducted in February 2015 at the University of Gävle Sweden. There were 25 students (14 females and 11 males) coming from bachelor and master study programmes in the Land Management Division (Geomatics, Land Surveying, Spatial Planning and Computer Science and Geographical Information Technology), who took part in the study. Their age ranged from 21 to 47 years.

The second user assessment (*Paper V*) took place at the University of Ghent in Belgium, in April 2015. There were two sessions held to accommodate two groups of bachelor students from the Engineering and Geography departments. The total number of students who participated were 83 (30 females and 53 males), with ages ranging from 20 to 27 years.

3.7.2 User evaluation 3

In the third user evaluation (*Paper VIII*), it was presumed that different certainty maps can lead participants to choose different locations, and the task to which a visualisation is applied can also influence their choices. Additionally, such decisions may or may not be affected by the background of the participants. Thus, an online survey was conducted to find out how users employ the different certainty maps in planning related tasks, and to know their perception of certainty maps as used in similar tasks and decision-making.

The survey was primarily designed to be conducted online, to allow more participants to be reached (Aerts et al., 2003; Roth, 2009), particularly the different groups of practitioners. The evaluation was developed in Psytoolkit (Stoet, 2010, 2017). There were two main parts of the survey. The quantitative parts included measuring performance of participants in solving two planning tasks and determining their map preference. The qualitative part of the survey comprised of questionnaires that participants had to answer.

Participants were contacted through e-mail explaining the purpose of survey and by describing how uncertainty was accounted for in the maps used in the different tasks. The link to the survey was also included in the e-mail. Instructions for each task were embedded in the survey. After performing the third task, the questionnaire followed. This was a self-paced survey, with no imposed time limit to solve the different tasks. It was emphasised in the e-mail that the main focus of the analysis was their answers.

Task procedure

There were three tasks included in the user assessment. The first two tasks involved making decisions based on the provided maps, while the third task was mainly for knowing the certainty map preference of the users. The nine certainty maps used as conditions in the different tasks are presented in Sec. 3.6.3. All certainty maps were presented together with the orthophoto of the area employing the map pair presentation approach (MacEachren, 1992).

Task 1

In this task, participants had to determine whether a requested site by a homeowner is to be allowed (*Yes*) or not allowed (*No*) for construction. This is similar to a planning task, wherein planners have to grant building permits depending on the condition of the requested location. There were four requested sites used for this task (Figure 33a). Each of the sites has its corresponding status depending on the map used (Table 15). Aside from providing a Yes/No answer, participants had also to give their confidence in their response through a Likert Scale of 1 (not confident) to 5 (highly confident), similar to the assessment made in (Roth, 2009) (Figure 33b).

Each participant had to solve 36 trials for this task (i.e. for the 4 different targets \times 9 certainty maps). Presentation order for each trial was randomised for all participants to avoid learning effect.

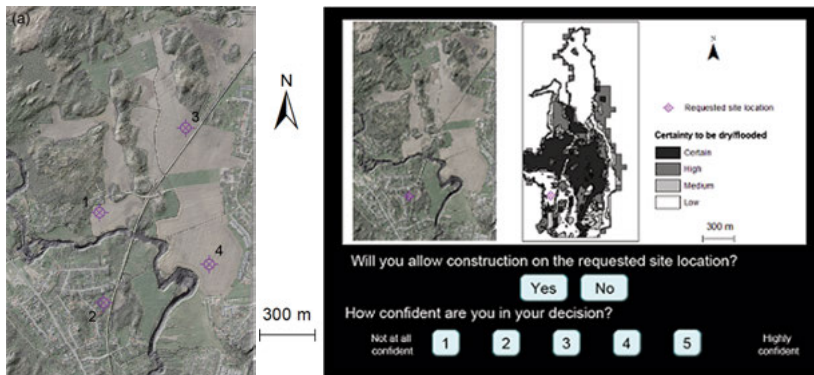


Figure 33. (a) The positions of the requested sites, and (b) a sample task to be solved, where they have to decide whether the requested location will be allowed or nor allowed for construction.

Table 15. The statuses of the sites in the different certainty maps.

FLOOD CERTAINTY MAP	TARGET 1	TARGET 2	TARGET 3	TARGET 4
Dual-ended (C_j), surface	1 (Flooded)	0.513	0.025	0.333
Dual-ended (C_j), choropleth	Certain to be flooded	Low certainty to be flooded	High certainty to be dry	Low certainty to be dry
Dual-ended (C_j), graduated symbol	Certain to be flooded	Low certainty to be flooded	High certainty to be dry	Low certainty to be dry
Sequential (probability), surface	100%	51.33%	2.5%	32.98%
Sequential (probability), choropleth	100%	60%	20%	40%
Sequential (S_j), surface	1 (Certain to be dry/flooded)	0	0.83	0.085
Sequential (S_j), choropleth	Certain	Low	High	Low
Sequential (S_j), graduated symbol	Certain	Low	High	Low
Binary	Flooded	Flooded	Uncertain	Uncertain

Task 2

In the second task, participants were given the choice to select a location for project development, based on the flooding condition in the area, and the land use from the orthophoto, which can both constrain decisions. This task is comparable to the ones undertaken as part of project planning, where prospective locations suitable for a specific project are identified. In identifying suitable project locations, different maps are often used in deciding the site.

To limit participants from randomly selecting locations, their choice was constrained by an area measuring 450 m × 450 m (Figure 34b). There were four target areas, where participants had to decide the location (Figure 34a) using the nine certainty maps, leading to 36 trials that had to be solved. As in Task 1, participants were also asked to rate their decision confidence in their location choices.

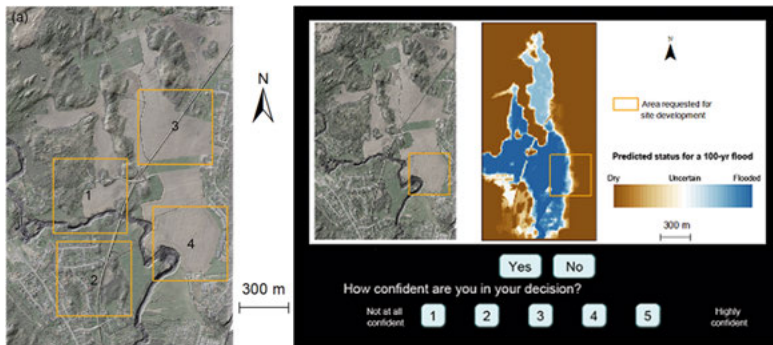


Figure 34. (a) Areas where participants had to select locations for project development, and (b) the sample task to be solved for Task 2.

Task 3

In evaluating the map preference of participants, the different certainty maps (Figures 26–30) were presented to them in pairs (Figure 35). For each pair, they had to select the map that was helpful in identifying the risk condition at the given site. Task 3 consisted of 36 pairwise comparisons ($\frac{9^2-9}{2}$), allowing all maps to be paired with each other.

Questionnaire design

There were about 35 open and close-ended questions that were answered by the participants for this study. The questions used consisted of deriving information on: participants' background (age, gender, education, GIS/hydrology knowledge); (uncertainty) decision-making perspectives; map familiarity and usage; certainty maps viewpoints and map preferences; insights on the tasks; and usage of contextual information.

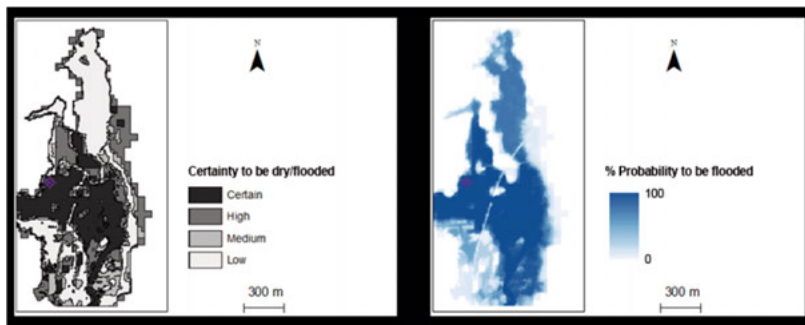


Figure 35. Example map pairs used for the pairwise comparison in Task 3.

Participants

Three groups of participants were chosen for the user evaluation, to be able to determine if there will be differences in their response to both the tasks and questionnaire. This can be an important determinant of their understanding of the certainty information provided to them (through the flood certainty maps) and the decisions they make (MacEachren, 1992). As shown in earlier studies, participants having different backgrounds solve decision-making tasks when presented with certainty information in different ways (Edwards & Nelson, 2001; Roth, 2009). Additionally, the results of Roth (2009) showed that different participant groups can have different ways of comprehending risks, which influence their decisions.

A total of 45 participants performed the quantitative part of the user evaluation by solving the different tasks. 13 of them were master and bachelor students from the University of Gävle within the Geospatial Information Science, Geomatics Spatial Planning and Land Surveying study programmes. The other two groups consisted of practitioners from Sweden (22) and the Philippines (10), who work mainly in municipalities and other government agencies.

Forty-two (11 students; 21 from Sweden; and 10 from the Philippines) out of the 45 participants answered the accompanying questionnaire. Age range of those who responded was 21 to 60 years old, with majority within the age bracket of 31 to 40 years of age. All respondents (with the exception of the three senior undergraduate students) have at least a bachelor's degree. Some participants, particularly from Sweden, have even their post graduate degrees. Participants from the Philippines are employed in different offices in the government. Nine of them work within general administration, while one is head of division. The Swedish group consisted of people working as planners, architects, researcher, GIS and project engineers, IT staffs, operations developer, environmental strategist, heads of department, as well as administrative workers. Most of the students and Swedes have knowledge in GIS or hydrology, while there was only one from the Philippine group who has this knowledge.

Chapter 4.

Summary of papers, discussion and contributions

Papers included in this dissertation focused on three areas to help answer the research problem: 1) modelling and uncertainty analyses (*Papers I, III IV and VI*); 2) mapping and geovisualisation (*Papers II, III, V, VII and VIII*); and 3) user assessment (*Papers III, V and VIII*) (Figure 36). The modelling part included GIS pre- and post-processing, hydraulic simulations, the sensitivity and uncertainty evaluation of model performance, and the mapping of uncertainties. It addresses the first and second research questions on how uncertainties can affect the model outputs and how they can be represented in maps. Map and geovisualisation model development focused on the conceptualisation and design of the uncertainty information derived in the flood modelling and uncertainty analyses parts. Research questions 2 to 4 are dealt with in this part. User assessment, which is centred on the design of tasks and carrying out quantitative (performance evaluation) and qualitative (questionnaire) studies, has its purpose to find out how the different uncertainty models developed from the previous steps are comprehended and utilised by users in decision-making tasks. This helps understand the effectiveness and usefulness of the uncertainty representations when making decisions (Research question 3 and 5), and how users perceive the inclusion of uncertainty information in the maps (Research question 6).

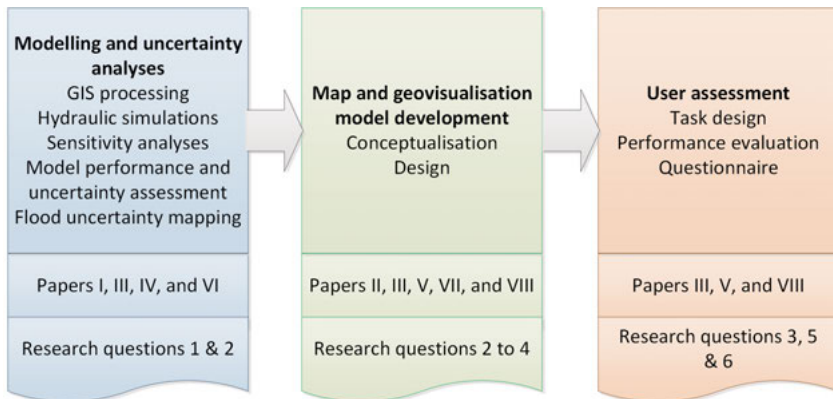


Figure 36. Main research topics in the dissertation.

4.1 Paper I: Importance of river bank and floodplain slopes on the accuracy of flood inundation mapping

Paper I investigates and quantifies the inaccuracies of flood results generated from a one-dimensional HEC-RAS model. There were two cases studied in this paper: the Eskilstuna River (Brandt, 2009) and Testebo River (Lim, 2011) in Sweden. The causes of uncertainties affecting prediction results (particularly the inundation extents) that were examined in the paper were the resolution of the DEM and the river side slope. For the Eskilstuna River, degenerated DEMs were used, while for the Testebo River, LiDAR combined with bathymetric data, and a 50 m elevation data from the *Swedish Mapping, cadastral and land registration authority* that was supplemented with bottom elevation were analysed.

There were four main findings derived from this study:

- 1) Regardless of the DEM resolution and the study area, inaccuracy in the results of the model became higher as the topography gets flatter. At steeper slopes, the disparity between the model and the validation data was smaller.
- 2) Lower resolution DEM further increased the inaccuracy of the model.
- 3) Errors induced by the modeller (in the cases used) were minimal compared with the effect of using lower resolution data.
- 4) How big the uncertainties accounted for also depended on the study area.

The first result was evident after plotting the river side slope against the measured disparity between the modelled and the reference data, using the different resolution DEMs in the two study areas. All results showed an inverse relationship, wherein higher disparities were derived at lower slopes (i.e. flat areas). From here, it can be deduced that in areas that are naturally flat, the results of the model in delineating the flood boundaries will be highly uncertain. In areas bounded by steep side slopes, water can be confined within a certain area. In this case, the water depth is increased vertically, rather than horizontally. Once the water level exceeded a vertical height threshold, it can expand laterally.

The increase in inaccuracy of results when using lower resolution data may be caused by the smoothing effect in the DEM, which can be brought about by the process of converting them from the original resolution to a lower resolution data. This leads to loss of details in the topography, making them flatter, especially with the lowest resolution Digital Elevation Models.

Errors brought about by the modellers are caused by the differences in the decisions they make throughout the modelling process. This is in terms of the data and the methods of processing them, the cross-section generation, handling the model and choice of model parameter and inputs used. But since the data and modelling performed were mostly similar to each other, the effect of the modellers to the prediction output was minimal. However, if there is a big discrepancy in modelling decisions made, as well as the type of data used, it is

possible that there can be greater error between the results produced by two modellers.

The two study areas, although having similarities in the disparity trends, produced different results in the uncertainty analysis. Poorer results were derived for the Testebo River, which can be attributed to the accuracy of the validation data that was used for deriving the disparity. As mentioned in the paper, the Eskilstuna River had no historic flood event to which the disparity can be accounted for. Instead it used the original resolution (non-degenerated) DEM. Furthermore, difference in results in the two study areas may also be affected by the dominant characteristic of the site being studied. If it is dominated by huge flat floodplains, then it is possible that there will be more inaccuracy in this area, than in an area dominated by steeper slopes.

4.2 Paper II: Geovisualisation of uncertainty in simulated flood maps

Geovisualisation of predicted flooding scenario for a specific flood event can be an important support tool that can aid planning and flood risk management. With flood visualisation, areas that are at risk of flooding can be identified or be used for creating scenarios. Thus, the aim of the paper was to show how uncertainties from hydraulic modelling can be visualised and incorporated in the 3D geovisualisation of predicted flooding conditions, and how they can be used for visual analysis of floods and exploration of spatial relationships. Additionally, an important phase in the development of the geovisualisation model was the process undergone by the different map layers and objects used, and their design. In order to meet the aim, a 3D visualisation model (Figure 37) was created using the Visualisation ToolKit. Prior to the creation of the model, there were several steps undertaken to prepare the different maps that constituted the information to be visualised. These were all described in Chapter 3, Sec. 3.6.1.

The design considerations applied in the geovisualisation have been important part of creating the model. These included the initial display of the visualisation, hierarchy of the spatial objects to be visualised, the type of geometry to represent the different features, the visual variables (size, colour, value) applied to the different geographic features in the map, the type of contextual information to be included, and the basic functionalities in the graphical user interface. The adoption of cartographic principles in the 3D representations was also significant part of the design, since geographic data are represented in the visualisation.

Moreover, in creating the model, it was also avoided to have much of the processing of the maps within the program. Since geovisualisation models utilise numerous map layers, and different transformation steps to attain their final forms, this was minimised by performing most of the transformation such as conversion and filtering, externally from the geovisualisation program. Most

of these tasks were performed in the data preparation stage. This allowed faster rendering of object and scenarios in the 3D scenes.

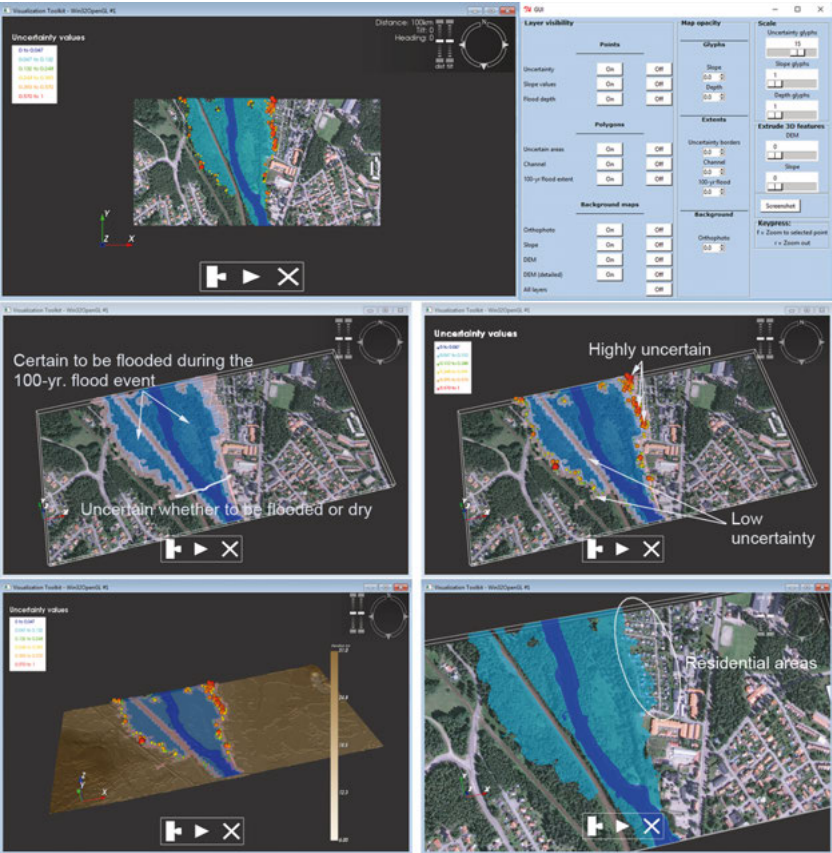


Figure 37. The 3D geovisualisation model with flood uncertainty information.

Nevertheless, it must be noted that the entire pipeline followed in both preparing the map layers and the development of the model (cf. Figure 14) also included different decisions that affected how the data appeared in the final visualisation. All these transformations that the data underwent are forms of abstraction (MacEachren et al., 2005). These steps are necessary in maps and other geovisualisation models, to avoid cluttered information, to attain more visually appealing visualisations or to augment the representation. However, they also altered the original data, causing information to be lost, as shown in Figure 38. Here, it was chosen to use more randomly distributed points instead of the original equally-spaced points (at 5 m) from the uncertainty information to avoid gridded appearance. But in the final output, it led to some locations having no entropy information, while in others, they were more clustered.

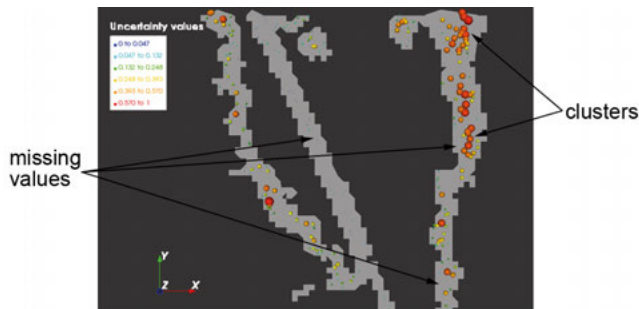


Figure 38. The effect of using randomly distributed points to represent uncertainty.

In some cases, it also became difficult to adhere to visualisation design principles. An example was the use of the colour representation for the entropy glyphs. The rainbow colour representation is not an optimal colour choice for representation due to its lack of perceptual ordering (Borland & Taylor, 2007). But in this case, it was used more for selective purpose, allowing one to easily identify the entropy and match it with the legend. This also makes them identifiable even when overlaid with the slope glyphs. Otherwise, it will be difficult for both glyphs to be distinguished from each other if the two of them follow a sequential colour scale, particularly for the lightest colour.

Moreover, the classification method used, i.e. natural breaks, also affected the representation of the information, particularly the uncertainties. If equal interval, for instance was used, the range of values will not be similar, leading to a different colour and size representation for the glyphs. As an example in the legend in Fig. 38, the last class was from 0.57 to 1 using natural breaks method for classification. This large range of values in the last uncertainty class will visualise most of the glyphs in red colour and with the largest sizes. If equal interval is used, there can be fewer red and large glyphs, since there will be smaller interval for the last class. Thus, this representation of colour and size according to class breaks may also influence how one views the uncertainty information. As what Brewer (2006) mentions, different classification schemes can produce various results and visual patterns. Yet, also according to her, this is a natural problem because there is no exact way of how to effectively class a data. This must be tested to the data that one is classifying and determine which method can convey well the message in the map.

The different user decisions in creating a geovisualisation model impact the visualisation and the information being conveyed, and its eventual interpretation by the user. This leads to another issue known as the *uncertainties in visualisation* (Brodie et al., 2012). Although there are already uncertainties in the modelling and assessment of model prediction output, there are also uncertainties involved in the visualisation pipeline that affect the final information being imparted.

4.3 Paper III: Visualisation and evaluation of flood uncertainties based on ensemble modelling

Three different uncertainty geovisualisation models, namely the aggregated entropy-like measure of uncertainty (S_j) with 2D and 3D contextual information, and the *performance bars* (Figures 22–24a), were evaluated through user assessment (cf. Sec. 3.7.1) to determine how users make geographic decisions using the information provided to them. Task performance of users was quantitatively measured in the task through: 1) the distance of their chosen location from the (target) stimuli given; 2) the predicted flooding status of their selected sites; and 3) the time they needed to solve the task. The questionnaire, on the other hand provided qualitative evaluation of the uncertainty geovisualisation models used and the task undertaken by the participants.

The location decisions made by the participants were influenced by the type of uncertainty information (aggregated S_j vs. *performance bars*), rather than the accompanying contextual information. There was significant difference in distance of the chosen location from the target when using the *performance bars* against the 2D and 3D S_j maps. Longer median distance was evident when the *performance bars* were used, but there was less variation in the response of the participants. This geovisualisation model also allowed them to totally avoid flooded areas, but at the same time, there were also more participants who chose uncertain locations using it. A possible reason for the better performance using the *performance bars* can be attributed to the visual variables used for representing uncertainty, particularly colour. As described in Sec. 3.6.2, the status of a given location where the cursor is pointed was represented by individual simulations results through 50 colour-coded bars (green=dry and red=flooded). The sizes of the bars indicate the likelihood of the particular simulation result to the reference data. If the bars are all red, it denotes that this location is flooded. Thus, it has to be avoided. The degree of certainty to be dry or flooded can easily be represented by the dominance of one colour in the series. This technique employed in using the *performance bars* also came out in the participants' answers in the questionnaire, when asked how they decided with the said visualisation. On the other hand, the S_j uncertainty map became more difficult to interpret, due to the same colour (black) used for representing certain to be flooded or dry areas. This loss of clear distinction between the statuses was due to the transformation made in applying the equation (Sec. 3.4.4), assigning the two statuses to a value of 0.

On the contrary, time varied among the different visualisations. Models integrated with functionalities, which allow users to interact with them, can take longer time to use. This was particularly the case for uncertainty map accompanied by 3D contextual information, followed by the *performance bars*.

However, the *performance bars* and the S_j uncertainty maps have also their own advantages in showing spatial patterns of the flooding condition. Although the *performance bars* visualisation is intuitive in representing the predicted conditions, it represents a point-based status. The *performance bars* indicates the condition of the particular cell where the cursor is currently pointed.

This condition is very specific to the cell and may change if it moves to another position. The value can also depend on the resolution of the underlying map. Moreover, since the information is point-based, it cannot immediately provide an overall geographic context of uncertainty, which can otherwise be provided by the entropy-based S_j map. This can be important especially in planning, where conditions of neighbouring areas are considered to see how flooding patterns will affect a location and nearby sites.

4.4 Paper IV: Visualising DEM-related flood map uncertainties using a disparity-distance equation algorithm

Earlier flood modelling results derived from the Eskilstuna River, and the analysis of the river side slope and model inaccuracy in *Paper I* led to the development of the disparity distance (D_d) equation algorithm that accounts for the inaccuracies brought about by the DEM resolution and the slope (Brandt, 2016). With the algorithm, an uncertain zone is generated around the flood extents produced from modelling performed using the 1D HEC-RAS model. Since the equation was empirically derived using the Eskilstuna case, this was tested to another river (i.e. the Testebo River), which has different topographic characteristics. This is mainly to identify the applicability of the equation to other cases aside from which it is based on, and to study how it can be used to assess or analyse model prediction uncertainties caused by the resolution of the data. This can also help determine the advantages and possible problems in implementing the method.

Results of this paper showed that the size of the uncertainty zones generated by the equation for the Testebo River was affected primarily by the resolution used. As can be seen from the result, the low resolution (50 m) DEM produced a larger uncertain area (0.93 km²), compared with the two results from the LiDAR data (0.22 km²), coming from the different modellers (Figure 39a–b). With the 50 m data, the terrain has become smoother, making the topography flatter. The issue with flat areas was also manifested in LiDAR-based results, particularly in locations that are already flat. But since the details in the terrain were preserved using high resolution DEM, it did not suffer as much uncertainty in the result as the 50 m resolution data.

Similar to *Paper I*'s results, the implemented algorithm showed that uncertainty in the model prediction (in terms of the zones generated) was affected more by resolution than the modellers. Again, the minimal effect by the modellers, who produce the simulations results, was caused by calibrations to match the reference data. Thus, uncertainties stemming from data processing, modelling and mapping were minimised.

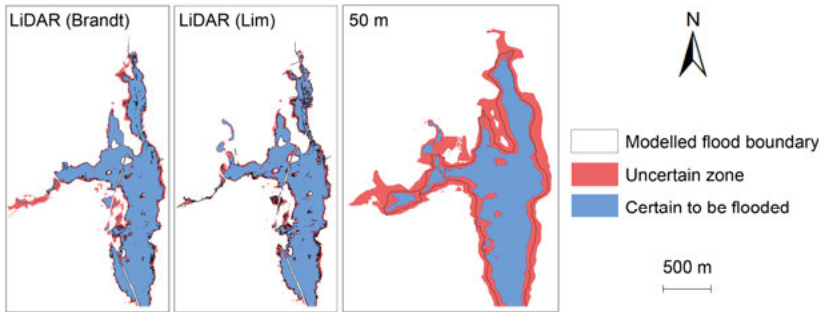


Figure 39. Uncertainty zones generated when using the LiDAR data and 50 m DEM.

It is also possible in the produced results for the Testebo case that uncertainties were underestimated. As mentioned, the equation in the algorithm was based on the Eskilstuna River, which lacks larger flat areas. Thus, the coefficient c (Equation 5) and exponent z (Equation 6) may be specific in accounting for the characteristics of the river to which it was based upon. This is a usual limitation with empirically derived equations. Therefore, they have to be tested and assessed for their applicability. Nevertheless, the method can be valuable in assessing further uncertainties of any prediction results as effect of the DEM resolution and the topography of an area. This method can be useful in adding uncertainty zones to deterministic (most optimal result) maps, to indicate their limitations.

4.5 Paper V: Color map design for visualisation in flood risk assessment

Paper III showed that the loss of information in indicating the exact status of the flooding condition, led to poorer user performance when using the entropy-like S_j map. To determine whether decisions will be improved when explicit flooding and dry statuses are represented as part of the uncertainty, a second user study was carried out to assess spatial decisions and task performance when utilising three different geovisualisation models: an S_j map accompanied by the 2D contextual information; the *performance bars* with altered colours to blue (flooded) and brown (dry); and a new dual-ended custom-designed C_j map, which shows a cost-weighted probability flooding status based on the aggregated ensemble results. The colour mapping scheme applied to the new map was conceptualised to follow different semantics and perceptual criteria to facilitate user interpretation of the map. Hence, the design aspects and procedure followed in developing the colour map became an important part of the method applied in this study (Sec. 3.6.2).

The findings of the user evaluation showed that the new dual-ended C_j map was the most effective and efficient for identifying and choosing dry locations among the geovisualisation models tested (Figure 40). Although there were also more participants who chose locations that were uncertain with this map, the statuses of these locations had higher certainty to be dry ($\tilde{C}_j=0.39$) or have lower risk to be flooded.

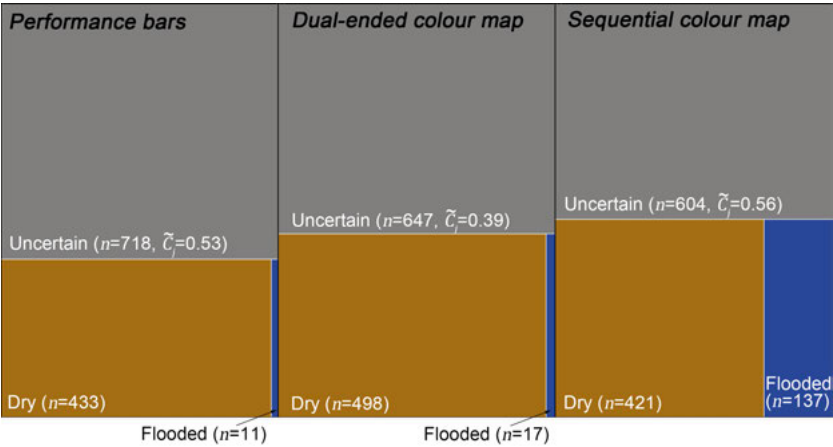


Figure 40. The proportion of the statuses chosen by participants when using the different geovisualisation models. Total n per visualisation was 1162.

Also similar to the result of *Paper III* was the findings derived for the *performance bars*. This geovisualisation model was the most effective for avoiding flooded status, wherein only 1% (11 out of the 1162 cases) were chosen in these sites. But at the same time, it led to the largest number of choices (62%) in highly uncertain locations.

The ineffectiveness of the S_j map when making decisions was demonstrated by the biggest number of locations chosen that have certain to be flooded status ($n=137$). Dry locations, on the other hand, were identified the fewest times using this map. This ambiguity in identifying flooded/non-flooded locations when using this information was also evident in the answers of the participants in the questionnaire when they rated the map. It also received the lowest rating in terms of comprehensibility, helpfulness in making decision and visual appeal. These results for the S_j map also agreed with the results of *Paper III*.

4.6 Paper VI: Flood map boundary sensitivity due to combined effects of DEM resolution and roughness

Model sensitivity to both the Digital Elevation Model and the roughness parameter (Manning's n) was looked at in this study to evaluate how they affect model prediction outputs, in terms of the flood boundaries generated. Most often, results from ensemble modelling and Monte Carlo simulations are limited in presenting such results due to the large number of outputs that have to be processed and produced. Yet, getting a spatial overview of the extents may help to further analyse the variabilities in the produced extents. Furthermore, the goodness-of-fit measure used can also have bias in assessing model sensitivity. These measures are used to quantify the results produced from using a given input/model parameter combination. Whether a model produces a good or poor result will be relative to the performance measure used. Thus, this paper investigates how flood map boundaries can be affected by both DEM resolution and the Manning's n used, and how the performance measure can further influence uncertainty assessment, as well as the deterministic maps used in flood inundation mapping. In the ensemble modelling conducted, 100 hydraulic simulations using ten DEMs (1 to 5 m, 10, 15, 20, 25 and 50 m) and 10 Manning's roughness values (0.01 to 0.1) were performed to assess the sensitivity of the prediction results. For estimating the model performance, four goodness-of-fit measures described in Sec. 3.4.3 were used.

The results of the extents produced from the different combinations of DEM and Manning's roughness are shown in Figure 41. Regardless of the resolution, all total flooding extents were under-estimated when using Manning's $n=0.01$ to 0.04, particularly in the northern and southern parts of the study area. However, the 25 m DEM only minimally under-estimated the southwest portion. The 50 m data, on the other hand, gradually produced an over-estimation in the extent as the roughness parameter was increased. At $n=0.05$ and 0.06, the northern portion was fully inundated in all resolutions. There were still under-estimations in the southern part, but mostly for higher resolution DEMs (1 to 10 m) that were paired with these Manning's n . With $n=0.07$ to 0.10, the 1977 flood extent was within the predicted extents in all resolution used, though the size of the overestimation in the northern and the entire western parts also became bigger as the roughness values were increased.

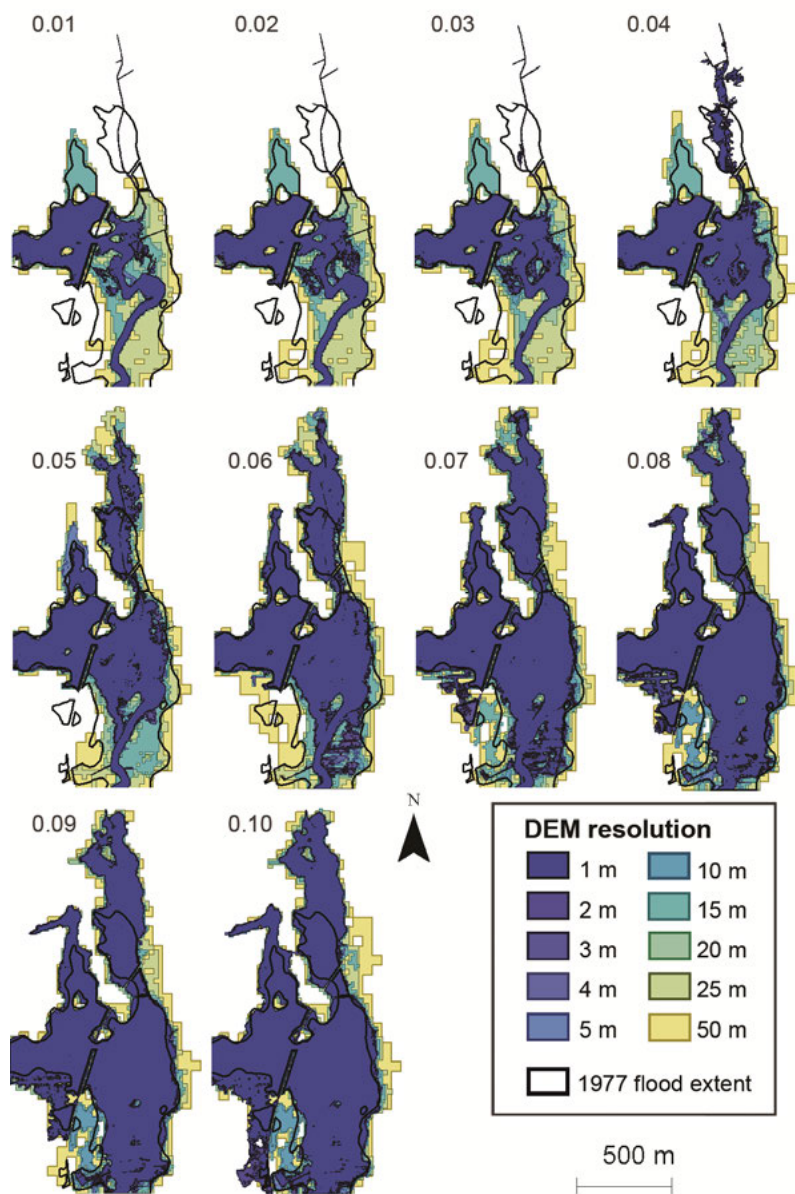


Figure 41. Flood extents grouped according to roughness value used.

The most optimal result varied with the goodness-of-fit measure used. Different combinations of DEM and Manning's roughness gave different highest performances (Figure 42). The lower resolution data produced maximum performance when using the three goodness-of-fit measures: 50 m for $F1$, and the 25 m for $F2$ and \bar{D} . The Manning's roughness paired with them also varied. For $F1$ and $F2$, lower Manning's n values produced the most optimal results with lower resolution data paired with them. While for both disparity measures, $n=0.07$ gave the highest performance for the 5 m and 25 m DEMs.

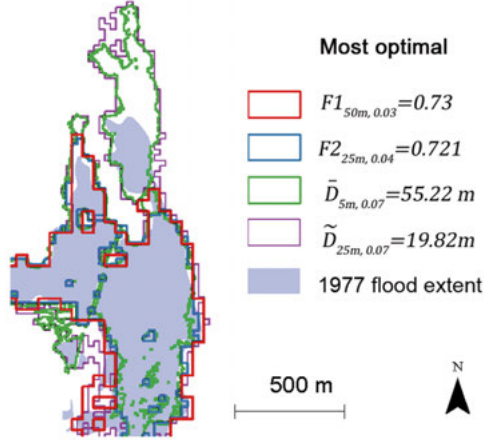


Figure 42. Optimal model performance from the different goodness-of-fit measures.

The number of high performances also differed with the method employed. When using $F1$, 74 of the 100 simulation results received performance ≥ 0.50 , while in $F2$, there were 18 simulations with the performance value. For the disparity measures, if the threshold used for high performance is ≤ 50 m, then no simulation will have good performance using mean disparity (\bar{D}), since the maximum is 55 m. If median disparity (\tilde{D}) is used, majority of the simulations (67) will be considered to have high performance.

Additionally, based on all the results of the different performance measures, the intermediate resolution 25 m received consistently high median performance among the different resolutions DEMs. It had also the lowest variability in the range of quantified performance, especially when $F1$ and the two disparity measures were used. For the roughness parameter, the highest median performance was 0.07 for $F1$, \bar{D} and \tilde{D} , and 0.04 for $F2$. All performance measures indicated the lowest median performance for the lowest roughness parameter due to the big underestimation in the model result, and bigger disparity between the model and the actual data.

The differences in the results of the goodness-of-fit measures were affected by how they account performance through the different equations implemented. The feature agreement statistics ($F1$ and $F2$), which are commonly used in flood modelling studies (e.g. Bates & de Roo, 2000; Aronica et al.,

2002; Hunter et al., 2005; Mason et al., 2009), consider mainly areal sizes (i.e. overlap, over- and underestimated) of the predicted flood in relation to the reference data. Both $F1$ and $F2$ also do not consider positional accuracies when comparing the extents produced in the model. They rely mainly on the total area sizes produced. In $F1$ the size of overlap is important in determining the overall performance of the model. Thus, a big overlap size (i.e. exceeding the combined size of the over-estimation and under-estimation of the model) can produce high performance. In $F2$, the size of overestimation, as well as the underestimation, determines how well the model performs. If both are very small, then performance of the model can be high. If the produced over-estimation (as well as underestimation) is high, then the model gets lower performance. So, in a study area that is flat with huge uncertainties in the model results, this performance measure can give low values.

The two disparity measures (\bar{D} and \tilde{D}) proposed in the study account for positional difference between the extents produced by the model and the reference data. However, the point sampling performed affected the values derived for the measure. Since this is based on the cross-sections, it will be sensitive to the cross-section's position, and also if the sampling is performed in locations where there are big disparities. If there are more locations with bigger disparities included in the sample, the mean will be larger. But if no sampling was performed in locations with big disparities, then the mean will be smaller.

Thus, only basing the results in the performance measures may miss looking at how well the flood extents were generated. For instance, low resolution (50 and 25 m) data received the maximum performance in three performance measures. Nevertheless, in the maps, the boundaries generated, may not be accurate due to the loss of details produced. Another example was when using $F2$. No high resolution data set (from 1 to 5 m) received a performance higher than 0.5, despite some of the results having better fit when compared to the reference map. If GLUE is implemented using this measure, and if the rejection criteria is set to 0.5, results from high resolution data sets will be eliminated, and most of the results that will be included in the probability map will be based on the intermediate and lower resolution DEMs.

As what is also seen in the results, these lower resolution data, particularly the 25 and 50 m DEMs, produce more errors in the generated water surface elevation. The effect was most prominent in flat areas, wherein coarser resolution data produced higher water surface elevation due to an increase in bottom elevation. This result was in agreement with the findings of Cook and Merwade (2009). At steeper slopes and narrower channels this effect was minimal in the WSE. The rise in bed was compensated by the increase in the width of the channel as effect of the grid size. This makes the WSE to not change significantly.

4.7 Paper VII: A cartographic framework for visualising flood uncertainties

Uncertainty communication is a complex process, involving different actors. In frameworks and guidelines recommended for flood uncertainty communication, there are different elements that are looked at (e.g. Faulkner et al., 2007; Beven et al., 2014, 2015) on how this can be carried out. One important aspect mentioned in these frameworks is the visualisation or presentation of the uncertainty. However, despite being mentioned as significant, there is no clear guideline or explanation on how this can be carried out to help modellers when visualising their results. Thus, *Paper VII* suggests a working framework that can be adopted by flood modellers or scientists when visualising map results from sensitivity or uncertainty analyses undertaken. This framework can partly address the communication issues between scientists and practitioners, by allowing the former to visualise and convey the information they produce, in a way that can easily be comprehended by the latter.

The guidelines adopted were grounded on cartographic principles, since maps were the main visualisation tools that the study focused on. Therefore, adhering to cartographic grammar became an important part of the suggested guidelines. Moreover, the suggestions for the usage of different visual uncertainty representations used, and those provided in the examples were based on earlier uncertainty visualisation studies that evaluate their intuitiveness in conveying information to their users.

The proposed framework consists of three primary stages: 1) flood modelling and uncertainty analyses; 2) output classification and characterisation; and 3) uncertainty mapping and visualisation. The first stage is crucial in producing the uncertainty map. This can be any method that will account for uncertainty in the model output. There are suggested ways on how this can be carried out as in Hall and Solomatine (2008). After the uncertainty information is produced, the data needs to be characterised with regards to its structure, types and the meanings associated with the information. The third stage focuses on the actual design and generation of the uncertainty representation. This is further divided in eight steps, namely:

1. determining the purpose of the information;
2. resolving the map scale to be used;
3. selecting a mapping method and symbolisation;
4. applying abstraction/generalisation/transformation;
5. choosing the visual variable for uncertainty representation, and the semantics to be used;
6. overlay consideration for contextual information;
7. inclusion of basic map elements; and,
8. visualisation technique.

The applicability of the proposed framework was also tested with uncertainty maps generated from flood uncertainty modelling. An important part of the proposed step that facilitated the design process was the second stage, where

the output data was characterised and typified. Here, the characterisation of whether the original data follows a sequential, double-ended, or binary scheme, or whether they come from individual simulation results that can be presented simultaneously in a map, helped facilitate decisions as to the mapping method, symbols and the uncertainty representation used. Thus, regardless of the uncertainty assessment method used, the suggestions for stages 2 and 3 can be adopted as long as they follow the same data characteristics. This may even be considered in other fields of application in uncertainty modelling.

The guidelines also include a step that is usually undertaken in visualisation, i.e. the application of abstraction in the modelling results. It can either be skipped or implemented in the framework, depending on the purpose of the map, or the information that is to be highlighted. Abstraction is often necessary steps in cartography to simplify the information (Dent, 1999; Kraak & Ormeling, 2003). It also allows users to easily interpret and find trends in the information. In the examples given, two ways of abstraction were presented in the uncertainty map: one is classing the original information to discrete conditions when using choropleth mapping techniques, and the other is the usage of graduated symbols to represent the flood statuses in a graduated symbol map. In choropleth mapping, reclassification is often undertaken to form homogeneous patterns that will help users of the maps to easily identify categories (Dent, 1999; Kraak & Ormeling, 2003), which can be crucial for extracting information from the map and for immediately making decisions based on it (Morss, Wilhelmi, Downton, & Gruntfest, 2005). Reclassification is usually employed in flood risk maps, where risks are classed into low, medium or high risks. The simplified information through the categories can immediately provide an estimate of risks. Nevertheless, in reclassifying the data, there can also be different schemes used for classing the original values (e.g. equal interval, natural jenks, quantile, standard deviation), and the number of classes to be discretised. They affect how the information is displayed or how they can be interpreted, as explained in *Paper II*. The graduated symbol grid map employs both reclassification and the assignment of symbols to each cell. The symbol's size gives emphasis to the quantities being represented in the map (Dent, 1999). However, during the process of creating the symbols, some details may have to be eliminated or refined, or the size and number of symbols may need to be increased or decreased to make the features more discernible, at the particular scale used in the visualisation medium, and the size of the grid. But regardless of the method used, abstraction alters the original data. This is the same issue presented in *Paper II* on how the entire visualisation process can also produce uncertainties in the visualisation (Brodlić et al., 2012). Therefore, a modeller must be aware of the effects of these alterations in the information they are showing, and how decisions can be influenced by them. At the same time, users shall be informed of these processes to make them aware of the limitations of the visualisation they are using.

4.8 Paper VIII: Assessment of spatial-based decisions and user perspectives in the utilisation of flood uncertainty maps

In this paper, different users, including practitioners and students, were assessed on how they understand and use different flood certainty maps, which indicate the certainty/uncertainty of the predicted flooding condition. These maps were derived from the uncertainty analyses conducted in *Paper VI* and from some of the examples generated in *Paper VII* in applying the proposed framework. Different mapping techniques were employed to produce these maps, where uncertainty was represented by different visual variables such as colour, value and size.

Decisions and confidence of the participants using the maps varied according to the task, as well as according to the group they belonged to. At certain to be flooded locations, participants were unanimous in not allowing construction in these locations. At the same time, they were also more confident in their response. However, the variation in response became evident when the sites to be decided were positioned in locations with varying degrees of certainty. Their decision became dependent on the dominant colour at the position of the site, as well as the condition of the neighbouring areas. The lightest colours were considered to be safer place in this case, particularly when using the C_j and probability maps, although for the former, this status is uncertain.

When users were to suggest locations for construction, they became more confident in their judgement. Also, the map type became important in the effectiveness of their decisions. Here, both the continuous dual-ended and probability maps made users to select dry locations. The continuous S_j map had again caused ambiguity in the choices made by the participants, wherein they chose less certain (i.e. most uncertain) areas the most number of times. But the abstraction performed in the choropleth and graduated symbol S_j maps had reduced the ambiguity when reading this information. Additionally, the elimination of the big certain to be dry area (outside the flood zone) allowed participants to be able to identify dry locations using these maps.

Although the three groups of participants had different backgrounds and line of work, a majority understood the information in a given map. Nevertheless, the variation between groups became obvious when they responded in the tasks, as well as their map preferences. The Swedish group (consisted of more experienced persons working with maps, more familiar with GIS, visualisation or hydrology) was the most careful in their decisions in both tasks. Participants in this group were less willing to take risks in their decisions by choosing locations that are certain or have high certainty to be dry. On the other hand, some students have taken more risky decisions, by selecting places with varying degrees of certainty the most frequently. This trend among students was also evident in the results from *Papers III* and *V*, regardless of the visualisation used. A possible reason that can explain this may be similar to Roth (2009), wherein he mentioned that domain novices, have the tendency to underestimate the risk in uncertain locations. Their lack of experience in making spatial decisions may also be a contributing factor. As also mentioned by Roth (2009),

non-experts tend to take more risks in their decisions because they misjudge the impact of the risk associated with flooding. With regards to certainty map preference, the less experienced groups preferred discretised (choropleth maps) over continuous surface maps. Nevertheless, if the performance will be looked at, the number of dry locations that were selected by them were higher for the continuous maps.

Overall, participants were positive with the inclusion of flood certainty statuses in a map, and how it can help improve their decisions. However, most of them are also aware that this is not the only information to the decisions they make. They mentioned for instance in their answers to the questionnaire that other maps are also needed when making location-related decisions. This is true in planning, and it is important for scientists and modellers to know this. Other information has also to be processed in relation to flood uncertainty condition (Morss et al., 2005). Therefore, it is vital that the visualisation is able to communicate its message directly and in an easy way that can be comprehended by the user. Yet, despite this positive reception on uncertainty flood maps, it is hardly seen that these practitioners use them in planning related tasks. It can be easier for them to see its importance when they practically know how to use them (Morss et al., 2005). This can also be a contributing reason why users were positive in all evaluations conducted (even in Papers *III* and *I*) to the inclusion of flood uncertainty information in decision-making. The usage of the information in the different tasks that the participants solved during the assessments, exemplified how these maps and geovisualisation models can be employed practically in planning-related tasks.

Chapter 5.

Conclusion, research contributions and future work

5.1 Conclusion

Flood maps are produced from using different data and involve different processes and modelling decisions. All these are reflected in the final map. The first aim of the study, which is to *determine how uncertainties in the modelling process, as brought about by the effects of the input DEM resolution, Manning's roughness parameters and methods for estimating model performance can affect the model prediction results, in terms of the flood inundation maps generated from them*, tried to show the effects of these problems, particularly to deterministic maps (i.e. maps only showing dry and flood areas for a given flood magnitude). *Papers I, IV and VI* showed that flood extents produced varied depending on the DEM resolution and the Manning's roughness parameter used, as well as the area's topography. Even the performance measure for quantifying how well a model produced its results in relation to a historical flood data showed to manifest biases when choosing an optimal model. As what was presented in *Paper VI*, the optimal outputs were different in all goodness-of-fit measures used.

Although there are imperfections brought by the modelling process to produce flood maps, they remain valuable tools for information. Without them, it is impossible to foresee and plan what can possibly happen during an extreme flood event, which is important for disaster risk management. However, these maps should be able to reflect the uncertainties in the flood prediction process. As part of this issue and the disadvantages of using deterministic maps, it was explored in the research how uncertainties can be represented or accounted for in maps and other geovisualisation models (i.e. the second aim of the study). *Papers II–V, VII and VIII* showed different ways of representing uncertainty information by employing probabilistic and uncertainty mapping (*Papers III, V, VIII*), or generating uncertain flood zones around deterministic maps (*Paper IV*). Different visual variables (colour, value size, arrangement, texture and fuzziness) recommended in earlier uncertainty geovisualisation literature and different mapping techniques were applied for representing flood uncertainties. The flood uncertainty representations presented in *Papers III, IV, V, VII and VIII* can be classified as dual-ended flood maps, probabilistic flood maps, sequential certainty and uncertainty maps, binary maps, overlain flood boundaries and *performance bars*. A description of these different uncertainty representations, together with their advantages and disadvantages, are found in the *Appendix*.

As part of addressing the second aim, it was also examined how cartographic design elements can be adopted in the visualisation. Here, the role of

cartography was considered to be important in facilitating communication of the information in maps. The cartographic aspect in flood uncertainty visualisation is often overlooked in flood uncertainty studies and the visualisation of results. This is the reason why a framework was also recommended in *Paper VII*, particularly the 8-step design considerations in flood uncertainty mapping and visualisation, following cartographic rules in the visual display of information. It aimed to help modellers and scientists to consider cartographic design aspects when visualising their results. Together with the suggested framework, the conceptualisation of the design aspects was adopted for the data derived from the different studies to exemplify how these guidelines can be flexibly applied to different types of flood uncertainty data.

To better understand the effectiveness of the uncertainty representations proposed in the different studies, user evaluations were conducted (*Papers III, V and VIII*). The assessments helped address the third aim, which is understanding how users make spatial decisions based on the different visualisation, and determining their perspectives on the uncertainty maps. The results of these evaluations showed that users were able to make spatial decisions according to the tasks given to them using the uncertainty maps. Therefore, there is no problem on how they understood the maps containing flood uncertainty statuses. However, the findings also showed that there can be uncertainty information that is more difficult to understand, and may be confusing, such as the entropy (S_j) maps based on Equation 19, which could have led users to a different decision or choice. Regardless of the semantics applied in this map (degrees of certainty or uncertainty), similar results in the evaluations (*Papers III, V and VIII*) were obtained. The difficulty in understanding this map was only reduced by discretising the original information and by using symbols for representing the statuses (*Paper VIII*). Here, the role of map abstraction became important to simplify and make the information more comprehensible.

Nevertheless, how well the decisions were made also depended on the backgrounds of the participants. From the different groups evaluated, it was shown that students tended to take more risk in their location choices. This was evident in all user evaluations (*Papers III, V and VIII*). The most experienced practitioners (i.e. Swedish group) were most careful with selecting sites in flooded areas. Different users were also positive on the inclusion of uncertainty in flood maps and adopting them in decision-making.

5.2 Research contributions

The entire research contributes to the comprehension of uncertainties affecting flood model results, in terms of the maps produced by them. Some of the causes of uncertainties that were looked at included the Digital Elevation Model's resolution, the roughness parameter, the inherent characteristics of the area, as well as the performance measures used. The DEM resolution was shown to have great effect in the extents of the flooding produced (*Papers I, IV and VI*), which can further be affected by the Manning's roughness that was paired with

it (*Paper VI*). Lower resolution data increased the inaccuracy in model results. Additionally, their effect was not only manifested in the extents of floods, but also in the water surface elevation, which became higher due to the increased in bottom elevation as effect of the smoothing in the DEM (*Paper VI*). This effect of resolution in both the spatial extents of flooding and the water surface elevation is seldom analysed in sensitivity analyses of 2D models, especially in relation to the performance of the model. In most studies, the focus is assessing the model based only on its performance. Since these performances are given as numeric values, the geographic variation in the results, and the discrepancies in the extents cannot be determined by just relying on them. This may therefore lead to concluding that a specific flood model result, even when based on lower resolution DEM, is acceptable as long as the performance derived is high. Nevertheless, as what was shown in *Paper VI*, coarser resolution affected the inaccuracies horizontally (in the expanse of flooding) and vertically (with the increase in water surface elevation) in the model. Thus, suggestions that it is acceptable to use coarser resolution DEMs in flood modelling (e.g. 25 m, 50 m or even lower than these two), may be misleading.

It was also shown that uncertainties in prediction results can further be influenced by the topography of the area. Uncertainties were bigger in flatter areas (*Papers I, IV and VI*). This was regardless of the resolution of the DEM, although higher resolution DEMs have shown to minimise these uncertainties (*Papers I and IV*). In flatter areas, the smoothening effect mentioned earlier, and the increase in bed elevation become more prominent (*Paper VI*). Unlike in steeper and narrower channels (having widths smaller than the cell size of the DEM), the increase in grid size is compensated by the rise in bed. Therefore, the extents and water surface elevation do not change much in these locations. This may be an explanation why flat areas produce more uncertainties in model results than steeper areas, especially when using lower quality DEMs.

Two new methods for quantifying model prediction performance were also presented in the research. These were the mean and median disparities. In contrast to the feature agreement statistics ($F1$ and $F2$), which are commonly employed in extent validation studies, the new measures account for model errors rather than areal size comparisons that are used in $F1$ and $F2$ (*Paper VI*). The usage of areal size comparisons in feature agreement statistics considers the totality of the sizes (overlap, over- and underestimated) generated by the model in comparison with the reference data. They do not account for any positional accuracies between the two. In $F1$, for example, a higher performance can be derived, as long the overlap size between the model and the reference is larger than the combined sizes of under- and over-estimation it produced. However, if the latter becomes larger than the size of overlap, a lower performance is given (i.e. <0.5 , where 1 is the maximum). An equal size of overlap to the combination of under- and overestimated sizes will produce an $F = 0.5$. In $F2$, a higher performance can be derived if the sizes of the over- and under-estimation is very low.

It was also shown in the results of the study, particularly in *Paper VI*, that the most optimal model result depended on the performance (goodness-of-fit)

measure used. Different performance measures gave varying best model results in the study conducted. Hence, these findings further supports Di Baldassarre et al. (2010) on why it is inappropriate to use deterministic flood maps. In the case of this research (*Paper VI*), however, it was attributed to the performance measure as causing subjectivity in the choice of an optimal model result. Since most deterministic flood maps used in planning are outcomes of calibrations and/or validation with historical data and are evaluated based on a specific performance measure, they may also suffer from uncertainties caused by the assumptions of the performance measure used when quantifying the generated model results.

In estimating uncertainty, the most commonly used method for assessment and producing flood inundation probability and uncertainty maps was applied by following the GLUE methodology framework. In addition to this, the implementation of the empirically derived *Disparity Distance* (D_d) algorithm was also presented in this study. Unlike the GLUE methodology, the D_d algorithm can consider the effects of different resolution DEMs in model results and the slope by generating uncertainty zones around these maps (*Paper IV*). The effect of various DEM resolution in prediction results is more difficult to account in the GLUE methodology, due to the implementation of Monte Carlo simulations. This will necessitate changing the DEM or its accuracy for each test, before conducting the simulation. Additionally, the DEM resolution and the study area's size can increase the simulation time, making it impractical to use in this context. Therefore, the D_d algorithm can serve as an alternative method to account for DEM uncertainties in the model.

Ways of visually communicating uncertainties through maps were investigated in the entire research, aside from evaluating how different users deal with flood uncertainty maps. Different flood uncertainty maps produced from uncertainty assessments were represented in different ways as shown in *Papers II, III, V, VII and VIII*. The characterisation of the data helped in conceptualising the design and the selection of graphical variable to be used in mapping. Different visualisations were also assessed and the findings from these evaluations led to the suggestions of representations that can be adopted in flood inundation mapping (see *Appendix* for the list). As part of representing flood uncertainty, a new dual-ended colour map scheme (*Paper V*) and an uncertainty visualisation model (i.e. *performance bars* in *Papers III and V*) were also introduced in the research. The former was specifically designed for flood risk assessment. Unlike any colour map used for flood risk applications, the new colour represents both probability and uncertainty of the flooding condition. Despite being specific to flooding application, the design process adopted to this colour map can also be applicable to diverging data manifesting uncertainty. An important step suggested in *Paper V* is to determine the colours at the ends of the scheme, which can be dependent on what is being represented by the data. The evaluation of this colour map also showed its effectiveness in preferring dry areas and efficiency in solving the tasks in the assessment. The *performance bars*, which is an interactive way of presenting ensemble results for a specific location, was effective especially in avoiding flooded areas (*Papers III and V*).

Furthermore, a cartographic framework for presenting and visualising flood certainty maps was proposed in *Paper VII* that can serve as guidelines for modellers and scientists. This framework partly addresses the call of some authors like Pappenberger and Beven (2006) and Beven et al. (2015) for guidelines that will enhance flood uncertainty communication process between producers and users of flood information. However, instead of focusing on the entire communication process, which is rather more complicated, the guidelines suggested centred on cartographic visualisation aspects that will help scientists and modellers when communicating the information that they derive. Moreover, the suggested framework can also be extended to other domains in environmental modelling, when visualising uncertainties in prediction results.

Evaluation of maps and representations are important steps to determine how visual representations of uncertainty is understood, and if it serves its purpose to communicate its message to users of the information (MacEachren et al., 2005). Yet, in specific domains, these studies are still limited. In flood inundation and uncertainty modelling studies, the focus is coming up with analyses and different representations of uncertainties, but leave out the part of conducting user evaluations. Therefore, this research contributes, not only in understanding the causes of uncertainties in flood maps and creating or designing visualisations based on them, but also in apprehending how users utilise and decide using the different information. The results of the user evaluations in *Papers III, V and VIII*, for instance, gave insights that different users can understand flood uncertainty information through the maps and use them in the tasks given to them. However, they also showed that decisions made varied among user groups, as brought about by the task to be solved, the visualisation used, as well as their backgrounds (*Papers III, V and VIII*). The last mentioned can further be affected by participants' reasoning on the choice of locations they prefer, wherein both their knowledge of risk and experience can play significant roles when making decisions (Roth, 2009). Thus, this make uncertainties also inherent when making decisions (Hutter & Schanze, 2008).

The tasks designed in the user evaluations exemplified practical ways on how flood uncertainty information can be used in spatial planning (e.g. suggesting locations where projects can possibly be developed, based on the information provided in the map, or granting construction based on the uncertain flooding status at that site). This could have led users to better understand the information and its usage, as well as its value in planning, making them more positive in its inclusion in planning-related tasks. Moreover, the findings of the research become relevant, since more practical (valid) tasks are solved in relation to understanding the use of flood uncertainty information in decision-making.

5.3 Future work

Based on the outcomes of the research, there are several recommendations suggested for future studies that can lead to better understanding of the uncertainties contributing to flood maps. High resolution DEMs and their effects in 2D

modelling, for instance, should be investigated more. With increasing computational power of computers, it is possible to simulate floods using high resolution data. The effect of the quality of the DEM should also be looked at in relation to the boundary conditions, the discharge as well as in different study areas having different characteristics. Moreover, when performing flood validation studies, investigation of both the flood extents and the depth of flood must be taken in consideration. This is because the horizontal expanse of water can also be affected by the vertical changes in the profile.

It has been explored in the study how the different performance measures affected the deterministic maps produced. Since these measures are also used in probabilistic mapping when employing the GLUE methodology, the effects of the goodness-of-fit methods in these maps should also be looked at. This is to see how the probability flood maps can also be affected by uncertainties in the performance measure used.

In estimating model prediction uncertainties as effect of the DEM and the river side slope, the D_d algorithm was implemented. However, the applicability of the said algorithm to different study areas and rivers with different characteristics need to be examined further. Currently, only the Testebo River (aside from the Eskilstuna river, where the equation was derived), has been tested for its implementation. Expanding the research to other study areas may give valuable results that help to adjust the equations, and to determine the validity of the results produced by the algorithm.

More user evaluations that will assess user comprehension in the usage of flood uncertainty maps are needed. This is to understand how they decide using these maps. In the evaluations to be conducted, it is further suggested to incorporate practical problem-solving tasks where they can employ decisions using these maps. Moreover, users (particularly planners who use the flood maps) coming from different backgrounds are also suggested to be involved in more studies, as these differences can affect how they decide using the map information presented to them, or how they take risks in their decisions, as shown in this research.

It is also suggested to future studies to incorporate uncertainty in flood depth maps and risk maps. Uncertainties in flood depths are often graphically represented instead of visualising them in maps. In addition, since flood risk maps depend on the different hazard maps, there will be uncertainties in the risk maps as effect of these underlying maps. Therefore, flood risk maps showing uncertainties should also be explored.

An important recommendation for scientists and modellers who investigate uncertainties is to make the results more comprehensible, less complex and the visualisation simpler. The usage of maps to present information should be used to visually represent uncertainty information. In producing these maps, it is suggested in this research that the application of basic cartographic design principles is adopted to facilitate communicating information.

As earlier stated, most practitioners do not have the same modelling background as hydraulic modellers and scientists. They may have difficulty to understand the modelling process and the uncertainties involved in these processes. It must also be considered that flood uncertainty information and maps

are only some of the information that is needed by practitioners when making decisions. There are numerous considerations that they need in planning or in the decision-making process. Hence, simplifying the information can help them extract the main information they need from the map.

It is also suggested to modellers and scientists to provide ways on how flood uncertainty maps can be adopted practically in planning and decision-making tasks. In this way, it will be easier for practitioners to understand and possibly use the information.

References

- Aerts, J. C. J. H., Clarke, K. C., & Keuper, A. D. (2003). Testing popular visualization techniques for representing model uncertainty. *Cartography and Geographic Information Science*, 30(3), 249–261.
- Apel, H., Thielen, A. H., Merz, B., & Blöschl, G. (2004). Flood risk assessment and associated uncertainty. *Natural Hazards and Earth System Sciences*, 4, 295–308.
- Aronica, G., Bates, P. D., & Horritt, M. S. (2002). Assessing the uncertainty in distributed model predictions using observed binary pattern information within GLUE. *Hydrological Processes*, 16(10), 2001–2016. <https://doi.org/10.1002/hyp.398>
- Aronica, G., Hankin, B., & Beven, K. (1998). Uncertainty and Equifinality in calibrating distributed roughness coefficients in a flood propagation model with limited data. *Advances in Water Resources*, 22(4), 349–365.
- Bates, P. D., & de Roo, A. P. J. (2000). A simple raster-based model for flood inundation simulation. *Journal of Hydrology*, 236, 54–77.
- Bates, P. D., Horritt, M. S., & Fewtrell, T. J. (2010). A simple inertial formulation of the shallow water equations for efficient two-dimensional flood inundation modelling. *Journal of Hydrology*, 387, 33–45. <https://doi.org/10.1016/j.jhydrol.2010.03.027>
- Bedient, P. B., Huber, W. C., & Vieux, B. E. (2013). *Hydrology and Floodplain Analysis* (5th ed.). Harlow Essex: Pearson Education Limited.
- Bertin, J. (1983). *Semiology of Graphics: Diagrams, networks, maps*. Madison, WI: University of Wisconsin Press.
- Beven, K. J. (2006). A manifesto for the equifinality thesis. *Journal of Hydrology*, 320, 18–36. <https://doi.org/10.1016/j.jhydrol.2005.07.007>
- Beven, K. J. (2009). *Environmental Modelling: An Uncertain Future*. CRC Press.
- Beven, K. J., & Binley, A. (1992). The future of distributed models: Model calibration and uncertainty prediction. *Hydrological Processes*, 6(3), 279–298. <https://doi.org/10.1002/hyp.3360060305>
- Beven, K. J., & Freer, J. (2001). Equifinality, data assimilation, and uncertainty estimation in mechanistic modelling of complex environmental systems using the GLUE methodology. *Journal of Hydrology*, 249(1), 11–29.
- Beven, K. J., Lamb, R., Leedal, D., & Hunter, N. (2015). Communicating uncertainty in flood inundation mapping : a case study. *International Journal of River Management Basin*, 13(3), 285–295. <https://doi.org/10.1080/15715124.2014.917318>
- Beven, K. J., Leedal, D., & McCarthy, S. (2014). *Framework for assessing uncertainty in fluvial flood risk mapping*. London: CIRIA.
- Bisantz, A. M., Stone, R. T., Pfautz, J., Fouse, A., Farry, M., Roth, E., ... Thomas, G. (2009). Visual representations of meta-information. *Journal of Cognitive Engineering and Decision Making*, 3(1), 67–91.
- Blazkova, S., & Beven, K. J. (2009). Uncertainty in flood estimation. *Structure and Infrastructure Engineering*, 4(4), 325–332. <https://doi.org/10.1080/15732470701189514>

- Borland, D., & Taylor, R. M. (2007). Rainbow Color Map (Still) Considered Harmful. *IEEE Computer Graphics and Applications*, 27(2), 14–17. <https://doi.org/10.1109/MCG.2007.323435>
- Brandt, S. A. (2009). *Betydelse av höjdmodellens kvalitet vid endimensionell översvämningsmodellering*. Högskolan i Gävle. Retrieved from <http://urn.kb.se/resolve?urn=urn:nbn:se:hig:diva-4120>
- Brandt, S. A. (2016). Modeling and visualizing uncertainties of flood boundary delineation: algorithm for slope and DEM resolution dependencies of 1D hydraulic models. *Stochastic Environmental Research and Risk Assessment*, 30(6), 1677–1690. <https://doi.org/10.1007/s00477-016-1212-z>
- Brandt, S. A., & Lim, N. J. (2016). Visualising DEM-related flood-map uncertainties using a disparity-distance equation algorithm. In A. H. Schumann (Ed.), *Proceedings of the International Association of Hydrological Sciences (IAHS): The spatial dimensions of water management - Redistribution of benefits and risks* (pp. 153–159). Bochum, Germany: Copernicus. <https://doi.org/10.5194/piahs-373-153-2016>
- Brewer, C. A. (1994). Color use guidelines for mapping and visualization. In A. M. MacEachren & D. R. F. Taylor (Eds.), *Visualization in Modern Cartography* (vol. 2) (pp. 123–148). Oxford: Pergamon.
- Brewer, C. A. (1996). Guidelines for Selecting Colors for Diverging Schemes on Maps. *The Cartographic Journal*, 33(2), 79–86.
- Brewer, C. A. (2006). Basic Mapping Principles for Visualizing Cancer Data Using Geographic Information Systems (GIS). *American Journal of Preventive Medicine*, 30(2), 25–36.
- Brewer, C. A., Hatchard, G. W., & Harrower, M. A. (2003). ColorBrewer in Print: A Catalog of Color Schemes for Maps. *Cartography and Geographic Information Science*, 30(1), 5–32. <https://doi.org/10.1559/152304003100010929>
- Brodie, K., Osorio, R. A., & Lopes, A. (2012). A review of uncertainty in data visualization. In J. Dill, R. Earnshaw, D. Kasik, J. Vince, & P. C. Wong (Eds.), *Expanding the Frontiers of Visual Analytics and Visualization* (pp. 81–109). London: Springer. https://doi.org/10.1007/978-1-4471-2804-5_6
- Casas, A., Benito, G., Thorndycraft, V. R., & Rico, M. (2006). The topographic data source of digital terrain models as a key element in the accuracy of hydraulic flood modelling. *Earth Surface Processes and Landforms*, 31(4), 444–456. <https://doi.org/10.1002/esp.1278>
- Cheong, L., Bleisch, S., Kealy, A., Tolhurst, K., Wilkening, T., & Duckham, M. (2016). Evaluating the impact of visualization of wildfire hazard upon decision-making under uncertainty. *International Journal of Geographical Information Science*, 30(7), 1377–1404. <https://doi.org/10.1080/13658816.2015.1131829>
- Chow, V. T. (1959). *Open Channel Hydraulics*. New York: McGraw Hill Book Co.
- Cook, A., & Merwade, V. (2009). Effect of topographic data, geometric configuration and modeling approach on flood inundation mapping. *Journal of Hydrology*, 377(1–2), 131–142. <https://doi.org/10.1016/j.jhydrol.2009.08.015>

- Coulthard, T. J., Neal, J. C., Bates, P. D., Ramirez, J., de Almeida, G. A. M., & Hanrock, G. R. (2013). Integrating the LISFLOOD-FP 2D hydrodynamic model with the CAESAR model: implications for modelling landscape evolution. *Earth Surface Processes and Landforms*, 38(15), 1897–1906. <https://doi.org/10.1002/esp.3478>
- Cruise, J. F., Sherif, M. M., & Singh, V. P. (2012). *Introduction to Hydraulics* (Philippine). Singapore: Cengage Learning Asia Pte. Ltd.
- Dent, B. D. (1999). *Cartography: Thematic Map Design* (5th ed.). WCB/McGraw-Hill.
- Di Baldassarre, G. (2012). *Floods in a Changing Climate: Inundation Modelling (Vol. 3)*. Cambridge: Cambridge University Press.
- Di Baldassarre, G., Laio, F., & Montanari, A. (2009). Effect of observation errors on the uncertainty of design floods. *Physics and Chemistry of the Earth*, 34, 606–611.
- Di Baldassarre, G., & Montanari, A. (2009). Uncertainty in river discharge observations: a quantitative analysis. *Hydrology and Earth System Sciences Discussions*, 13, 913–921.
- Di Baldassarre, G., Schumann, G., Bates, P. D., Freer, J., & Beven, K. (2010). Flood-plain mapping: a critical discussion of deterministic and probabilistic approaches. *Hydrological Sciences Journal*, 55(3), 364–376. <https://doi.org/10.1080/02626661003683389>
- Domeneghetti, A., Vorogushyn, S., Castellarin, A., Merz, B., & Brath, A. (2013). Probabilistic flood hazard mapping: effects of uncertain boundary conditions. *Hydrological Earh System Science*, 17, 3127–3140. <https://doi.org/10.5194/hess-17-3127-2013>
- Dottori, F., Di Baldassarre, G., & Todini, E. (2013). Detailed data is welcome, but with a pinch of salt: Accuracy, precision, and uncertainty in flood inundation modeling. *Water Resources Research*, 49(9), 6079–6085. <https://doi.org/10.1002/wrcr.20406>
- Drecki, I. (2002). Visualisation of uncertainty in geographical data. In W. Shi, P. Fisher, & M. F. Goodchild (Eds.), *Spatial Data Quality* (pp. 144–163). London: Taylor & Francis.
- Edwards, L. D., & Nelson, E. S. (2001). Visualizing data certainty A case study using graduated circles maps. *Cartographic Perspectives*, 38, 19–36. <https://doi.org/10.14714/CP38.793>
- EXCIMAP. (2007). *Handbook on good practices for floodmapping in Europe*.
- Faulkner, H., Parker, D., Green, C., & Beven, K. J. (2007). Developing a Translational Discourse to Communicate Uncertainty in Flood Risk between Science and the Practitioner. *AMBIO: A Journal of the Human Environment*, 36(8), 692–704.
- Fedra, K. (1993). GIS and Environmental Modeling. In M. F. Goodchild, B. O. Parks, & L. T. Steyaert (Eds.), *Environmental modeling with GIS* (pp. 35–50). Oxford University Press.
- Fewtrell, T. J., Bates, P. D., Horritt, M. S., & Hunter, N. (2008). Evaluating the effect of scale in flood inundation modelling in urban environments. *Hydrological Processes*, 22, 5107–5118. <https://doi.org/10.1002/hyp.7148>
- Fewtrell, T. J., Neal, J. C., Bates, P. D., & Harrison, P. J. (2011). Geometric and structural river channel complexity and the prediction of urban inundation. *Hydrological Processes*, 25, 3173–3186.

- French, R. H. (1986). *Open-channel hydraulics*. New York: McGraw-Hill Book Company.
- Goodchild, M. F. (1992). Geographical information science. *International Journal of Geographical Information Systems*, 6(1), 31–45.
- Goodchild, M. F., Battenfield, B. P., & Wood, J. (1994). Introduction to visualizing data validiy. In H. Hearnshaw & D. J. Unwin (Eds.), *Visualization in Geographical Information Systems* (pp. 141–149). Chichester: Wiley.
- Hall, J. W., & Solomatine, D. P. (2008). A framework for uncertainty analysis in flood risk management decisions. *International Journal of River Basin Management*, 8(2), 85–98. <https://doi.org/10.1080/15715124.2008.9635339>
- Hall, J. W., Tarantola, S., Bates, P. D., & Horritt, M. S. (2005). Distributed sensitivity analysis of flood inundation model calibration. *Journal of Hydraulic Engineering*, 131(2), 117–126.
- Horritt, M. S. (2006). A methodology for the validation of uncertain flood inundation models. *Journal of Hydrology*, 326(1–4), 153–165. <https://doi.org/10.1016/j.jhydrol.2005.10.027>
- Horritt, M. S., & Bates, P. D. (2001a). Effects of spatial resolution on a raster based model of flood flow. *Journal of Hydrology*, 253(1), 239–249.
- Horritt, M. S., & Bates, P. D. (2001b). Predicting floodplain inundation: raster-based modelling versus the finite-element approach. *Hydrological Processes*, 15(5), 825–842. <https://doi.org/10.1002/hyp.188>
- Horritt, M. S., & Bates, P. D. (2002). Evaluation of 1D and 2D numerical models for predicting river flood inundation. *Journal of Hydrology*, 268, 87–99.
- Howard, D., & MacEachren, A. M. (1996). Interface design for geographic visualization: Tools for representing reliability. *Cartography and Geographic Information Systems*, 23(2), 59–77.
- Hunter, G. J., & Goodchild, M. F. (1997). Modeling the Uncertainty of Slope and Aspect Estimates Derived from Spatial Databases. *Geographical Analysis*, 29(4), 35–49. <https://doi.org/https://doi.org/10.1111/j.1538-4632.1997.tb00944.x>
- Hunter, G. J., Goodchild, M. F., & Robey, M. (1994). A Toolbox for Assessing Uncertainty in Spatial Databases. In E. G. Masters (Ed.), *AURISA 94: Proceedings of the 22nd Annual Conference of the Australasian Urban and Regional Information Systems Association* (pp. 367–379). Sydney, Australia.
- Hunter, N., Bates, P. D., Horritt, M. S., De Roo, A. P. J., & Werner, M. (2005). Utility of different data types for calibrating flood inundation models within a GLUE framework. *Hydrology and Earth System Sciences Discussions*, 9(4), 412–430. <https://doi.org/10.5194/hess-9-412-2005>
- Hunter, N., Bates, P. D., Horritt, M. S., & Wilson, M. D. (2007). Simple spatially-distributed models for predicting flood inundation: A review. *Geomorphology*, 90(3–4), 208–225.
- Hunter, N., Bates, P. D., Néelz, S., Pender, G., Villanueva, I., Wright, N. G., ... Mason, D. (2008). Benchmarking 2D hydraulic models for urban flooding. *Water Management*, 161, 13–30.
- Hunter, N., Horritt, M. S., Bates, P. D., Wilson, M., & Werner, M. (2005). An adaptive time step solution for raster-based storage cell modelling of floodplain inundation. *Advances in Water Resources*, 28, 975–991. <https://doi.org/10.1016/j.advwatres.2005.03.007>

- Hutter, G., & Schanze, J. (2008). Learning how to deal with uncertainty of flood risk in long-term planning. *International Journal on River Basin Management*, 6, 175–184.
- Interrante, V. (2000). Harnessing natural textures for multivariate visualization. *IEEE Computer Graphics and Applications*, 10(6), 6–11. <https://doi.org/10.1109/MCG.2000.888001>
- Johnson, C. R., & Sanderson, A. (2003). A next step: visualizing errors and uncertainty. *Computer Graphics and Applications, IEEE*, 23(5), 6–10. <https://doi.org/10.1109/MCG.2003.1231171>
- Kraak, M.-J., & Ormeling, F. (2003). *Cartography: Visualization of Geospatial Data* (2nd ed.). Harlow Essex: Pearson Education Limited.
- Kubíček, P., & Šašík, Č. (2011). Thematic uncertainty visualization usability - comparison of basic methods. *Annals of GIS*, 17(4), 253–263. <https://doi.org/10.1080/19475683.2011.625978>
- Kunz, M., Grêt-Regamey, A., & Hurni, L. (2011). Visualization of uncertainty in natural hazards assessments using an interactive cartographic information system. *Natural Hazards*, 59(3), 1735–1751. <https://doi.org/10.1007/s11069-011-9864-y>
- Länstyrelsen Gävleborg. (2016). *Bevaredeplan för Natura 2000-området (SE0630164 Testeboån)*. Gävle.
- Leedal, D., Neal, J. C., Beven, K. J., Young, P., & Bates, P. D. (2010). Visualization approaches for communicating real-time flood forecasting level and inundation information. *Journal of Flood Risk Management*, 3(2), 140–150. <https://doi.org/10.1111/j.1753-318X.2010.01063.x>
- Leitner, M., & Bittenfield, B. P. (1997). Cartographic Guidelines on the Visualization of Attribute Accuracy. In *Proceedings of AUTO-CARTO 13*. Seattle.
- Leitner, M., & Bittenfield, B. P. (2000). Guidelines for the Display of Attribute Certainty. *Cartography and Geographic Information Science*, 27(1), 3–14. <https://doi.org/10.1559/152304000783548037>
- Lillesand, T. M., Kiefer, R. W., & Chipman, J. W. (2004). *Remote Sensing and Image Interpretation* (5th ed.). John Wiley & Sons, Inc.
- Lim, N. J. (2009). *Topographic data and roughness parameterisation effects on 1D flood inundation models*. University of Gävle, Sweden.
- Lim, N. J. (2011). *Performance and uncertainty estimation of 1- and 2-dimensional flood models*. University of Gävle, Sweden.
- Lim, N. J., Brandt, S. A., & Seipel, S. (2016). Visualisation and evaluation of flood uncertainties based on ensemble modelling. *International Journal of Geographical Information Science*, 30(2), 240–262. <https://doi.org/10.1080/13658816.2015.1085539>
- Litrico, X., & Fromion, V. (2009). *Modeling and Control of Hydrosystems*. London: Springer London.
- Loucks, D. P., & Beek, E. Van. (2005). *Water Resources Systems Planning and Management: An Introduction to Methods, Models and Applications*. United Nations Educational, Scientific and Cultural Organization (UNESCO).
- MacEachren, A. M. (1992). Visualizing uncertain information. *Cartographic Perspectives*, 13, 10–19. <https://doi.org/10.14714/CP13.1000>
- MacEachren, A. M. (1995). *How Maps Work: Representation, Visualization and Design*. Guilford Press.

- MacEachren, A. M., Robinson, A., Hopper, S., Gardner, S., Murray, R., Gahegan, M., & Hetzler, E. (2005). Visualizing geospatial information uncertainty: what we know and what we need to know. *Cartography and Geographic Information Science*, 32(3), 139–160. <https://doi.org/10.1559/1523040054738936>
- MacEachren, A. M., Roth, R. E., O'Brien, J., Li, B., Swingley, D., & Gahegan, M. (2012). Visual semiotics & uncertainty visualization: an empirical study. *IEEE Transactions on Visualization and Computer Graphics*, 18(12), 2496–2505. <https://doi.org/10.1109/TVCG.2012.279>
- Mahoney, D. P. (1999). The picture of uncertainty. *Computer Graphics World*, 33(11).
- Mark, D. M. (2000). Geographic Information Science: Critical Issues in an Emerging Cross-Disciplinary Research Domain. *Journal of the Urban and Regional Information Systems Association*, 12(1), 45–54.
- Mason, D. C., Bates, P. D., & Dall'Amico, J. T. (2009). Calibration of uncertain flood inundation models using remotely sensed water levels. *Journal of Hydrology*, 368(1–4), 224–236. <https://doi.org/10.1016/j.jhydrol.2009.02.034>
- Mason, D. C., Cobby, D. M., Horritt, M. S., & Bates, P. D. (2003). Floodplain friction parameterization in two-dimensional river flood-models using vegetation heights derived from airborne scanning laser altimetry. *Hydrological Processes*, 17(9), 1711–1732. <https://doi.org/10.1002/hyp.1270>
- Merwade, V., Cook, A., & Coonrod, J. (2008). GIS techniques for creating river terrain models for hydrodynamic modeling and flood inundation mapping. *Environmental Modelling & Software*, 23(10–11), 1300–1311. <https://doi.org/10.1016/j.envsoft.2008.03.005>
- Merz, B., & Thielen, A. H. (2005). Separating natural and epistemic uncertainty in flood frequency analysis. *Journal of Hydrology*, 309, 114–132. <https://doi.org/10.1016/j.jhydrol.2004.11.015>
- Merz, B., Thielen, A. H., & Gochi, M. (2007). Flood Risk Mapping at the Local Scale: Concepts and Challenges. In S. Begun, M. J. F. Stive, & J. W. Hall (Eds.), *Flood Risk Management in Europe* (pp. 231–251). Springer.
- Mitasova, H., Harmon, R. S., Weaver, K. J., Lyons, N. J., & Overton, M. F. (2012). Scientific visualization of landscapes and landforms. *Geomorphology*, 137(1), 122–137. <https://doi.org/10.1016/j.geomorph.2010.09.033>
- Moel, H., van Alphen, J., & Aerts, J. C. J. H. (2009). Flood Maps in Europe—methods, availability and use. *Natural Hazards Earth System Science*, 9(2), 289–301.
- Morss, R. E., Wilhelmi, O. V., Downton, M. W., & Grunfest, E. (2005). Flood Risk, Uncertainty, and Scientific Information for Decision Making: Lessons from an Interdisciplinary Project. *Bulletin of the American Meteorological Society*, 86(11), 1593–1601. <https://doi.org/10.1175/BAMS-86-11-1593>
- Mulligan, M., & Wainwright, J. (2004). Modelling and Model Building. In J. Wainwright & M. Mulligan (Eds.), *Environmental Modelling: Finding Simplicity in Complexity* (pp. 7–73). John Wiley & Sons, Ltd.
- Neal, J. C., Bates, P. D., Fewtrell, T. J., Hunter, N., Wilson, M. D., & Horritt, M. S. (2009). Distributed whole city water level measurements from Carlisle 2005 flood event and comparison with hydraulic model simulations. *Journal of Hydrology*, 368, 42–55.

- Neal, J. C., Villanueva, I., Wright, N., Willis, T., Fewtrell, T. J., & Bates, P. D. (2012). How much physical complexity is needed to model flood inundation? *Hydrological Processes*, 26, 2264–2282. <https://doi.org/10.1002/hyp.8339>
- Néelz, S., & Pender, G. (2009). *Desktop review of 2D hydraulic modelling packages*. Bristol.
- Olofsson, S., & Berggren, O. (1966). *Redogörelse för utförda observationer av vattenstånd i Testeboån på sträckan Strömsbro - Åbyggeby under våren 1966*.
- Pang, A. T. (2001). Visualizing uncertainty in geo-spatial data. In *Proceedings of the Workshop on the Intersections between Geospatial Information and Information Technology* (pp. 1–14). Washington, D.C.: National Academies Committee of the Computer Science and Telecommunications Board.
- Pang, A. T. (2008). Visualizing uncertainty in natural hazards. In A. Bostrom, S. P. French, & S. J. Gottlieb (Eds.), *Risk Assessment, Modeling and Decision Support: Strategic Directions* (pp. 261–294). Springer-Verlag Berlin Heidelberg.
- Pang, A. T., Witterbrink, C. M., & Lodha, S. K. (1997). Approaches to uncertainty visualization. *The Visual Computer*, 13(8), 370–390. <https://doi.org/10.1007/s003710050111>
- Papaioannou, G., Vasilades, L., Loukas, A., & Aronica, G. T. (2017). Probabilistic flood inundation mapping at ungauged streams due to roughness coefficient uncertainty in hydraulic modelling. *Advances in Geosciences*, 44, 23–34. <https://doi.org/10.5194/adgeo-44-23-2017>
- Pappenberger, F., & Beven, K. J. (2006). Ignorance is bliss: or seven reasons not to use uncertainty analysis. *Water Resources Research*, 42(5), 1–8. <https://doi.org/10.1029/2005WR004820>
- Pappenberger, F., Beven, K. J., Horritt, M. S., & Blazkova, S. (2005). Uncertainty in the calibration of effective roughness parameters in HEC-RAS using inundation and downstream level observations. *Journal of Hydrology*, 302(1), 46–49.
- Pappenberger, F., Beven, K. J., Hunter, N., Bates, P. D., Gouweleeuw, B. T., Thielen, J., & De Roo, A. P. J. (2005). Cascading model uncertainty from medium range weather forecasts (10 days) through a rainfall-runoff model to flood inundation predictions within the European Flood Forecasting System (EFFS). *Hydrology and Earth System Sciences*, 9, 381–393. <https://doi.org/10.5194/hess-9-381-2005>
- Pappenberger, F., Frodsham, K., Beven, K., Romanowicz, R., & Matgen, P. (2007). Fuzzy set approach to calibrating distributed flood inundation models using remote sensing observations. *Hydrological Earth System Science*, 11, 739–752.
- Pappenberger, F., Matgen, P., Beven, K. J., Henry, J.-B., Pfister, L., & de Frapoint, P. (2006). Influence of uncertainty boundary conditions and model structure on flood inundation predictions. *Advances in Water Resources*, 1430–1449.
- Pender, G., & Néelz, S. (2007). Use of computer models of flood inundation to facilitate communication in flood risk management. *Environmental Hazards*, 7(2), 106–114. <https://doi.org/10.1016/j.envhaz.2007.07.006>
- Price, R. K., & Vojinovic, Z. (2008). Urban flood disaster management. *Urban Water Journal*, 5(3), 259–276. <https://doi.org/10.1080/15730620802099721>
- Robinson, A. H., Morrison, J. L., Muehrcke, P. C., Kimerling, A. J., & Guptill, S. C. (1995). *Elements of Cartography* (6th ed.). John Wiley & Sons, Inc.

- Romanowicz, R., & Beven, K. (2003). Estimation of flood inundation probabilities as conditioned on event inundation maps. *Water Resources Research*, 39(3). <https://doi.org/10.1029/2001WR001056>
- Roth, R. E. (2009). The Impact of User Expertise on Geographic Risk Assessment under Uncertain Conditions. *Cartography and Geographic Information Science*, 36(1), 29–43. <https://doi.org/10.1559/152304009787340160>
- Samuels, P. G. (2006). The European perspective and research on flooding. In D. W. Knight & A. Y. Shamseldin (Eds.), *River Basin Modelling for Flood Risk Mitigation* (pp. 21–58). London: Taylor & Francis.
- Sanyal, J., Zhang, S., Bhattacharya, G., Amburn, P., & Moorhead, R. J. (2009). A User Study to Compare Four Uncertainty Visualization Methods for 1D and 2D Datasets. *IEEE Transactions on Visualization and Computer Graphics*, 15(6), 1209–1218.
- Savage, J. T. S., Pianosi, F., Bates, P. D., Freer, J., & Wagener, T. (2016). Quantifying the importance of spatial resolution and other factors through global sensitivity analysis of a flood inundation model. *Water Resource Research*, 52(11), 9146–9163. <https://doi.org/10.1002/2015WR018198>
- Schanze, J. (2006). Flood Risk Management - A Basic Framework. In J. Schanze, E. Zeman, & J. Marsalek (Eds.), *Flood Risk Management: Hazards, Vulnerability and Mitigation Measures* (pp. 1–20). Springer.
- Scholz, R. W., & Lu, Y. (2014). Uncertainty in Geographic Data on Bivariate Maps: An Examination of Visualization Preference and Decision Making. *ISPRS International Journal of Geo-Information*, 3(4), 1180–1197.
- Schroeder, W., Martin, K., & Lorensen, B. (2006). *The Visualization Toolkit* (4th ed.). Kitware.
- Schumann, G., Matgen, P., Cutler, M. E. J., Black, A., Hoffmann, L., & Pfister, L. (2008). Comparison of remotely sensed water stages from LiDAR, topographic contours and SRTM. *ISPRS Journal of Photogrammetry and Remote Sensing*, 63(3), 283–296.
- Schumann, G., Matgen, P., Hoffmann, L., Hostache, R., Pappenberger, F., & Pfister, L. (2007). Deriving distributed roughness values from satellite radar data for flood inundation modelling. *Journal of Hydrology*, 344(1–2), 96–111.
- Seipel, S., & Lim, N. J. (2017). Color map design for visualization in flood risk assessment. *International Journal of Geographical Information Science*, 31(11), 2286–2309. <https://doi.org/10.1080/13658816.2017.1349318>
- Skidmore, A. (2002). Taxonomy of environmental models in the spatial sciences. In A. Skidmore (Ed.), *Environmental Modelling with GIS and Remote Sensing*. London: Taylor & Francis.
- Slocum, T. A., Cliburn, D. C., Feddema, J. J., & Miller, J. R. (2003). Evaluating the usability of a tool for visualizing the uncertainty of the future global water balance. *Cartography and Geographic Information Science*, 30(4), 299–317.
- Smith-Jackson, T. L., & Wogalter, M. S. (2000). Users' Hazard Perceptions of Warning Components: An Examination of Colors and Symbols. In *Proceedings of the Human Factors and Ergonomics Society Annual Meeting* (pp. 6–55).
- Stoet, G. (2010). PsyToolkit - A software package for programming psychological experiments using Linux. *Behavior Research Methods*, 42(4), 1096–1104. <https://doi.org/10.3758/BRM.42.4.1096>

- Stoet, G. (2017). PsyToolkit: A novel web-based method for running online questionnaires and reaction-time experiments. *Teaching of Psychology*, 44(1), 24–31. <https://doi.org/10.1177/0098628316677643>
- Sveriges Meteorologiska och Hydrologiska Institut (SMHI). (2002). *Översiktlig översvämningskartering längs Testeboån (sträckan från Åmot till utloppet i Bottenhavet) (Rapport 30, 2002-05-28)*. Karlstad.
- Tak, S., & Toet, A. (2014). Color and Uncertainty: It is not always Black and White. In N. Elmqvist, M. Hlawitschka, & J. Kennedy (Eds.), *EuroVis - Short Papers*. The Eurographics Association. <https://doi.org/10.2312/eurovisshort.20141157>
- Tate, E., Maidment, D., Olivera, F., & Anderson, D. (2002). Creating a Terrain Model for Floodplain Mapping. *Journal of Hydrologic Engineering*, 7(2), 100–108. [https://doi.org/10.1061/\(ASCE\)1084-0699\(2002\)7:2\(100\)](https://doi.org/10.1061/(ASCE)1084-0699(2002)7:2(100))
- Teng, J., Jakeman, A. J., Vaze, J., Croke, B. F. ., Dutta, D., & Kim, S. (2017). Flood inundation modelling: A review of methods, recent advances and uncertainty analysis. *Environmental Modelling and Software*, 90, 201–216. <https://doi.org/10.1016/j.envsoft.2017.01.006>
- Thomson, J., Hetzler, B., MacEachren, A., MarkGahegan, & Pavel, M. (2005). A typology for visualizing uncertainty. In R. F. Erbacher, J. C. Roberts, M. T. Grohn, & K. Borner (Eds.), *Proceedings of SPIE (vol. 5669) - Visualization and Data Analysis 2005* (pp. 146–157). San Jose, CA. <https://doi.org/10.1117/12.587254>
- Van der Wel, F. J. M., Hootsmans, R. M., & Ormeling, F. (1994). Visualization of data quality. In A. M. MacEachren & D. R. F. Taylor (Eds.), *Visualization in Modern Cartography (vol. 2)* (pp. 313–331). Oxford: Pergamon.
- Vivoni, E. R., Ivanov, V., Bras, Rafael, L., & Entekhabi, D. (2005). On the effects of triangulated terrain resolution on distributed hydrologic model response. *Hydrological Processes*, 19, 2101–2122. <https://doi.org/10.1002/hyp.5671>
- WSP. (2015). *Översvämningskartering utmed Testeboån (Sträckan från Åmot till utloppet i Bottenhavet) (Rapport 30, 2015-05-11)*. Karlstad.
- Wurbs, R. A. (1997). *Computer Models for Water Resources Planning and Management*. Alexandria, Virginia: US Army Corps of Engineers.
- Yu, D., & Lane, S. N. (2006). Urban fluvial flood modelling using a two-dimensional-wave treatment, part 1: mesh resolution effects. *Hydrological Processes*, 20, 1541–1565.

Appendix

Different uncertainty maps derived from the uncertainty analyses

FLOOD UNCERTAINTY REPRESENTATION	CHAR. AND SOURCE OF INFORMATION	SUGGESTED MAP TYPE AND VISUAL VARIABLE	ADVANTAGES	DISADVANTAGES
Dual-ended certainty map	<ul style="list-style-type: none"> Two opposing certain status at both ends: dry (minimum) and flooded (maximum). Uncertainty is in the middle. C_j equation 	<ul style="list-style-type: none"> Surface map for continuous data and choropleth map for discrete data. Certain to be dry and flooded are represented by the darkest brown and blue colours, respectively. Degrees of certainty is represented by lightness, wherein the more uncertain, the lighter the colour it becomes. The application of the colour map design suggested in Paper V (Sec. 3.6.2) can also be an alternative. Here, the indicated pivot points are used for colour interpolation. 	<ul style="list-style-type: none"> Easy for identifying flooded and dry zones. Highly preferred by users in the evaluations. 	<ul style="list-style-type: none"> When deciding on an uncertain location using value as to indicate degrees of certainty, the lightest (blue/brown) colours in the continuous map became confusing as to whether it is safe or unsafe. The choropleth map can lead to more choices of uncertain locations, but they have high certain to be dry status.
Flood probability map	<ul style="list-style-type: none"> Shows the probability to be flooded status. Values range from 0 to 100, where 100 has the highest probability to be flooded C_j equation 	<ul style="list-style-type: none"> Surface map for continuous data and choropleth map for discrete data. Blue as the base colour. Lightness increases as the probability decreases. 	<ul style="list-style-type: none"> Easy to identify areas that are to be flooded, with the dark colour, as well as safe areas. Uncertain areas are also can be identified and avoided due to the medium blue colour. 	<ul style="list-style-type: none"> The continuous map is not highly preferred by novices

FLOOD UNCERTAINTY REPRESENTA- TION	CHAR. AND SOURCE OF IN- FORMATION	SUGGESTED MAP TYPE AND VISUAL VARIABLE	ADVANTAGES	DISAD- VANTAGES
Certainty map	<ul style="list-style-type: none"> Shows the degree of certainty of the prediction (from low to certain conditions). Inverted S_j equation 	<ul style="list-style-type: none"> Choropleth map where white represents the lowest certainty and black for the certain condition. Graduated symbol map with size as the only visual variable. Lowest certainty represented by smallest size and largest is certain condition. All symbols should have the same [black] colour. Elimination of the big certain to be dry area facilitates reading the map information. 	<ul style="list-style-type: none"> These two maps are easier to read than the continuous certainty map from the original inverted data. 	<ul style="list-style-type: none"> Both maps can also lead to more choices of locations that have uncertain status.
Uncertainty map	<ul style="list-style-type: none"> Emphasises the degree of uncertainty is emphasised (from low/minimum to high/maximum uncertainty) S_j equation 	<ul style="list-style-type: none"> Continuous: black for the lowest/minimum uncertainty and white for the highest/maximum uncertainty 	<ul style="list-style-type: none"> Good for indicating uncertain areas. 	<ul style="list-style-type: none"> Confusing in indicating flooded/non-flooded areas Led to poor user performance when used in the tasks
Binary map	<ul style="list-style-type: none"> Represents two conditions: flooded and uncertain. Discretisation of the resulting map from the C_j equation or from the application of the D_d equation. 	<ul style="list-style-type: none"> Discrete map representing certain to be flooded locations with, while uncertain is red. 	<ul style="list-style-type: none"> More direct in indicating the status of certain to be flooded and uncertain locations. 	<ul style="list-style-type: none"> Uncertain condition can be interpreted as either safe or unsafe location.

FLOOD UNCERTAINTY REPRESENTA- TION	CHAR. AND SOURCE OF IN- FORMATION	SUGGESTED MAP TYPE AND VISUAL VARIABLE	ADVANTAGES	DISAD- VANTAGES
Overlain flood extent map	<ul style="list-style-type: none"> – Flood bound- aries as re- sults of dif- ferent cali- brations that are overlain to each other 	<ul style="list-style-type: none"> – Line representation with varying colours and/or thickness to distinguish the bound- aries from each other. 	<ul style="list-style-type: none"> – Easy for dif- ferentiating the extents of flooding pro- duced 	<ul style="list-style-type: none"> – The number of boundaries overlain can affect the legibility of the map
Performance bars	<ul style="list-style-type: none"> – Interactive method for visualising flood uncer- tainty from ensemble modelling – Each bar rep- resents the flooding sta- tus from sim- ulation result. 	<ul style="list-style-type: none"> – Flooding status is rep- resented by the colour of the bar (blue=flooded; brown=dry) – Size of the bar indi- cates the likelihood of the model result to the observed data (longest bars=highest likeli- hood) 	<ul style="list-style-type: none"> – Effective for determining flooded areas – Number of bars visual- ised with a specific col- our can indi- cate degrees of certainty and uncer- tainty in the map. 	<ul style="list-style-type: none"> – Point-based. The status is determined at the cell where the cursor is pointed. – Overall spa- tial pattern of uncertainty and flooding could not be determined from the vis- ualisation – Can lead us- ers to choose more uncer- tain locations

Papers

Associated papers have been removed in the electronic version of this thesis.

For more details about the papers see: <http://urn.kb.se/resolve?urn:nbn:se:hig:diva-27995>